12-9-2011

Integrated Optimal and Robust Control of Spacecraft in Proximity Operations

Hejia Pan

INTEGRATED OPTIMAL AND ROBUST CONTROL OF SPACECRAFT IN PROXIMITY OPERATIONS

By

Hejia Pan

A Dissertation
Submitted to the Faculty of
Mississippi State University
in Partial Fulfillment of the Requirements
for the Degree of Doctor of Philosophy
in Aerospace Engineering
in the Department of Aerospace Engineering

Mississippi State, Mississippi

December 2011

INTEGRATED OPTIMAL AND ROBUST CONTROL OF SPACECRAFT IN PROXIMITY OPERATIONS

By

Hejia Pan

Approved:

Ming Xin Assistant Professor of Department of Aerospace Engineering (Major Advisor and Director of Dissertation)	Keith Koenig Professor of Department of Aerospace Engineering (Committee Member)
Yang Cheng Assistant Professor of Department of Aerospace Engineering (Committee Member)	Burak Eksioglu Associate Professor of the Industrial and Systems Engineering Department (Committee Member)
Randolph F. Follett Assistant Professor of Electrical and Computer Engineering Department (Committee Member)	J. Mark Janus Graduate Coordinator of Aerospace Engineering
Sarah A. Rajala Dean of the James Worth Bagley College of Engineering	

Name: Hejia Pan

Date of Degree: December 9, 2011

Institution: Mississippi State University

Major Field: Aerospace Engineering

Major Professor: Dr. Ming Xin

Title of Study: INTEGRATED OPTIMAL AND ROBUST CONTROL OF SPACECRAFT IN PROXIMITY OPERATIONS

Pages in Study: 118

Candidate for Degree of Doctor of Philosophy

With the rapid growth of space activities and advancement of aerospace science and technology, many autonomous space missions have been proliferating in recent decades. Control of spacecraft in proximity operations is of great importance to accomplish these missions. The research in this dissertation aims to provide a precise, efficient, optimal, and robust controller to ensure successful spacecraft proximity operations. This is a challenging control task since the problem involves highly nonlinear dynamics including translational motion, rotational motion, and flexible structure deformation and vibration. In addition, uncertainties in the system modeling parameters and disturbances make the precise control more difficult. Four control design approaches are integrated to solve this challenging problem. The first approach is to consider the spacecraft rigid body translational and rotational dynamics together with the flexible motion in one unified optimal control framework so that the overall system performance and constraints can be addressed in one optimization process. The second approach is to formulate the robust control objectives into the optimal control cost function and prove the equivalency between the robust stabilization problem and the transformed optimal

control problem. The third approach is to employ the θ-D technique, a novel optimal control method that is based on a perturbation solution to the Hamilton-Jacobi-Bellman equation, to solve the nonlinear optimal control problem obtained from the indirect robust control formulation. The resultant optimal control law can be obtained in closed-form, and thus facilitates the onboard implementation. The integration of these three approaches is called the integrated indirect robust control scheme. The fourth approach is to use the inverse optimal adaptive control method combined with the indirect robust control scheme to alleviate the conservativeness of the indirect robust control scheme by using online parameter estimation such that adaptive, robust, and optimal properties can all be achieved.

To show the effectiveness of the proposed control approaches, six degree-of-freedom spacecraft proximity operation simulation is conducted and demonstrates satisfying performance under various uncertainties and disturbances.

DEDICATION

To

my parents,

Jiansan Pan and Xiuying He,

who made all of this possible,

for their endless encouragement and love.

ACKNOWLEDGEMENTS

I wish to express my sincere gratitude to my advisor, Prof. Ming Xin, for helping spark my interest in this topic, for his sage advice and guidance on every aspect of my research, and for helping me cultivate good research habits. He has helped me clarify many ambiguities in my research, thus expedite my research progress. I deeply appreciate all his efforts. I would also like to thank Dr. Keith Koenig, Dr. Yang Cheng, Dr. Burak Eksioglu, and Dr. Randy Follett for being part of my dissertation committee on top of their busy schedules. Finally, I would like to thank the department head, Dr. Pasquale Cinnella and academic coordinator, Ms. Machaunda Bush for their unfailing patience and courtesy in helping me with everything I need in my study.

My special thanks go to my colleagues: Mr. Jianan Wang and Mr. Bin Jia, for their constant support during these years. At home, I have to thank Dongmei for her faith in me. I would also like to thank my parents for absolutely everything. I hope I did not let you down.

TABLE OF CONTENTS

Page

LIST OF TABLES

LIST OF FIGURES

CHAPTER I

INTRODUCTION

1.1 Background

Spacecraft proximity operation has been recognized as a very important task for many space missions since the 1960s. As stated in [1], those who envisioned humans going to the moon and exploring other worlds, those who dreamed of humanity's long-term presence in space, and those who actually made it happen, realized that orbital rendezvous and proximity operation would play a crucial role in making these miracles happen. With the rapid growth of space activities and the progress of aerospace science and technology, many autonomous space missions such as space station assembly, inspection and servicing, space refueling, correction of launch failure, and removal of space debris, have proliferated in recent decades. The research on proximity operation is of great importance to accomplish these missions. Our research aims to provide a precise and efficient controller that possesses both optimality and robustness such that successful spacecraft proximity operations can be ensured.

During the early development of space technology, spacecraft proximity rendezvous and docking efforts were piloted mostly by astronauts. The rendezvous and docking process was mission unique, labor-intensive and expensive, requiring extensive crew training and system redundancy to insure mission success [2].

The first docking between two spacecrafts can be dated back to the Gemini mission in the winter of 1965 [3]. That rendezvous operation was the first astronaut-

controlled maneuver in space. The Gemini spacecraft was launched later than the target spacecraft Agena, and driven to a relative distance of 30 cm to 90 m with respect to the target Agena vehicle. On March 16, 1966, Neil Armstrong and Dave Scott docked Gemini VIII with the target vehicle and completed the first spacecraft docking. Unfortunately, the success did not last long, since one of the spacecraft thrusters failed and caused near-fatal spinning and tumbling. This led to the first emergency landing of a manned U.S. space mission. At that time, the rendezvous and docking scenario relied heavily on the involvement of astronauts in guidance, navigation and control (GN&C) [1].

Based on these preliminary space missions, scientists had accumulated many experiences. Most of the following missions, such as Apollo program [4] and Skylab project[5], are quite successful. Space technology enters a new stage of development. Due to the fast expansion of human activities into space, complex spacecraft proximity operations require more accurate control and fast response even in large scale complex maneuvers. Besides, the engaging space vehicles not only contain large and bulky spacecraft piloted by astronauts, but also include small satellites operating in conditions where human involvement is impractical or undesirable. The cooperation between the engaging space vehicles may not exist. To handle with these cases, new control methods are required, thus the autonomous spacecraft proximity operation is moved up the agenda. It is desired to reduce the work load on human missions, or accomplish the servicing and retrieval of a variety of target objects that may be functioning or malfunctioning, alien or familiar, passive or active, cooperative or non-cooperative. These high mission requirements drive the rendezvous and proximity operation technique to advance rapidly and brought about a series of space programs with or without the involvement of astronauts.

Figure 1.1 demonstrates the timeline and significant events in the autonomous rendezvous and proximity operation history. We will take the DART mission and ATV mission for example and analyze these two proximity operation applications.

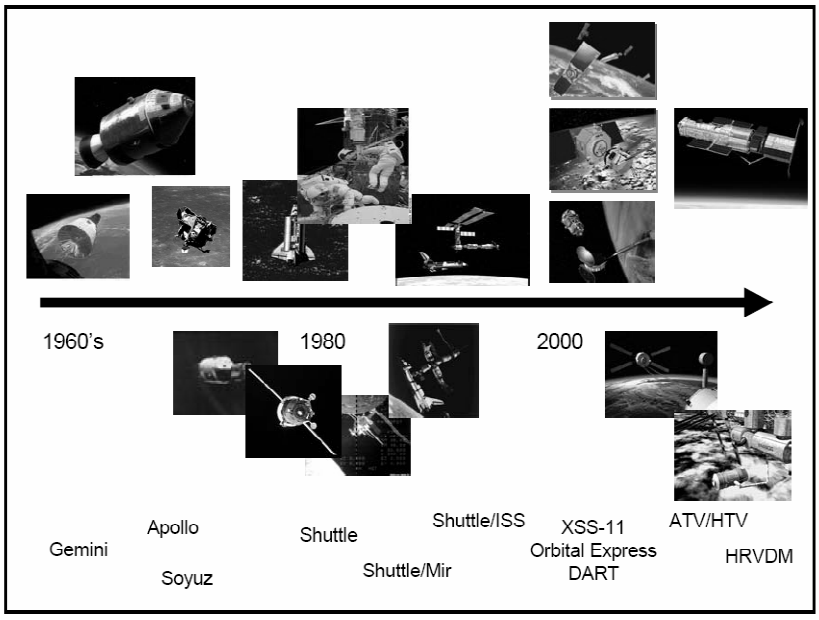

Figure 1.1 Autonomous rendezvous and docking program timeline [6]

The Demonstration of Autonomous Rendezvous Technology (DART) spacecraft, launched by NASA in April 15, 2005, is a key step in NASA's history to establish autonomous rendezvous capabilities for the US space program by performing autonomous rendezvous without assistance from ground personnel [7, 8].

DART was designed to rendezvous with and perform a variety of maneuvers in close proximity to the target Multiple Paths, Beyond-Line-of-Sight Communication (MUBLCOM) satellite. 27 objectives were developed to measure the performance of the DART spacecraft for a successful mission, especially the spacecraft's ability of independent rendezvous or meet up with a non-maneuvering and cooperative satellite while being a pre-programmed and unaided spacecraft [8]. During the proximity

operation phase, DART was programmed to move into MUBLCOM's orbit with a series of scheduled maneuvers

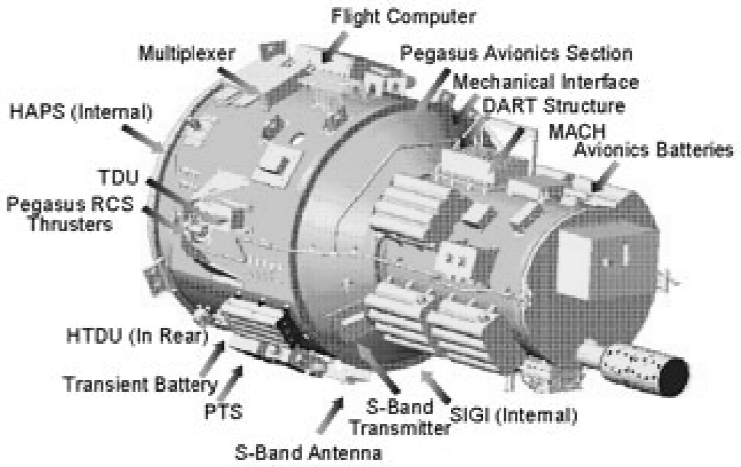

Figure 1.2 Demonstration for Autonomous Rendezvous Technology (DART) component diagram [7]

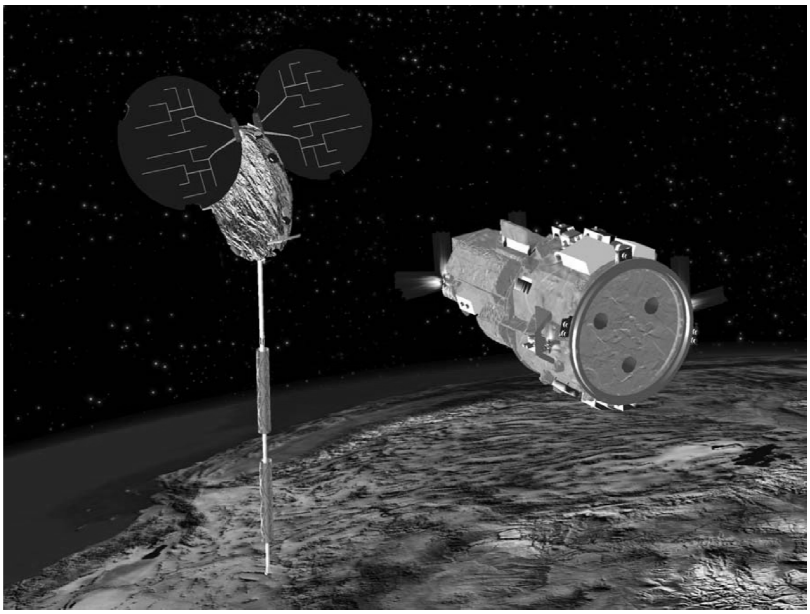

Figure 1.3 Artistic concept of Demonstration for Autonomous Rendezvous Technology [9]

and stay about 1 kilometer behind the target. Then DART was ordered to evaluate its proximity operation performance by a series of precise, close-range maneuvers, including various pre-planned holds and a collision avoidance maneuver at a predetermined position [9]. Unfortunately, because of over usage of the propellant and guidance system malfunction, the DART spacecraft made contact with and boosted the rendezvous MUBLCOM satellite's orbit 2.2 km higher and ended the mission prematurely.

The DART mission clearly supports the fact that autonomous spacecraft rendezvous, proximity operations, and capture capabilities will continue to be critically important to successful space exploration. As stated in [8], while DART's transition to such a high-visibility and important project did not proceed as planned, the lessons learned from the mishap will help enable the future development of autonomous capabilities.

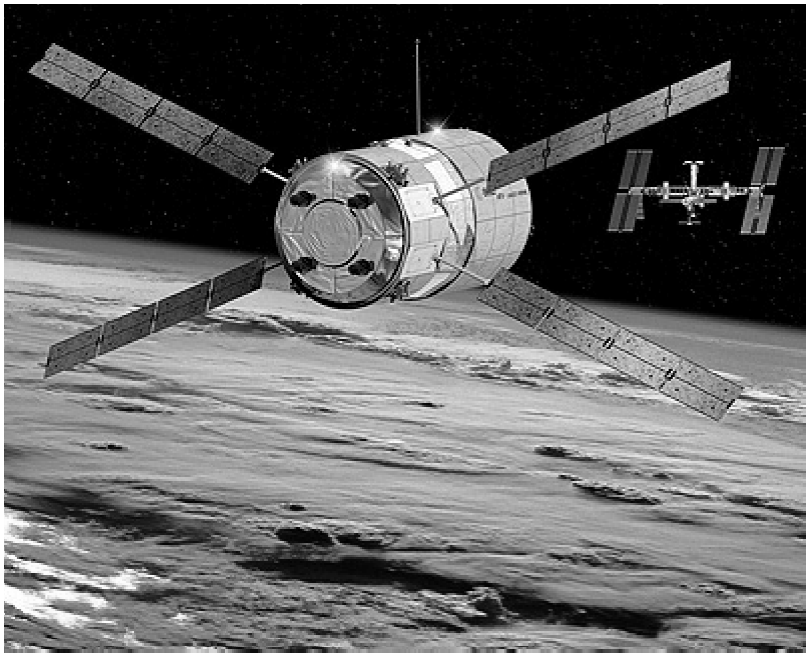

Figure 1.4 ATV becomes a fully automatic spaceship navigating towards ISS after lift-off and is ready to dock with ISS[10]

ESA's Automated Transfer Vehicle(ATV) [10-12] is the largest, heaviest and most complex space vehicle ever developed in Europe. As introduced in [12], ATV is designed to serve the orbiting International Space Station (ISS) as a cargo carrier, storage facility and as a 'tug' vehicle to adjust the Space Station's orbit.

Figure 1.5 ATV-2 Johannes Kepler proximity operation Strategy [11]

Major contributions of ATV can be divided into two aspects. First, the ATV provides express delivery service to ISS. The International Space Station has been permanently inhabited since 2000. It relies on logistic vehicles like ATV to upload all kinds of cargo, as well as propellants to maintain the orbit. ATV-2 was launched on Feburary 16, 2011 at French Guiana. Seventy minutes after lift-off, ATV-2 Johannes Kepler navigated and docked to the station automatically. It was monitored and commanded from the ATV Control Center. During the last 250 meters of the docking scenario, ATV's state-of-the-art automatic rendezvous system utilized a series of sensors to guide the ATV to the docking port on the Russia Zvezda module. ATV-2 docked with the ISS with the precision of about 8 cm. The whole process is fully automatic even though under the surveillance of control center and the space station crews. Second, the ATV is also designed to re-boost the ISS into a high altitude to compensate for the atmosphere drag [10]. The ATV propulsion system will use more than 4 tons of fuel to

fulfill another two functions aside from raising the station's orbit: perform necessary attitude control and perform ISS debris avoidance maneuvers. The ATV-2 Johannes Kepler mission is a total success, not only fulfilling the tasks for ISS, but also providing invaluable experience in practicing the existing GN&C technologies and designing the following ATVs.

1.2 Research overview

From the background sketched in Section 1.1, we can see that autonomous space missions have three flight segments characterized by unique mission design emphasis and proper GN&C support systems. These three phases are: the orbit adjusting phase, the relative navigation phase, and the close proximity operations phase.

The relative navigation phase starts once the spacecraft or shuttle enters the proximity range (100 km) of the target. By using proper navigation and guidance scheme, when the relative range decreases to two kilometers and the relative velocity is under 2 m/s, the proximity operation phase begins. During this phase, a series of maneuvers is conducted to adjust the attitude and position of the pursuer spacecraft so that servicing missions or docking can be conducted thereafter. Since the satellite rendezvous technique is relatively mature, in our research, we confine the scenario into the phase when the pursuer spacecraft has completed its orbit transferring process and is less than 1 km from the final stage [13]. Under the proper GNC method, the pursuer spacecraft will rendezvous with the target. We will control the translational and rotational motion of a pursuer spacecraft such that it has no relative motion (position and attitude) with respect to the target space body in the target body frame. For example, their docking ports will face towards each other.

Determined by whether the target body can maneuver actively, the target can be regarded as a cooperative target or a non-cooperative target [14]. The technologies of autonomous rendezvous and capturing of non-cooperative targets are becoming more and more important for future on-orbit servicing missions. Capturing a non-cooperative target is a very challenging task since the pursuer must synchronize its motion with the non-cooperative motion of the target [15]. Therefore, a highly robust and precise control strategy is of necessity for the pursuer to successfully accomplish the proximity operation.

Typical non-cooperative free tumbling targets include space debris or malfunctioning satellites. Conventional GNC methods in proximity operations for debris removal include self-removal and external removal. Knowing that the vast majority of space debris, especially smaller debris, cannot be removed under its own power, a variety of proposals have been put forward to directly remove the debris from orbit [16-23]. In these proposals, conventional large spacecraft capture is a method that may be applicable to most of the debris. Compared with the newly developed laser broom system [24], the conventional debris capture methods generate less secondary debris. Erika Carlson [16] proposed a design scheme that incorporates a transfer vehicle and a netting vehicle. Once debris has been detected, the transfer vehicle will proceed to rendezvous with the debris and deploy the netting vehicle. After expanding the nets, the netting vehicle returns and docks back to the transfer vehicle. It is apparent that in this procedure, precise rendezvous with the debris and docking of the transfer vehicle with the netting vehicle is essential. In [19-23], Sin-Ichiro et al. proposed a multiple space debris removal mission scenario. The servicing vehicle is required to rendezvous with a debris object (target), measure its motion and attempt a synchronized capture motion. Jerome Pearson and his research

group applied this technique to the Electro-Dynamic Debris Eliminator (EDDE) system [17, 18]. Debris is rendezvoused and captured by a series of EDDE vehicles and dragged to low altitude orbit such that the orbit life of the debris is reduced to a few months.

For a real spacecraft system in proximity operation, we will consider not only its translational motion and rotational motion, but also disturbances and uncertainties that will affect the overall system performance. Disturbances and uncertainties can be classified as structural uncertainty and environmental disturbances.

Structural uncertainty comes from flexible deployable structures [25, 26], mass expulsion torques, propellant slosh loads, crew motion, and other internal torques [27].

Typical deployable structures includes solar arrays, deployable beams, and articulating platforms. Most of them are hinged flexible structures that will generate deformation and oscillation when a fast and large scale attitude maneuver occurs. Empirically, flexibility must be considered by the control designer if the vibration's lowest frequency mode is less than six times the desired control bandwidth. Otherwise there is a high possibility that this mode will be destabilized by the control system [26]. The Hubble Space Telescope (HST) encountered such a problem. Though designers of the attitude stabilization system of HST took most of the vibration of the solar panels into account, one of the panels still vibrated more than predicted after launch. An extra HST servicing mission 3B [28] had to be conducted to fix the solar panel and consumed millions of dollars.

Fuel sloshing also contributes to system uncertainties. During thrust maneuvers, the sloshing of fuel in partially filled tanks can interact with the controlled system in such a way as to cause the overall system to be unstable [29]. Fuel slosh instability in the booster caused the failure of the first US attempt to place a spacecraft into orbit [30].

Parametric uncertainties also contribute to deterioration of the system performance. Successful autonomous rendezvous and docking missions critically rely on a fault-tolerant sensor system to obtain real-time relative position and attitude information of two spacecraft during proximity operations. In realistic environments, pre-launch measurement and ground measurement by means of radar or optical observations are usually not sufficiently accurate. Currently there are different vision systems capable of estimating the relative state information of moving objects [31]. All measurement systems, however, provide discrete and noisy position and orientation data at a relatively low rate. Besides, due to its importance, on-orbit or ground estimation of the spacecraft moment of inertia has become a hot topic in recent studies.

External disturbances include solar radiation pressure, gas leaks, gravity gradient torque, magnetic torque, aerodynamic drag, and other environmental disturbances.

As stated in [26], by careful design, the solar radiation torque can be reduced to 10^{-5} or even 10^{-6} Newton-meters at the Earth's distance from the sun. The gas leakage from a reaction control system can be held to values on the order of 10^{-5} Newton-meters. Gravity gradient torque is caused by the orbited planet's gravity gradient. Magnetic torque is caused by the orbited planet's magnetic field acting on the residual magnetic dipole moment of the spacecraft. Aerodynamic drag becomes significant below an altitude of 1000 kilometers. Most of these disturbances are state related and must be taken into account in order to design a controller with satisfying performance. In fact, all these disturbance torques can also be used as control torques. A controlled gas leak is a thruster; a solar sail uses radiation pressure; gravity gradient, magnetic, and aerodynamic torques can be (and have been) used for de-saturating reactions or momentum wheels. But one has to realize that when dealing with tracking problems, a spacecraft maneuver

must be completed in a relatively short time span. Thus external torques must be treated as disturbance torques rather than control torques.

1.3 Research objective and approaches

For the challenging spacecraft proximity control problem that involves highly nonlinear dynamics including coupled translational motion, rotational motion, and induced flexible structure vibration, we will design a robust controller that is able to accommodate not only complicated nonlinear dynamics, but the influence of modeling uncertainties and external or internal disturbances on system performance.

To achieve these challenging objectives, we propose an integrated design strategy in the following sections. The design scheme includes four design approaches.

The first approach is to consider the spacecraft rigid-body translational and rotational dynamics as well as the flexible motion in a unified optimal control framework so that the overall system performance and constraints can be addressed in one optimization process.

The second approach is to formulate the robust control problem into an equivalent optimal control problem and prove the robust stability and optimality. This approach is called the indirect robust control design strategy.

The third approach is to employ the θ-D technique, which is based on a perturbation solution to the Hamilton-Jacobi-Bellman equation, to solve this nonlinear optimal control problem obtained from the indirect robust control formulation. The resultant optimal control law can be obtained in closed-form and thus facilitates the onboard implementation.

The fourth approach is to use the inverse optimal adaptive control method combined with the indirect robust control scheme to alleviate the conservativeness of the robust control scheme by using online parameter estimation such that adaptive, robust, and optimal properties can be all achieved.

We emphasize that by utilizing the relationship among the optimal control, robust control and adaptive control method, the disturbances and uncertainties can be accounted for in an innovative way such that stabilization and optimality can be guaranteed simultaneously.

CHAPTER II

LITERATURE REVIEW

In the course of spacecraft technology development, various methods have been proposed to address the proximity control problem. In terms of the control theory development, there have been intensive researches on robust or adaptive control of spacecraft using linear control methods based on linearization of the spacecraft dynamics or nonlinear control methods to address the true nonlinear dynamics directly. For large maneuvers like the proximity operations, linear-based control methods cannot guarantee satisfactory performance because the linearization is not able to capture the complex characteristics of the nonlinear and coupled dynamics. Nonlinear approaches are thus applied widely in modern proximity control scenarios. The following literature reviews will summarize some typical nonlinear spacecraft control methodologies and discuss the control designs specifically for spacecraft translational motion, rotational motion, and flexible spacecraft structures.

2.1 Overview of spacecraft proximity operation control techniques

Before we start to investigate specific control scenario in spacecraft proximity operations, it is important for us to review some widely used spacecraft control methods. As stated in the previous section, the highly nonlinear and coupled spacecraft dynamics and modeling uncertainties and disturbances need advanced nonlinear robust control techniques to guarantee satisfactory performance. Typical nonlinear spacecraft control methods include: the Lyapunov direct control scheme, the adaptive control method, the

variable structure robust control, and the optimal control method. : the Lyapunov direct control scheme, the adaptive control method, the variable structure robust control, and the optimal control method

2.1.1 Lyapunov direct control scheme

Based on the Lyapunov stability theory, the Lyapunov direct control scheme aims to find an appropriate Lyapunov function candidate for the dynamic system and construct a corresponding feedback control law to satisfy the stability condition. For simple systems with explicit energy function that is also a good Lyapunov function candidate, this method is efficient and capable of ensuring system stability. However, when applied to complex nonlinear systems such as spacecraft proximity operations, finding an appropriate Lyapunov function is very difficult, not to mention the complexity of designing the controller. Tsiotras [33] designs a linear passivity-based asymptotically stabilizing controller and control laws without angular velocity measurements for the rigid body attitude motion. The corresponding Lyapunov functions are carefully designed based on the storage functions. In [34], a Euler-Poisson form is used to describe the equations of motion. Internal modal principle is applied to eliminate the sinusoidal disturbance. Global asymptotic stability for both axisymmetric and asymmetric spacecraft is proved by combining the Lyapunov direct method with LaSalle's theorem. Using the polhode representation, the tumbling motion dynamics can be expressed by linear equations in [35]. Lyapunov direct method is applied thereafter to find the analytical controller.

2.1.2 Adaptive control method

Adaptive control method actively integrates the disturbance compensation and uncertainty estimation into controller design by introducing update law. The unknown parameters and dynamics are estimated by the known system parameters and outputs. Lyapunov stability theorem is then applied to ensure system stability. In [36], the author reviews several adaptive control methods in spacecraft attitude tracking with standard model reference based techniques. In the absence of disturbance and parametric uncertainty, a generic form of the passivity based control law is derived by the direct Lyapunov control method. When the parametric uncertainty is present, adaptive control is used. The similar general framework for spacecraft attitude control problem is presented in [37]. After proposing several passivity controllers based on the Lyapunov direct control method, adaptive controllers are proposed to account for parametric uncertainties. In references [38-40], authors present several adaptive control methods based on spacecraft moment of inertia identification. Sanyal et al. [38-40] proposes an adaptive controller for the spacecraft attitude tracking without using moment of inertia. The disturbance rejection can be also achieved with knowledge of the disturbance spectrum but without knowledge of either the amplitude or phase. In [41], a new adaptive robust control framework was proposed. Parameter adaptation is used along with robust filter structures to attenuate the effect of model uncertainties as much as possible. Considering the problem of whether parameter estimates converge to constant values, [42] and [43] give affirmative answers. Notice that it is not mandatory for the estimated parameters to converge to their real values in adaptive control problems.

2.1.3 Variable structure control method

Another widely used nonlinear robust control method to address input constraints, parameter uncertainties and external disturbances is the variable structure control. Sliding mode control (SMC) is a typical variable structure control design technique. SMC is advantageous in being both insensitive to parameter uncertainties and robust against external disturbances. Variable structure control method can be combined with other design methods, such as backstepping method [44] and adaptive integral control method [45]. SMC was used for flexible spacecraft attitude control in [46]. Reference [47] discussed the application of the fuzzy control method combined with the variable structure technique in determining controller parameters. Neural network based sliding mode controller was investigated in [48] and [49]. Typical drawback of the variable structure control method is the chattering phenomenon that may cause the implementation problem since the controller contains the discontinuous nonlinearity. Continuous approximation of the SMC are not sensitive to the chattering problem and can be made to mimic the sliding-mode controllers [50].

2.1.4 Optimal control method

Although adaptive control methods are widely used, it is worth noting that a major drawback of conventional adaptive control methods is that it utilizes the nonlinear cancellation technique. Controllers that cancel nonlinearities are, in general, non-optimal since the nonlinearities may be actually beneficial in stabilization and/or minimizing the cost function. Therefore, optimal control method is desired for not only stabilization, but also performance optimization. The difficulty of conventional optimal control methods lies in solving the Hamilton-Jacobi-Bellman (HJB) equation, which is a nonlinear partial

differential equation. Methods of directly solving the HJB equation are investigated in [51] and [52]. Optimal control with higher order performance criteria is discussed in [53]. When parametric uncertainties, unmodeled dynamics, and disturbances are present, the optimal control method can be combined with robust or adaptive control schemes. Reference [54] proposes an optimal controller for the general plant model with uncertain parameters. Control of internal plant disturbance is accomplished with an optimal disturbance cancellation mechanism. This mechanism is designed to minimize the plant output disturbance power. An adaptive filter, with the neural network based parameter training method, is introduced. Nguyen and Ishihara [55] propose an adaptive optimal controller that can achieve adaptation with a large adaptive gain. To minimize the tracking error, the L_2 norm of the tracking error is formulated as the performance index.

Inverse optimal control design, on the other hand, avoids solving the HJB equation directly in the conventional optimal control design. The difference between the direct and the inverse optimal control problems is that the former seeks a controller that minimizes a *given* cost, while the latter is concerned with finding a controller that minimizes some derived "meaningful" cost. In the inverse optimal approach, a controller is designed by using a control Lyapunov function (clf) obtained from solving the stabilization problem. The clf employed in the inverse optimal design is, in fact, a solution to the HJB equation with a meaningful cost. In [56], an inverse optimal control method is designed to minimize a meaningful cost function that incorporates integral penalty on the tracking error and the control as well as a terminal penalty on the parameter estimation error. The controller compensates for the effect of parameter adaptation transients in order to achieve optimality of the overall system. The inverse optimal controller also possesses margins in the sense of input-to-state stability [57].

After finding a stable regulator for an auxiliary system using the Lyapunov direct control approach, inverse optimal design can find the corresponding stabilizing controller for the original system with certain optimality. Application of the inverse optimal control to rigid spacecraft attitude control is discussed in [58]. In [59], unmodeled disturbance, parametric uncertainty, and system stabilization are addressed in a unified inverse optimal framework and solved simultaneously. The relationship between optimal control and adaptive control was discussed in [60] and [61].

The certain equivalency between robust stabilization of uncertain nonlinear systems and the optimal control problem has been established by several researchers. Haddad and Chellaboina [62-64] have shown that the Lyapunov function guaranteeing closed-loop stability is a solution to the steady-state Hamilton-Jacobi-Bellman (HJB) equation for the optimal-controlled nominal system with a modified cost function including uncertainty bounds. In addition, Bernstein proves that the upper bound of the cost function can be calculated by the Lyapunov function [65, 66]. From another unique perspective, Lin et al. [67, 68] prove that the robust nonlinear control problem under the matching condition is equivalent to an optimal control problem by defining a proper cost function that reflects the uncertainty bounds. The result is then extended to input matrix uncertainty cases and unmatched uncertainty cases [69, 70]. By solving the transformed optimal control problem, both robust stability and optimality can be achieved. Applications utilizing this equivalency relationship include control of robot manipulators [71], PVTOL aircraft [72], and space robot arms [73].

To solve the nonlinear optimal control problem, a number of methods have been proposed. One of the widely used techniques is the state-dependent Riccati equation (SDRE) method [74], which is a systematic nonlinear regulator and state estimation

approach. In the recent decade, the SDRE optimal control method has been applied in solving a wide range of engineering problems under various conditions and restrictions [75], [76] and [77]. However, the SDRE technique needs to solve the algebraic Riccati equation repetitively at every integration step, which demands an intensive computation load. In this dissertation, a novel approach called the θ-D method [78] is employed to solve the nonlinear optimal control problem in our indirect robust control formulation. The θ-D method is based on an approximate solution to the HJB equation via a perturbation process. The optimal control law can be obtained in an analytical form by solving a series of algebraic Lyapunov equations. This closed-form feedback control law is much more efficient to implement onboard because it does not require excessive computational power [79]. By combining the advantages of the indirect robust control formulation and the θ-D method, we can solve a broad range of highly nonlinear robust control problems.

2.2 Control of rigid spacecraft motion

In Section 2.1, we have reviewed various control techniques in spacecraft proximity operations. In the following sections, we will review each control aspect from the spacecraft dynamics perspective.

The typical way of designing the spacecraft controller is to consider the translational motion, rotational motion, and flexible structure motion in a separate framework. However, in the spacecraft proximity operations, these motions will be highly coupled. In this section, we will review the literature on the control of these motions separately and set up the stage to propose our integrated design scheme in the next section. Based upon this, we divide the rigid body proximity motion control into the

translational control and rotational control. Previous corresponding works will be reviewed in Section 2.2.1 and 2.2.2. We want to emphasize that this separation is merely to facilitate the understanding of the dynamics. We do not require the translational motion synchronization or the attitude synchronization to converge in any particular order. The integrated control design will be given in Section 2.4.

2.2.1 Control of rigid spacecraft translational motion

Spacecraft relative motion dynamics are first given by Clohessy and Wiltshire in 1960s. The relative motion dynamics are derived by utilizing a Hill-like rotating Cartesian coordinate frame [80]. The Clohessy-Wiltshire (CW) linear formulation assumes small deviations from a circular reference orbit and used the initial conditions as the constants of the unperturbed motion [81]. The resultant relative equation of motion is named CW equation.

Based on the CW equation, the problem of spacecraft rendezvous was investigated by various methods. Gao et al [82] explore the multi-objective spacecraft rendezvous using the linear matrix inequality (LMI) properties and Lyapunov approach. Optimal control methods focusing on time-optimal or fuel-optimal control were also studied by many researchers. In [83], Yang et al. investigate the homing phase of autonomous spacecraft rendezvous and formulated an output tracking control problem. Tang et al. [84] utilize the non-dominated sorting genetic algorithm (NSGR) to solve the multi-objective optimization problem for impulsive rendezvous. Uncertainties and disturbance are included in the control design to improve the robustness. Simulated annealing (SA), a stochastic optimization algorithm with global convergence, is employed in Luo's work [85] to solve an optimal rendezvous problem. Compared with

[85], direct solving the Riccati equation is used in [86] to find the closed loop optimal controller. Genetic algorithm is also widely adopted in solving the optimal rendezvous problem [87-89].

2.2.2 Control of rigid spacecraft rotational motion

Attitude tracking control problem has been studied in many works [29, 37, 90]. The spacecraft attitude control problem is to find a feedback control law such that the spacecraft attitude error and angular velocity error asymptotically converge to zero as time evolves.

Various control algorithms have been proposed for solving the attitude tracking control problem. The Lyapunov direct control method [91-93] is widely used to construct the passivity based control law. In [94], a stabilizing controller for XTE spacecraft attitude tracking is proposed when no disturbance and uncertainty are considered. A relatively complex Lyapunov function is used in deriving the controller. When disturbance and uncertainties are present, the adaptive or robust control methods are more applicable. Reference [36] reviews the adaptive control methods when the spacecraft moment of inertia is not known. In [95] and [96], the disturbance torques are modeled as outputs of an auxiliary Lyapunov-stable system and estimated by appropriate update law. In [97], adaptive attitude tracking controller is designed based on a feed-forward learning adaptive filter. In [98] and [99], the adaptive control method is combined with the backstepping technique to solve the attitude tracking problem.

To enhance the control performance with respect to a specific performance index, optimal control is preferable. In [100], the state-dependent Riccati equation (SDRE) technique is employed to control the position and attitude of a spacecraft approaching a

tumbling target. Robust symmetric controller is applied in ETS-VIII satellite [101] using the LMI optimization approach. Optimal control combined with backstepping [102] and variable structure control [103] are used for attitude tracking control to improve robustness and achieve optimality.

Variable structure control method is also widely used in the robust attitude control design. In [104], extended state observer (ESO) is introduced with the SMC to stabilize the system under disturbance torques. Conventional boundary layer method is adopted to alleviate the chattering phenomenon. Chakrabortty [105] uses two high-gain filters in the controller design so that the disturbance and estimation error can be eliminated simultaneously. SMC is applied to provide the robust performance. Fuzzy sliding mode control is applied in [106] and a finite-time sliding mode control is proposed in [49] for the robust attitude tracking.

2.2.3 Control of rigid spacecraft translational and rotational motion

There are some research works that consider the rigid spacecraft translational motion and rotational motion together. In [107], an output feedback based adaptive control law is developed for spacecraft rendezvous and docking problems. The control law incorporates disturbance attenuation, parameter error compensation, and measurement noise estimation. Subbarao and Welsh [108] follow the method of decoupling the translational motion and rotational motion for the control of proximity operation. The control synthesis combines the feedback linearization technique with the adaptive control to handle the disturbance and uncertainties.

2.3 Control of flexible spacecraft motion

Flexible spacecraft, as introduced in the previous sections, are spacecraft systems involving interconnected rigid structures and flexible appendages. In the previous rigid spacecraft control sections, we have reviewed a number of techniques with which disturbance and uncertainties are accounted for. The flexible structure deformation can be considered as disturbance to the rigid structure, or as part of the overall system dynamics. Moreover, the flexible deformation can be actively dealt with by active suppression methods. Actuators like piezoelectric layers [109] on the flexible structure can act as extra actuators for the flexible deformation suppression.

Control techniques reviewed in Section 2.1 can be applied directly to the flexible spacecraft control. Feedback linearization technique and direct Lyapunov control scheme were applied in [110-113] for flexible space structure control. Since the generalized modal coordinates of the flexible motion are hard to measure, adaptive control method is frequently used in estimating the flexible system states. Gennaro [114] proposed a class of nonlinear controllers for flexible spacecraft using static controller or dynamic controller based on available sets of measurements. If the spacecraft rotational parameter (typically the moment of inertia matrix) is unknown, adaptive control method can also be applied assuming the full state feedback [115-119].

Variable structure control method is also widely used in the flexible structure control to ensure stability and robustness. PD type controllers with the variable structure were proposed in [120-122] using the passivity-based control technique. Neural network based sliding mode control was adopted in [123]. Closed-loop input shaping control scheme was developed and applied to flexible spacecraft control in [124] and [125]. When the input saturation is imposed, saturation compensator can be combined with the

input shaping and variable structure method to handle this problem in spite of disturbance and uncertainties [126]. In [127], reference model variable structure output feedback control (RMVSOFC) was proposed with the input shaping method for the flexible spacecraft control problem.

When the flexible damping modes are considered as part of system states and are incorporated in the controller design, the conventional control method, such as adaptive based control method [128-130] and robust control method [131], can still be applied.

When the flexible deformation is actively controlled, extra actuators are placed on the flexible structure to increase the control performance. Typical active flexible deformation suppression methods include: modal velocity feedback (MVF) compensator [132-135], positive position feedback (PPF) control [136-138], and strain rate feedback control [139, 140].

2.4 Integrated indirect robust control scheme

As described in Section 2.2 and 2.3, complete spacecraft dynamics include the rigid-body translational and rotational motions coupled with the flexible structure dynamics. External disturbances and model uncertainties must be taken into account as well. Most of the previous works deal with these three dynamics separately when designing the controller. But since these three aspects are coupled in the proximity operations, a unified framework is necessary. In this dissertation, an integrated optimization approach is proposed to simultaneously control the rigid-body translational motion, rotational motion and flexible structure vibration. By doing so, the overall system performance and constraints can be addressed in one optimization process. However, to

solve this optimal control problem is a very challenging task especially when various model uncertainties and external disturbances must be addressed as well.

Our research investigates the robust control of spacecraft in proximity operations from a new perspective by utilizing the close relationship between optimal control and robust control of uncertain nonlinear systems. We name this method the indirect robust control scheme. By properly choosing a cost function that reflects the uncertainty, state regulation, and control, the solution to the optimal control problem can be proved to be a solution to the robust control problem.

Compared with the conventional direct robust control scheme, this new indirect robust control method avoids the difficulty in selecting the Lyapunov function candidate. The computation load will also be reduced greatly. The challenge of the indirect robust control scheme lies in solving the induced nonlinear optimal control problem. In particular, solving the corresponding Hamilton-Jacobi-Bellman (HJB) equation is always a challenging problem in the optimal control theory. To handle this difficulty, we employ the novel θ-D optimal control method [78], which can provide an approximate solution to the HJB equation and closed-form optimal control law such that the indirect robust control law can be efficiently implemented onboard without intensive computation load.

The typical robust control scheme involves the uncertainty bounds in the control design and may be conservative if the bounds are hard to determine. Therefore, we propose the inverse optimal adaptive control method [59-61] combined with the indirect robust control scheme to alleviate the conservativeness of the robust control scheme by using online parameter estimation such that adaptive, robust, and optimal properties can be all achieved.

Remaining parts of the dissertation are organized as follows: in Chapter III, the spacecraft proximity control problem is described including the relevant coordinate frames, equations of motion, standing assumptions, and control objectives. The indirect robust control formulation and the review of the θ-D method are presented in Chapter IV. Integrated control of position, attitude, and flexible motion with uncertainties is designed in a unified framework in Chapter V. Controller design based on the inverse optimal adaptive control method will be presented in Chapter VI. Numerical results based on 6-DOF simulations are given in Chapter VII to demonstrate the effectiveness of both controller design technique. Comparison and concluding remarks will be given in the last chapter.

CHAPTER III

PROBLEM FORMULATION

In this dissertation, we address the robust control of spacecraft position, attitude, and flexible motion in proximity operations in the presence of parameter uncertainties and bounded disturbances.

Specifically, one servicing spacecraft denoted as pursuer *S* attempts to approach a space body denoted as target *T*. The target is uncontrolled and free tumbling but its full state information is assumed to be available, which can be obtained either from target sensors or from the pursuer's observation and estimation [141]. The control objective is to have the pursuer position at a certain safe distance with respect to the target while keeping its docking port facing the docking port of the target. The attitude of the two vehicles must be kept synchronized during the maneuver so that subsequent operations, capturing or docking for instance, can be carried out safely.

3.1 Coordinate systems and notations

Four coordinate systems need to be defined to describe the dynamics and equations of motion as shown in Fig. 3.1 and Fig. 3.2. The inertial coordinate system is represented by the geocentric-equatorial frame $\{\boldsymbol{I}\} = \{\hat{\boldsymbol{I}}_x, \hat{\boldsymbol{I}}_y, \hat{\boldsymbol{I}}_z\}$. The local-vertical-local-horizontal (LVLH) frame $\{\boldsymbol{L}\} = \{\hat{\boldsymbol{L}}_x, \hat{\boldsymbol{L}}_y, \hat{\boldsymbol{L}}_z\}$ centered on the target has $\hat{\boldsymbol{L}}_x$ axis along the target radius vector from the Earth, $\hat{\boldsymbol{L}}_z$ axis along the direction of the orbital normal, and $\hat{\boldsymbol{L}}_y$ axis completing the triad. Body-fixed coordinate frames of the pursuer and the target are defined as $\{\boldsymbol{B}_s\} = \{\hat{\boldsymbol{b}}_{sx}, \hat{\boldsymbol{b}}_{sy}, \hat{\boldsymbol{b}}_{sz}\}$ and $\{\boldsymbol{B}_t\} = \{\hat{\boldsymbol{b}}_{tx}, \hat{\boldsymbol{b}}_{ty}, \hat{\boldsymbol{b}}_{tz}\}$, respectively.

Without loss of generality, it is assumed that $\hat{\boldsymbol{b}}_{sx}$ axis of the pursuer and $\hat{\boldsymbol{b}}_{tx}$ axis of the target are their respective outward normal directions of the docking ports. During the proximity operation, $\hat{\boldsymbol{b}}_{sx}$ axis must align with the $\hat{\boldsymbol{b}}_{tx}$ axis and point to the opposite direction of $\hat{\boldsymbol{b}}_{tx}$ axis.

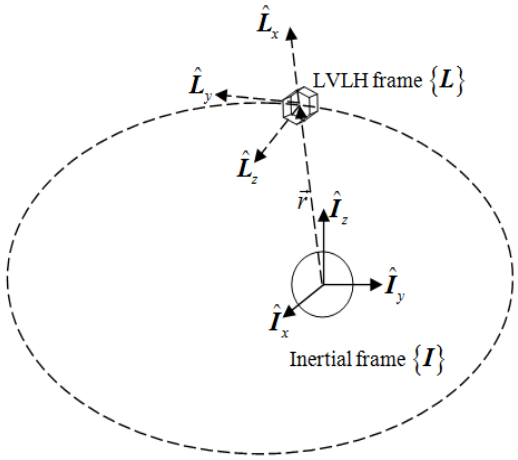

Figure 3.1 Earth inertial frame $\boldsymbol{I}$ and the local-vertical-local-horizontal frame $\boldsymbol{L}$

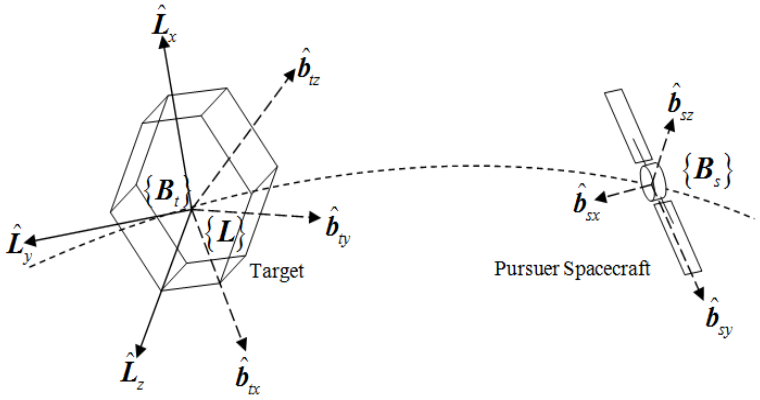

Figure 3.2 Pursuer spacecraft body frame $\boldsymbol{B_s}$ and target body frame $\boldsymbol{B_t}$

3.2 Rigid spacecraft translational dynamics

The relative translational dynamics are developed based on their relative position with respect to the LVLH frame fixed to the target. Define the relative position vector from the target to the pursuer as $\mathbf{r}_L$ and its velocity as $\mathbf{v}_L$:

$$\mathbf{r}_L = x\hat{\boldsymbol{L}}_x + y\hat{\boldsymbol{L}}_y + z\hat{\boldsymbol{L}}_z \tag{3.1}$$

$$\mathbf{v}_L = \dot{x}\hat{\boldsymbol{L}}_x + \dot{y}\hat{\boldsymbol{L}}_y + \dot{z}\hat{\boldsymbol{L}}_z \tag{3.2}$$

where $[x, y, z]^T$ are three components of $\mathbf{r}_L$ vector in the LVLH frame. The relative translational dynamics are governed by [142]:

$$\ddot{x} - 2\dot{v}\dot{y} - \ddot{v}y - \dot{v}^2 x = -\mu(\bar{r} + x)\Big/\left[(\bar{r} + x)^2 + y^2 + z^2\right]^{\frac{3}{2}} + \mu/\bar{r}^2 + a_x \tag{3.3}$$

$$\ddot{y} + 2\dot{v}\dot{x} + \ddot{v}x - \dot{v}^2 y = -\mu y\Big/\left[(\bar{r} + x)^2 + y^2 + z^2\right]^{\frac{3}{2}} + a_y \tag{3.4}$$

$$\ddot{z} = -\mu z\Big/\left[(\bar{r} + x)^2 + y^2 + z^2\right]^{\frac{3}{2}} + a_z \tag{3.5}$$

where μ is the gravitational constant, $\boldsymbol{a} = [a_x, a_y, a_z]^T$ is pursuer's control acceleration vector represented in the LVLH frame. $\bar{r}$ is the distance from the Earth center of mass to the target. v is true anomaly. For a circular orbit, the equations of motion become the linear Clohessy-Wiltshire (CW) equation [80]. The evolutions of $\bar{r}$ and v parameters are governed by [142]:

$$\ddot{\bar{r}} = \bar{r}\dot{v}^2 - \mu/\bar{r}^2 \tag{3.6}$$

$$\ddot{v} = -2\dot{\bar{r}}\dot{v}/\bar{r} \tag{3.7}$$

3.3 Coupled rotational dynamics and flexible structure dynamics

As introduced in the previous sections, flexible structure deformation should be considered while the spacecraft performs large angular maneuvers. In our research, the rigid-body rotational dynamics coupled with the flexible motion are considered in the controller design.

Figure 3.3 shows the model [26] of a relatively large class of spacecraft that are required to undergo large maneuvers.

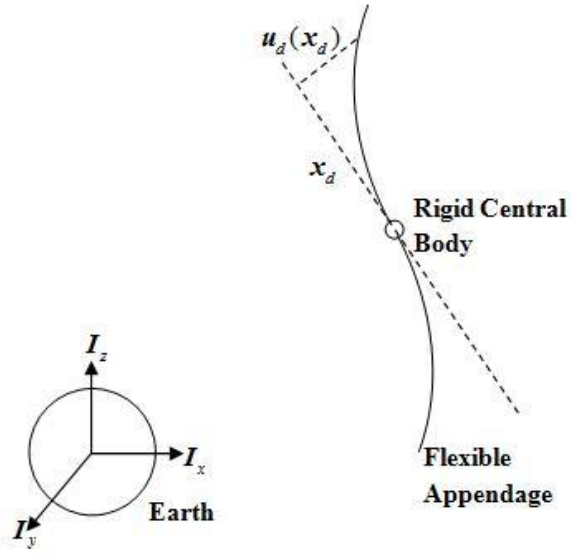

Figure 3.3 Schematic representation of flexible spacecraft system with two axisymmetric beams

Several assumptions are made to facilitate the formulation and control design:

1) The maneuver of the spacecraft is limited to the orbit normal axis (pitch maneuver). But the elastic deflections of the appendages, which are assumed to be small, are not confined only in the orbital plane but in all three directions.

2) The maneuver is assumed to excite the two flexible appendages anti-symmetrically. The shift in the spacecraft center-of-mass caused by the flexible deflection is thus negligible.

Method of assumed modes is used to represent the flexible deflection. Appendages are considered to behave as simple Euler-Bernoulli beams to simplify the analysis.

By the method of assumed modes [143], the deflections in all three directions are expressed in terms of a set of admissible or shape functions:

$$\boldsymbol{u}_d(x_d) = \sum_{k=1}^{N} \eta_k(t)\boldsymbol{\phi}_k(x_d) \tag{3.8}$$

where, x_d is the distance from the center of the rigid body, $\eta_k(t)$ represents the kth time-varying amplitude, also known as generalized coordinates associated with the admissible shape function $\boldsymbol{\phi}_k(x_d) = [\phi_x(x_d), \phi_y(x_d), \phi_z(x_d)]$. Components $\phi_x(x_d)$, $\phi_y(x_d)$ and $\phi_z(x_d)$ are shape functions along the three axes, respectively. Certain boundary conditions must be satisfied by the shape function:

$$\phi_k(0) = \dot{\phi}_k(0) = \ddot{\phi}_k(L) = \dddot{\phi}_k(L) = 0 \tag{3.9}$$

L is the appendage length. N in (3.8) represents the number of terms used in the approximation and it is also known as the number of significant modes.

The governing dynamic equations for the flexible spacecraft rotational motion can be derived based on the Lagrangian procedure [144].

$$J_s\dot{\boldsymbol{\omega}}_s + \delta^T\ddot{\boldsymbol{\eta}} = -\tilde{\boldsymbol{\omega}}_s J_s\boldsymbol{\omega}_s - \tilde{\boldsymbol{\omega}}_s\delta^T\dot{\boldsymbol{\eta}} + \boldsymbol{\Gamma}_s \tag{3.10}$$

$$\ddot{\boldsymbol{\eta}} + \delta\dot{\boldsymbol{\omega}}_s + C\dot{\boldsymbol{\eta}} + K\boldsymbol{\eta} = 0 \tag{3.11}$$

where $\boldsymbol{\omega}_s = [\omega_{s_x}, \omega_{s_y}, \omega_{s_z}]^T$ is the angular velocity vector of the pursuer expressed in its own body frame; J_s is the pursuer's moment of inertia matrix and $\boldsymbol{\Gamma}_s$ is the control torque, which is defined in pursuer's body frame $\{\boldsymbol{B}_s\}$, $\tilde{\boldsymbol{\omega}}_s$ is the cross product matrix defined as:

$$\tilde{\boldsymbol{\omega}}_s = \begin{bmatrix} 0 & -\omega_{s_z} & \omega_{s_y} \\ \omega_{s_z} & 0 & -\omega_{s_x} \\ -\omega_{s_y} & \omega_{s_x} & 0 \end{bmatrix} \tag{3.12}$$

$\boldsymbol{\eta}(t) = [\eta_1(t) \quad \eta_2(t) \quad \dots \quad \eta_N(t)]^T$ is the modal deformation coordinate vector. δ is the coupling matrix between the flexible and rigid body dynamics. C and K denote the damping and stiffness matrices, respectively, which are defined as:

$$\begin{aligned} C &= diag(2\zeta_i \omega_{ni}, i = 1, 2, \dots, N) \\ K &= diag(\omega_{ni}^2, i = 1, 2, \dots, N) \end{aligned} \tag{3.13}$$

with appendage damping coefficient ζ_i and natural frequency ω_{ni}.

Quaternion representation is used to describe the spacecraft attitude kinematics:

$$\dot{\boldsymbol{q}}_s = \frac{1}{2}\Omega(\boldsymbol{\omega}_s)\boldsymbol{q}_s \tag{3.14}$$

where $\boldsymbol{q}_s = [q_{s_0}, q_{s_1}, q_{s_2}, q_{s_3}]^T$ is the pursuer's attitude quaternion defined by: $q_{s_0} = \cos(\varphi_{euler}/2), q_{s_i} = c_{s_i}\sin(\varphi_{euler}/2), i = 1, 2, 3$; φ_{euler} is the rotation angle about the Euler-axis; $(c_{s_1}, c_{s_2}, c_{s_3})$ are the direction cosines of the Euler axis with respect to the reference frame. $\Omega(\boldsymbol{\omega}_s)$ is defined as:

$$\Omega(\boldsymbol{\omega}_s) = \begin{bmatrix} 0 & -\omega_{s_x} & -\omega_{s_y} & -\omega_{s_z} \\ \omega_{s_x} & 0 & \omega_{s_z} & -\omega_{s_y} \\ \omega_{s_y} & -\omega_{s_z} & 0 & \omega_{s_x} \\ \omega_{s_z} & \omega_{s_y} & -\omega_{s_x} & 0 \end{bmatrix}$$

The free-tumbling target is considered as a rigid body and has similar attitude dynamics except that the external torque and flexible dynamics are not present:

$$\dot{\boldsymbol{q}}_t = \frac{1}{2}\Omega(\boldsymbol{\omega}_t)\boldsymbol{q}_t \tag{3.15}$$

$$J_t\dot{\boldsymbol{\omega}}_t + \tilde{\boldsymbol{\omega}}_t J_t\boldsymbol{\omega}_t = 0 \tag{3.16}$$

Where $\boldsymbol{\omega}_t = [\omega_{t_x} \quad \omega_{t_y} \quad \omega_{t_z}]^T$ is the target angular velocity expressed in the target body frame; $\boldsymbol{q}_t = [q_{t_0} \quad q_{t_1} \quad q_{t_2} \quad q_{t_3}]^T$ is the target quaternion; J_t is the target's moment of inertia matrix.

The attitude control aims to synchronize the two objects' angular velocity and have the pursuer's docking port face the docking port of the target. Without loss of generality, the outward normal directions of the pursuer and target docking ports are assumed to be along the $\boldsymbol{x}$ axis of their individual body frames. In other words, the $\hat{\boldsymbol{b}}_{sx}$ axis is required to point toward the opposite direction of the $\hat{\boldsymbol{b}}_{tx}$ axis. For the convenience of control formulation, a *virtual target* is assumed as the desired attitude for the pursuer to track. This virtual target has a body frame $\{\boldsymbol{B}_d\}$ fixed on the target. Here $\{\boldsymbol{B}_d\}$ is obtained through rotating the original target body frame by 180 degrees about $\hat{\boldsymbol{b}}_{tz}$ axis. The transformation from the target frame $\{\boldsymbol{B}_s\}$ to the virtual target frame $\{\boldsymbol{B}_d\}$ can be represented by the direct cosine matrix of:

$$C_{dt} = \begin{bmatrix} \cos 180^\circ & \sin 180^\circ & 0 \\ -\sin 180^\circ & \cos 180^\circ & 0 \\ 0 & 0 & 1 \end{bmatrix} = \begin{bmatrix} -1 & 0 & 0 \\ 0 & -1 & 0 \\ 0 & 0 & 1 \end{bmatrix} \tag{3.17}$$

It can also be represented as quaternion: $\boldsymbol{q}_{dt} = \begin{bmatrix} 0 & 0 & 0 & 1 \end{bmatrix}^T$. Thus, the angular velocity of the target expressed in the virtual target frame becomes:

$$\boldsymbol{\omega}_d^{\boldsymbol{B}_d} = C_{dt}\boldsymbol{\omega}_t = \begin{bmatrix} -\omega_{t_x} & -\omega_{t_y} & \omega_{t_z} \end{bmatrix}^T \tag{3.18}$$

The desired quaternion for the pursuer spacecraft to track is:

$$\boldsymbol{q}_d = \boldsymbol{q}_t \cdot \boldsymbol{q}_{dt} = \begin{bmatrix} -q_{t_3} & q_{t_2} & -q_{t_1} & q_{t_0} \end{bmatrix}^T \tag{3.19}$$

The attitude synchronization is reduced to the problem of tracking the virtual target's attitude $\boldsymbol{q}_d$ and its angular velocity $\boldsymbol{\omega}_d^{\boldsymbol{B}_d}$. To facilitate the attitude control design, define the tracking error in the pursuer's body frame as:

$$\boldsymbol{\omega}_e = \boldsymbol{\omega}_s - \boldsymbol{\omega}_d^{\boldsymbol{B}_s} = \boldsymbol{\omega}_s - T_{\boldsymbol{I}}^{\boldsymbol{B}_s} T_{\boldsymbol{B}_d}^{\boldsymbol{I}} \boldsymbol{\omega}_d^{\boldsymbol{B}_d} \tag{3.20}$$

$$\boldsymbol{q}_e = \boldsymbol{q}_d^{-1}\boldsymbol{q}_s = Q_d^{-1}\boldsymbol{q}_s \tag{3.21}$$

where $\boldsymbol{\omega}_d^{\boldsymbol{B}_s}$ is the virtual target angular velocity expressed in the pursuer's body frame $\{\boldsymbol{B}_s\}$, $T_{\boldsymbol{B}_d}^{\boldsymbol{I}}$ is the virtual target body-to-inertial coordinate transformation matrix and $T_{\boldsymbol{I}}^{\boldsymbol{B}_s}$ is the inertial-to-pursuer body coordinate transformation matrix. They can be calculated by the corresponding quaternions:

$$T_{\boldsymbol{B}_d}^{\boldsymbol{I}} = \begin{bmatrix} q_{d_0}^2 + q_{d_1}^2 - q_{d_2}^2 - q_{d_3}^2 & 2\left(q_{d_1}q_{d_2} - q_{d_0}q_{d_3}\right) & 2\left(q_{d_1}q_{d_3} + q_{d_0}q_{d_2}\right) \\ 2\left(q_{d_1}q_{d_2} + q_{d_0}q_{d_3}\right) & q_{d_0}^2 - q_{d_1}^2 + q_{d_2}^2 - q_{d_3}^2 & 2\left(q_{d_2}q_{d_3} - q_{d_0}q_{d_1}\right) \\ 2\left(q_{d_1}q_{d_3} - q_{d_0}q_{d_2}\right) & 2\left(q_{d_2}q_{d_3} + q_{d_0}q_{d_1}\right) & q_{d_0}^2 - q_{d_1}^2 - q_{d_2}^2 + q_{d_3}^2 \end{bmatrix} \tag{3.22a}$$

$$T_{\boldsymbol{I}}^{\boldsymbol{B}_s} = \begin{bmatrix} q_{s_0}^2 + q_{s_1}^2 - q_{s_2}^2 - q_{s_3}^2 & 2\left(q_{s_1}q_{s_2} + q_{s_0}q_{s_3}\right) & 2\left(q_{s_1}q_{s_3} - q_{s_0}q_{s_2}\right) \\ 2\left(q_{s_1}q_{s_2} - q_{s_0}q_{s_3}\right) & q_{s_0}^2 - q_{s_1}^2 + q_{s_2}^2 - q_{s_3}^2 & 2\left(q_{s_2}q_{s_3} + q_{s_0}q_{s_1}\right) \\ 2\left(q_{s_1}q_{s_3} + q_{s_0}q_{s_2}\right) & 2\left(q_{s_2}q_{s_3} - q_{s_0}q_{s_1}\right) & q_{s_0}^2 - q_{s_1}^2 - q_{s_2}^2 + q_{s_3}^2 \end{bmatrix} \tag{3.22b}$$

Q_d matrix in (3.21) is defined as:

$$Q_d = \begin{bmatrix} q_{d_0} & -q_{d_1} & -q_{d_2} & -q_{d_3} \\ q_{d_1} & q_{d_0} & -q_{d_3} & q_{d_2} \\ q_{d_2} & q_{d_3} & q_{d_0} & -q_{d_1} \\ q_{d_3} & -q_{d_2} & q_{d_1} & q_{d_0} \end{bmatrix} \tag{3.23}$$

In Section 3.2 and Section 3.3, spacecraft translational and rotational dynamics have been described in detail. As parametric uncertainties and disturbances are inevitable, in the following section, we will establish uncertain system equations for the robust controller design.

3.4 Coupled rotational dynamics with parametric uncertainties

In this dissertation, we consider the parametric uncertainties due to the spacecraft moment of inertia uncertainty ΔJ and the coupling matrix uncertainty $\Delta\delta$ between rigid-body dynamics and flexible motion. Other parametric uncertainties can be similarly attacked. When the uncertainties ΔJ and $\Delta\delta$ are introduced, one can derive the perturbed attitude dynamics from (3.10) and (3.11):

$$J_s\dot{\boldsymbol{\omega}}_s + \delta^T\ddot{\boldsymbol{\eta}} = -\tilde{\omega}_s J_s\boldsymbol{\omega}_s - \tilde{\omega}_s\delta^T\dot{\boldsymbol{\eta}} + \boldsymbol{\Gamma}_s + (-\Delta J\dot{\boldsymbol{\omega}}_s - \tilde{\omega}_s\Delta J\boldsymbol{\omega}_s - \tilde{\omega}_s\Delta\delta^T\dot{\boldsymbol{\eta}} - \Delta\delta^T\ddot{\boldsymbol{\eta}}) \tag{3.24}$$

$$\ddot{\boldsymbol{\eta}} + C\dot{\boldsymbol{\eta}} + K\boldsymbol{\eta} = -\delta\dot{\boldsymbol{\omega}}_s - \Delta\delta\dot{\boldsymbol{\omega}}_s \tag{3.25}$$

In the following manipulations, we rewrite the above two equations as the first-order state equations and separate the attitude dynamics into the nominal part and the perturbation part to facilitate subsequent robust control design.

By eliminating the $\ddot{\boldsymbol{\eta}}$ term using (3.25), (3.24) can be rewritten as:

$$\begin{aligned} M_0\dot{\boldsymbol{\omega}}_s = {} & (\delta^T C - \tilde{\omega}_s\delta^T)\dot{\boldsymbol{\eta}} + \delta^T K\boldsymbol{\eta} - \tilde{\omega}_s J_s\boldsymbol{\omega}_s \\ & + \boldsymbol{\Gamma}_s + [c_1\dot{\boldsymbol{\omega}}_s - \tilde{\omega}_s\Delta J\boldsymbol{\omega}_s - (\tilde{\omega}_s\Delta\delta^T - \Delta\delta^T C)\dot{\boldsymbol{\eta}} + \Delta\delta^T K\boldsymbol{\eta}] \end{aligned} \tag{3.26}$$

where $M_0 = J_s - \delta^T\delta$, $c_1 = (\delta^T\Delta\delta - \Delta J + \Delta\delta^T\delta + \Delta\delta^T\Delta\delta)$.

In order to eliminate $\dot{\boldsymbol{\omega}}_s$ on the right hand side of the equation, we will still use (3.24) and (3.25) to find a proper representation of $\dot{\boldsymbol{\omega}}_s$ by state variables $\boldsymbol{\omega}_s, \boldsymbol{\eta}, \dot{\boldsymbol{\eta}}$. If we set $\delta' = \delta + \Delta\delta$, $J_s' = J_s + \Delta J$ and $\tilde{M}_0 = (J_s' - \delta'^T \delta')$, then:

$$\dot{\boldsymbol{\omega}}_s = \tilde{M}_0^{-1}(\delta'^T C - \tilde{\omega}_s \delta'^T)\dot{\boldsymbol{\eta}} + \tilde{M}_0^{-1}\delta'^T K\boldsymbol{\eta} - \tilde{M}_0^{-1}\tilde{\omega}_s J_s'\boldsymbol{\omega}_s + \tilde{M}_0^{-1}\boldsymbol{\Gamma}_s \tag{3.27}$$

Using (3.27) in the $\dot{\boldsymbol{\omega}}_s$ term on the right hand side of (3.26) yields:

$$\begin{aligned}\dot{\boldsymbol{\omega}}_s &= M_0^{-1}[(\delta^T C - \tilde{\omega}_s \delta^T)\dot{\boldsymbol{\eta}} + \delta^{\mathrm{T}} K\boldsymbol{\eta} - \tilde{\omega}_s J_s \boldsymbol{\omega}_s + \boldsymbol{\Gamma}_s] \\ &\quad + M_0^{-1}\{[c_1\tilde{M}_0^{-1}(\delta'^T C - \tilde{\omega}_s \delta'^T) - (\tilde{\omega}_s \Delta\delta^T - \Delta\delta^T C)]\dot{\boldsymbol{\eta}} \\ &\quad + (c_1\tilde{M}_0^{-1}\delta'^T K + \Delta\delta^T K)\boldsymbol{\eta} - (c_1\tilde{M}_0^{-1}\tilde{\omega}_s J_s' + \tilde{\omega}_s \Delta J)\boldsymbol{\omega}_s \\ &\quad + c_1\tilde{M}_0^{-1}\boldsymbol{\Gamma}_s\}\end{aligned} \tag{3.28}$$

The perturbed part in (3.28) can be denoted as:

$$\begin{aligned}&M_0^{-1}\{[c_1\tilde{M}_0^{-1}(\delta'^T C - \tilde{\omega}_s \delta'^T) - (\tilde{\omega}_s \Delta\delta^T - \Delta\delta^T C)]\dot{\boldsymbol{\eta}} \\ &\quad + (c_1\tilde{M}_0^{-1}\delta'^T K + \Delta\delta^T K)\boldsymbol{\eta} - (c_1\tilde{M}_0^{-1}\tilde{\omega}_s J_s' + \tilde{\omega}_s \Delta J)\boldsymbol{\omega}_s \\ &\quad + c_1\tilde{M}_0^{-1}\boldsymbol{\Gamma}_s\} \\ &= \mathrm{P}_1\dot{\boldsymbol{\eta}} + \mathrm{P}_2\boldsymbol{\eta} + \mathrm{P}_3\boldsymbol{\omega}_s + \mathrm{P}_4\boldsymbol{\Gamma}_s\end{aligned} \tag{3.29}$$

where P_1, P_2, P_3 and P_4 denote the corresponding coefficient matrices. Their dimensions are $3\times 4, 3\times 4, 3\times 3,$ and 3×3, respectively.

Following the similar procedure, one can establish the dynamic equation for $\ddot{\boldsymbol{\eta}}$:

$$\begin{aligned}\ddot{\boldsymbol{\eta}} &= -\delta\dot{\boldsymbol{\omega}}_s - \Delta\delta\dot{\boldsymbol{\omega}}_s - C\dot{\boldsymbol{\eta}} - K\boldsymbol{\eta} \\ &= \left[-\delta M_0^{-1}\left(\delta^T C - \tilde{\omega}_s \delta^T\right) - C\right]\dot{\boldsymbol{\eta}} + \left(-\delta M_0^{-1}\delta^T K - K\right)\boldsymbol{\eta} \\ &\quad + \delta M_0^{-1}\tilde{\omega}_s J_s \boldsymbol{\omega}_s - \delta M_0^{-1}\boldsymbol{\Gamma}_s + \left[-\delta'\mathrm{P}_1 - \Delta\delta M_0^{-1}\left(\delta^T C - \tilde{\omega}_s \delta^T\right)\right]\dot{\boldsymbol{\eta}} \\ &\quad + \left(-\delta'\mathrm{P}_2 - \Delta\delta M_0^{-1}\delta^T K\right)\boldsymbol{\eta} + \left(-\delta'\mathrm{P}_3 + \Delta\delta M_0^{-1}\tilde{\omega}_s J_s\right)\boldsymbol{\omega}_s \\ &\quad + \left(-\delta'\mathrm{P}_4 - \Delta\delta M_0^{-1}\right)\boldsymbol{\Gamma}_s\end{aligned} \tag{3.30}$$

In this equation, the perturbation part due to parametric uncertainties is:

$$\begin{aligned}&[-\delta' \mathrm{P}_1 - \Delta\delta M_0^{-1}(\delta^T C - \tilde{\omega}_s \delta^T)]\dot{\boldsymbol{\eta}} + (-\delta' \mathrm{P}_2 - \Delta\delta M_0^{-1}\delta^T K)\boldsymbol{\eta} \\ &+(-\delta' \mathrm{P}_3 + \Delta\delta M_0^{-1}\tilde{\omega}_s J_s)\boldsymbol{\omega}_s + (-\delta' \mathrm{P}_4 - \Delta\delta M_0^{-1})\boldsymbol{\Gamma}_s \\ &= \mathrm{P}_5\dot{\boldsymbol{\eta}} + \mathrm{P}_6\boldsymbol{\eta} + \mathrm{P}_7\boldsymbol{\omega}_s + \mathrm{P}_8\boldsymbol{\Gamma}_s\end{aligned} \tag{3.31}$$

where P_5, P_6, P_7 ,and P_8 denote the corresponding coefficient matrices. Their dimensions are 4×4, 4×4, 4×3 , and 4×3, respectively.

Note that Equations (3.29) and (3.31) will become zero if parametric uncertainties do not exist. The robust control will be designed in the next chapter such that the system stability and optimal performance can be guaranteed.

CHAPTER IV

INDIRECT ROBUST CONTROL DESIGN SCHEME

In this section, the indirect approach is introduced to convert the nonlinear robust control problem to an equivalent optimal control problem. Then a new nonlinear optimal control technique, the θ-D method, is employed to solve the resulting problem in closed-form.

4.1 Indirect robust control method

Robust stabilization under uncertainties has been shown in [62-70] to possess certain equivalency with respect to the optimal control problem. The Lyapunov function guaranteeing closed-loop stability is in fact the solution to the steady-state HJB equation for the optimal-controlled nominal system with a modified cost function including uncertainty bounds. In this dissertation, we extend these results to a general framework to handle parametric uncertainties and control input uncertainties, which are considered in this robust spacecraft control problem. The following theorem gives the main result of the indirect robust control method[145-150].

Theorem 4.1: Consider the following nonlinear systems:

$$\dot{\boldsymbol{x}} = \boldsymbol{f}_n(\boldsymbol{x}) + \mathrm{B}_n(\boldsymbol{x})\boldsymbol{u}(\boldsymbol{x}) + \mathrm{B}_n(\boldsymbol{x})h(\boldsymbol{x})\boldsymbol{u}(\boldsymbol{x}) + \boldsymbol{d}_n(\boldsymbol{x}) \tag{4.1}$$

where $\boldsymbol{x} \in \mathbb{R}^n, \boldsymbol{u} \in \mathbb{R}^m$; $h(\boldsymbol{x})$ and $\boldsymbol{d}_n(\boldsymbol{x})$ are bounded uncertainties. Assume $\boldsymbol{f}_n(\boldsymbol{0}) = 0$ and $\boldsymbol{d}_n(\boldsymbol{0}) = 0$ so that $\boldsymbol{x} = \boldsymbol{0}$ is an equilibrium point. Consider the following two problems:

P1: *Robust Control Problem*:

Find a feedback control law $\boldsymbol{u}(\boldsymbol{x})$ such that the closed-loop system (4.1) is globally asymptotically stable for all bounded uncertainties $h(\boldsymbol{x})$ and $\boldsymbol{d}_n(\boldsymbol{x})$.

P2: *Optimal Control Problem*:

For system:

$$\dot{\boldsymbol{x}} = \boldsymbol{f}_n(\boldsymbol{x}) + \mathrm{B}_n(\boldsymbol{x})\boldsymbol{u}(\boldsymbol{x}) + (I - \mathrm{B}_n(\boldsymbol{x})\mathrm{B}_n(\boldsymbol{x})^+)\mathbf{v}(\boldsymbol{x}) \tag{4.2}$$

where I is an identity matrix and $\mathrm{B}_n(\boldsymbol{x})^+$ is the pseudo-inverse of $\mathrm{B}_n(\boldsymbol{x})^+$, find a feedback control law $\boldsymbol{u}(\boldsymbol{x})$ and an auxiliary control $\mathbf{v}(\boldsymbol{x})$ to minimize the following cost function:

$$J = \int_0^\infty (H_{\max}^2(\boldsymbol{x}) + \rho^2 g_{\max}^2(\boldsymbol{x}) + \boldsymbol{x}^T\tilde{Q}\boldsymbol{x} + 2\boldsymbol{u}^T\tilde{R}^T\tilde{R}\boldsymbol{u} + \rho^2\|\mathbf{v}\|^2)dt \tag{4.3}$$

where $H_{\max}(\boldsymbol{x})$ and $g_{\max}(\boldsymbol{x})$ are bounds for uncertainties; $\tilde{Q} \in \mathbf{R}^{n\times n}$ and $\tilde{R} \in \mathbb{R}^{m\times m}$ are positive definite matrices; ρ is a positive tunable parameter.

If one can find the solution for this optimal control problem **P2** and satisfy the following conditions:

$$\|\boldsymbol{d}_n(\boldsymbol{x})\|^2 \le g_{\max}^2(\boldsymbol{x}) \tag{4.4}$$

$$4\|\tilde{R}h(\boldsymbol{x})\boldsymbol{u}\|^2 \le H_{\max}^2(\boldsymbol{x}) \tag{4.5}$$

$$2\rho^2\|\mathbf{v}\|^2 + 4\|\tilde{R}\mathrm{B}_n(\boldsymbol{x})^+\|^2 g_{\max}^2(\boldsymbol{x}) < \gamma'^2\|\boldsymbol{x}\|^2 \tag{4.6}$$

for some $|\gamma'|^2 \le |\gamma|^2 = \lambda_{\min}(\tilde{Q})$, where $\lambda_{\min}(\bullet)$ is the minimum eigenvalue, then the $\boldsymbol{u}$ component of the optimal control solution is a solution to the robust control problem **P1**.

Proof:

Consider the optimal control problem (4.2) and (4.3). Let us first define:

$$V(\boldsymbol{x}) = \min_{\boldsymbol{u},\mathbf{v}} \int_t^\infty (H_{\max}^2(\boldsymbol{x}) + \rho^2 g_{\max}^2(\boldsymbol{x}) + \boldsymbol{x}^T\tilde{Q}\boldsymbol{x} + 2\boldsymbol{u}^T\tilde{R}^T\tilde{R}\boldsymbol{u} + \rho^2\|\mathbf{v}\|^2)dt \tag{4.7}$$

as the minimum cost-to-go. From the steady-state Hamilton-Jacobi-Bellman equation [151] and the optimality condition, one can get the following equations:

$$H_{\max}^2(\boldsymbol{x}) + \rho^2 g_{\max}^2(\boldsymbol{x}) + \boldsymbol{x}^T \tilde{Q}\boldsymbol{x} + 2\boldsymbol{u}^T \tilde{R}^T \tilde{R}\boldsymbol{u} + \rho^2 \|\mathbf{v}\|^2 + V_x^T [\boldsymbol{f}_n(\boldsymbol{x}) + \mathrm{B}_n(\boldsymbol{x})\boldsymbol{u} + (I - \mathrm{B}_n(\boldsymbol{x})\mathrm{B}_n(\boldsymbol{x})^+)\mathbf{v}] = 0 \tag{4.8}$$

$$4\boldsymbol{u}^T \tilde{R}^T \tilde{R} + V_x^T \mathrm{B}_n(\boldsymbol{x}) = 0 \tag{4.9}$$

$$2\rho^2 \mathbf{v}^T + V_x^T (I - \mathrm{B}_n(\boldsymbol{x})\mathrm{B}_n(\boldsymbol{x})^+) = 0 \tag{4.10}$$

These three equations will be used to prove that $V(\boldsymbol{x})$ is a Lyapunov function for the original robust control problem **P1**. It can be proved easily that $V(\boldsymbol{x}) > 0$ for $\boldsymbol{x} \neq 0$ and $V(\boldsymbol{x}) = 0$ for $\boldsymbol{x} = 0$.

$$\begin{aligned} \dot{V} = V_x^T \dot{\boldsymbol{x}} &= V_x^T [\boldsymbol{f}_n(\boldsymbol{x}) + \mathrm{B}_n(\boldsymbol{x})\boldsymbol{u} + \mathrm{B}_n(\boldsymbol{x})h(\boldsymbol{x})\boldsymbol{u} + \boldsymbol{d}_n(\boldsymbol{x})] \\ &= V_x^T [\boldsymbol{f}_n(\boldsymbol{x}) + \mathrm{B}_n(\boldsymbol{x})\boldsymbol{u} + \boldsymbol{d}_n(\boldsymbol{x})] + V_x^T \mathrm{B}_n(\boldsymbol{x})h(\boldsymbol{x})\boldsymbol{u} \\ &= V_x^T [\boldsymbol{f}_n(\boldsymbol{x}) + \mathrm{B}_n(\boldsymbol{x})\boldsymbol{u} + \boldsymbol{d}_n(\boldsymbol{x})] - 4\boldsymbol{u}^T \tilde{R}^T \tilde{R}h(\boldsymbol{x})\boldsymbol{u} \end{aligned} \tag{4.11}$$

(Note that the condition (4.9) is applied).

1) For the term $-4\boldsymbol{u}^T \tilde{R}^T \tilde{R}h(\boldsymbol{x})\boldsymbol{u}$, one can use the following relationship:

$$[\tilde{R}\boldsymbol{u} + 2\tilde{R}h(\boldsymbol{x})\boldsymbol{u}]^T [\tilde{R}\boldsymbol{u} + 2\tilde{R}h(\boldsymbol{x})\boldsymbol{u}] = \left\|\tilde{R}\boldsymbol{u}\right\|^2 + 4\boldsymbol{u}^T \tilde{R}^T \tilde{R}h(\boldsymbol{x})\boldsymbol{u} + 4\left\|\tilde{R}h(\boldsymbol{x})\boldsymbol{u}\right\|^2 \geq 0$$

to derive:

$$-4\boldsymbol{u}^T \tilde{R}^T \tilde{R}h(\boldsymbol{x})\boldsymbol{u} \leq \left\|\tilde{R}\boldsymbol{u}\right\|^2 + 4\left\|\tilde{R}h(\boldsymbol{x})\boldsymbol{u}\right\|^2 \leq \left\|\tilde{R}\boldsymbol{u}\right\|^2 + H_{\max}^2(\boldsymbol{x}) \tag{4.12}$$

(Note that the condition (4.5) is applied).

2) For the term $V_x^T [\boldsymbol{f}_n(\boldsymbol{x}) + \mathrm{B}_n(\boldsymbol{x})\boldsymbol{u} + \boldsymbol{d}_n(\boldsymbol{x})]$, we have:

$$
\begin{aligned}
&V_x^T[\boldsymbol{f}_n(\boldsymbol{x})+\mathrm{B}_n(\boldsymbol{x})\boldsymbol{u}+\boldsymbol{d}_n(\boldsymbol{x})] \\
&=V_x^T[\boldsymbol{f}_n(\boldsymbol{x})+\mathrm{B}_n(\boldsymbol{x})\boldsymbol{u}+(I-\mathrm{B}_n(\boldsymbol{x})\mathrm{B}_n(\boldsymbol{x})^+)\mathbf{v}]+V_x^T\boldsymbol{d}_n(\boldsymbol{x})-V_x^T(I-\mathrm{B}_n(\boldsymbol{x})\mathrm{B}_n(\boldsymbol{x})^+)\mathbf{v} \\
&=V_x^T[\boldsymbol{f}_n(\boldsymbol{x})+\mathrm{B}_n(\boldsymbol{x})\boldsymbol{u}+(I-\mathrm{B}_n(\boldsymbol{x})\mathrm{B}_n(\boldsymbol{x})^+)\mathbf{v}]+V_x^T(I-\mathrm{B}_n(\boldsymbol{x})\mathrm{B}_n(\boldsymbol{x})^+)\boldsymbol{d}_n(\boldsymbol{x}) \\
&\qquad -V_x^T(I-\mathrm{B}_n(\boldsymbol{x})\mathrm{B}_n(\boldsymbol{x})^+)\mathbf{v}+V_x^T\mathrm{B}_n(\boldsymbol{x})\mathrm{B}_n(\boldsymbol{x})^+\boldsymbol{d}_n(\boldsymbol{x}) \\
&=-H_{\max}^2(\boldsymbol{x})-\rho^2 g_{\max}^2(\boldsymbol{x})-\boldsymbol{x}^T\tilde{Q}\boldsymbol{x}-2\boldsymbol{u}^T\tilde{R}^T\tilde{R}\boldsymbol{u}+\rho^2\|\mathbf{v}\|^2 \\
&\quad -2\rho^2\mathbf{v}^T\boldsymbol{d}_n(\boldsymbol{x})-4\boldsymbol{u}^T\tilde{R}^T\tilde{R}\mathrm{B}_n(\boldsymbol{x})^+\boldsymbol{d}_n(\boldsymbol{x})
\end{aligned}
\tag{4.13}
$$

Note that the conditions (4.8-4.10) are applied.

Now applying (4.12) and (4.13) to (4.11) leads to:

$$
\dot{V}\le-\left\|\tilde{R}\boldsymbol{u}\right\|^2-\rho^2 g_{\max}^2(\boldsymbol{x})-\boldsymbol{x}^T\tilde{Q}\boldsymbol{x}+\rho^2\|\mathbf{v}\|^2-2\rho^2\mathbf{v}^T\boldsymbol{d}_n(\boldsymbol{x})-4\boldsymbol{u}^T\tilde{R}^T\tilde{R}\mathrm{B}_n(\boldsymbol{x})^+\boldsymbol{d}_n(\boldsymbol{x}) \tag{4.14}
$$

For $-\left\|\tilde{R}\boldsymbol{u}\right\|^2-4\boldsymbol{u}^T\tilde{R}^T\tilde{R}\mathrm{B}_n(\boldsymbol{x})^+\boldsymbol{d}_n(\boldsymbol{x})$, completing the square term yields:

$$
\begin{aligned}
&-\left\|\tilde{R}\boldsymbol{u}\right\|^2-4\boldsymbol{u}^T\tilde{R}^T\tilde{R}\mathrm{B}_n(\boldsymbol{x})^+\boldsymbol{d}_n(\boldsymbol{x}) \\
&=4\left\|\tilde{R}\mathrm{B}_n(\boldsymbol{x})^+\boldsymbol{d}_n(\boldsymbol{x})\right\|^2-\left\|\tilde{R}\boldsymbol{u}+2\tilde{R}\mathrm{B}_n(\boldsymbol{x})^+\boldsymbol{d}_n(\boldsymbol{x})\right\|^2 \\
&\le 4\left\|\tilde{R}\mathrm{B}_n(\boldsymbol{x})^+\boldsymbol{d}_n(\boldsymbol{x})\right\|^2
\end{aligned}
\tag{4.15}
$$

Thus (4.14) becomes

$$
\begin{aligned}
\dot{V}&\le-\rho^2 g_{\max}^2(\boldsymbol{x})-\boldsymbol{x}^T\tilde{Q}\boldsymbol{x}+\rho^2\|\mathbf{v}\|^2-2\rho^2\mathbf{v}^T\boldsymbol{d}_n(\boldsymbol{x})+4\left\|\tilde{R}\mathrm{B}_n(\boldsymbol{x})^+\boldsymbol{d}_n(\boldsymbol{x})\right\|^2 \\
&\le-\rho^2 g_{\max}^2(\boldsymbol{x})-\boldsymbol{x}^T\tilde{Q}\boldsymbol{x}+\rho^2\|\mathbf{v}\|^2+\rho^2[\mathbf{v}^T\mathbf{v}+\boldsymbol{d}_n(\boldsymbol{x})^T\boldsymbol{d}_n(\boldsymbol{x})]+4\left\|\tilde{R}\mathrm{B}_n(\boldsymbol{x})^+\boldsymbol{d}_n(\boldsymbol{x})\right\|^2 \\
&\le-\rho^2 g_{\max}^2(\boldsymbol{x})-\boldsymbol{x}^T\tilde{Q}\boldsymbol{x}+2\rho^2\|\mathbf{v}\|^2+\rho^2 g_{\max}^2(\boldsymbol{x})+4\left\|\tilde{R}\mathrm{B}_n(\boldsymbol{x})^+\boldsymbol{d}_n(\boldsymbol{x})\right\|^2 \\
&=-\boldsymbol{x}^T\tilde{Q}\boldsymbol{x}+2\rho^2\|\mathbf{v}\|^2+4\left\|\tilde{R}\mathrm{B}_n(\boldsymbol{x})^+\boldsymbol{d}_n(\boldsymbol{x})\right\|^2 \\
&\le-\lambda_{\min}(\tilde{Q})\|\boldsymbol{x}\|^2+2\rho^2\|\mathbf{v}\|^2+4\left\|\tilde{R}\mathrm{B}_n(\boldsymbol{x})^+\right\|^2 g_{\max}^2(\boldsymbol{x})
\end{aligned}
\tag{4.16}
$$

Therefore, if the condition (4.6), $4\left\|\tilde{R}\mathrm{B}_n(\boldsymbol{x})^+\right\|^2 g_{\max}^2(\boldsymbol{x}) + 2\rho^2\|\mathbf{v}\|^2 < \gamma'^2\|\boldsymbol{x}\|^2$, is satisfied, then:

$$\dot{V} \le -\left(\gamma^2 - \gamma'^2\right)\|\boldsymbol{x}\|^2 < 0 \tag{4.17}$$

Thus, according to the Lyapunov stability theorem, there exists a neighborhood of 0, $N_c = \{\boldsymbol{x} : \|\boldsymbol{x}\| < c\}$ for some $c > 0$ such that if $\boldsymbol{x}(t)$ enters N_c, then $\boldsymbol{x}(t) \to 0$ as $t \to \infty$.

Furthermore, $\boldsymbol{x}(t)$ cannot always stay outside N_c. If $\|\boldsymbol{x}(t)\| \ge c$ for all $t > 0$, then:

$$\begin{aligned} V(\boldsymbol{x}(t)) - V(\boldsymbol{x}(0)) &= \int_0^t \dot{V}(\boldsymbol{x}(\tau))d\tau \le \int_0^t -(\gamma^2 - \gamma'^2)\|\boldsymbol{x}\|^2 d\tau \\ &\le -\int_0^t (\gamma^2 - \gamma'^2)c^2 d\tau \le -(\gamma^2 - \gamma'^2)c^2 t \end{aligned} \tag{4.18}$$

If *t* goes to infinity, it is obvious that $V(\boldsymbol{x}(t))$ will go to negative, which contradicts the assumption that $V(\boldsymbol{x}(t)) > 0$ for all $\boldsymbol{x}(t)$. Therefore $\boldsymbol{x}(t)$ cannot always stay outside of N_c. Once it enters N_c, it will go to 0 as *t* increases. This proves that by using the control $\boldsymbol{u}$ obtained from solving the optimal control problem **P2**, the robust control problem **P1** has a globally asymptotically stable solution. □

Remark 4.1: *Theorem* 4.1 applies to systems with both matched uncertainty and unmatched uncertainty. The auxiliary control $\mathbf{v}(\boldsymbol{x})$ in (4.2) and (4.3) is used to facilitate the formulation of robust control for unmatched uncertainty. In the case of matched uncertainty, i.e. $\boldsymbol{d}_n(\boldsymbol{x})$ is in the range of $\mathrm{B}_n(\boldsymbol{x})$, *Theorem* 4.1 can be simplified to:

Theorem 4.2: Consider the following nonlinear systems:

$$\dot{\boldsymbol{x}} = \boldsymbol{f}_n(\boldsymbol{x}) + \mathrm{B}_n(\boldsymbol{x})\boldsymbol{u}(\boldsymbol{x}) + \mathrm{B}_n(\boldsymbol{x})h(\boldsymbol{x})\boldsymbol{u}(\boldsymbol{x}) + \mathrm{B}_n(\boldsymbol{x})\boldsymbol{d}_n(\boldsymbol{x})$$

where $\boldsymbol{d}_n(\boldsymbol{x})$ is the uncertainty and $\|\boldsymbol{d}_n(\boldsymbol{x})\| \le d_{\max}(\boldsymbol{x})$. The feedback control law $\boldsymbol{u}(\boldsymbol{x})$ that globally asymptotically stabilizes the closed-loop system can be obtained from solving the following optimal control problem:

Find a feedback control law $\boldsymbol{u}(\boldsymbol{x})$ that minimizes:

$$J = \int_0^\infty (H_{\max}^2(\boldsymbol{x}) + \rho^2 g_{\max}^2(\boldsymbol{x}) + \boldsymbol{x}^T \tilde{Q}\boldsymbol{x} + 2\boldsymbol{u}^T \tilde{R}^T \tilde{R}\boldsymbol{u})dt$$

subject to: $$\dot{\boldsymbol{x}} = \boldsymbol{f}_n(\boldsymbol{x}) + \mathrm{B}_n(\boldsymbol{x})\boldsymbol{u}(\boldsymbol{x})$$

where $H_{\max}(\boldsymbol{x})$ and $g_{\max}(\boldsymbol{x})$ are uncertainty bounds such that:

$$4\left\|\tilde{R}\boldsymbol{d}_n(\boldsymbol{x})\right\|^2 \le g_{\max}^2(\boldsymbol{x}), \quad 4\left\|\tilde{R}h(\boldsymbol{x})\boldsymbol{u}\right\|^2 \le H_{\max}^2(\boldsymbol{x})$$

□

One can follow the similar steps in *Theorem* 4.1 to prove *Theorem* 4.2.

4.2 θ-D nonlinear optimal control technique

The above indirect approach is capable of transforming the nonlinear robust control problem to the nonlinear optimal control problem. However, the resultant optimal control problem is still very difficult to solve for general nonlinear dynamic systems. In this dissertation, we employ the θ-D method to find an approximate analytical solution via a perturbation process. As detailed in Chapter 2, the θ-D technique can provide a closed-form suboptimal feedback control law and is thus much more efficient to implement onboard because it does not require excessive computational load. The θ-D technique can be summarized as follows.

Consider a class of nonlinear time-invariant systems described by:

$$\dot{\boldsymbol{x}} = \boldsymbol{f}(\boldsymbol{x}) + \mathrm{B}\boldsymbol{u} \tag{4.19}$$

The objective is to find a stabilizing control $\boldsymbol{u}$ and minimize the cost function:

$$J = \frac{1}{2}\int_0^\infty (\boldsymbol{x}^T \mathrm{Q}\boldsymbol{x} + \boldsymbol{u}^T \mathrm{R}\boldsymbol{u})dt \tag{4.20}$$

where $\boldsymbol{x} \in \Omega \subset \mathbb{R}^n, \boldsymbol{f} \in \mathbb{R}^n, \mathrm{B} \in \mathbb{R}^{n\times m}, \boldsymbol{u} \in \mathbb{R}^m, \mathrm{Q} \in \mathbb{R}^{n\times n}, \mathrm{R} \in \mathbb{R}^{m\times m}$

Here we assume that Ω is a compact subset in $\mathbb{R}^n$, Q is a positive semi-definite matrix, R is a positive definite constant matrix. Also assume that $\boldsymbol{f}$ is of class C^1 in $\boldsymbol{x}$ on Ω and $\boldsymbol{f}(\mathbf{0})=\mathbf{0}$.

The optimal solution to this infinite-horizon nonlinear regulator problem can be obtained by solving the Hamilton-Jacobi-Bellman (HJB) equation [151]:

$$\frac{\partial V}{\partial \boldsymbol{x}} \boldsymbol{f}(\boldsymbol{x}) - \frac{1}{2}\left(\frac{\partial V}{\partial \boldsymbol{x}}\right)^T \mathrm{B}\mathrm{R}^{-1}\mathrm{B}^T \frac{\partial V}{\partial \boldsymbol{x}} + \frac{1}{2}\boldsymbol{x}^T \mathrm{Q}\boldsymbol{x} = 0 \tag{4.21}$$

where $V(\boldsymbol{x})$ is the optimal cost-to-go, i.e.

$$V(\boldsymbol{x}) = \min_{\boldsymbol{u}} \frac{1}{2}\int_t^\infty \left[\boldsymbol{x}^T \mathrm{Q}\boldsymbol{x} + \boldsymbol{u}^T \mathrm{R}\boldsymbol{u}\right] dt \tag{4.22}$$

Assume that $V(\boldsymbol{x})$ is continuously differentiable and $V(\boldsymbol{x})>0$ with $V(\mathbf{0})=\mathbf{0}$. The optimal control is given by:

$$\boldsymbol{u} = -\mathrm{R}^{-1}\mathrm{B}^T \frac{\partial V}{\partial \boldsymbol{x}} \tag{4.23}$$

The HJB equation (4.21) is very difficult to solve in general. The θ-D method gives an approximate closed-form solution by introducing perturbations to the cost function [78], i.e.

$$J_p = \frac{1}{2}\int_0^\infty \left\{\boldsymbol{x}^T \left[\mathrm{Q} + \sum_{i=1}^{\infty} \mathrm{D}_i \theta^i\right]\boldsymbol{x} + \boldsymbol{u}^T \mathrm{R}\boldsymbol{u}\right\} dt \tag{4.24}$$

where $\sum_{i=1}^{\infty} \mathrm{D}_i \theta^i$ is a perturbation series in terms of an instrumental variable θ. The construction of this series will be discussed afterwards. Rewrite the state equation (4.19) in a linear factorization structure [78], i.e.

$$\dot{\boldsymbol{x}} = \boldsymbol{f}(\boldsymbol{x}) + \mathrm{B}\boldsymbol{u} = \mathrm{F}(\boldsymbol{x})\boldsymbol{x} + \mathrm{B}\boldsymbol{u} = \left\{ \mathrm{A}_0 + \theta \left[\frac{\mathrm{A}(\boldsymbol{x})}{\theta} \right] \right\} \boldsymbol{x} + \mathrm{B}\boldsymbol{u} \tag{4.25}$$

where A_0 is a constant matrix; $(\mathrm{A}_0, \mathrm{B})$ is a controllable pair and $\{\mathrm{F}(\boldsymbol{x}), \mathrm{B}\}$ is pointwise controllable. Then the new optimal control problem (4.24) and (4.25) can be solved through the perturbed HJB equation:

$$\left(\frac{\partial V}{\partial \boldsymbol{x}} \right)^T \left[\mathrm{A}_0 + \theta \frac{\mathrm{A}(\boldsymbol{x})}{\theta} \right] \boldsymbol{x} - \frac{1}{2} \left(\frac{\partial V}{\partial \boldsymbol{x}} \right)^T \mathrm{B}\mathrm{R}^{-1}\mathrm{B}^T \frac{\partial V}{\partial \boldsymbol{x}} + \frac{1}{2} \boldsymbol{x}^T \left(\mathrm{Q} + \sum_{i=1}^{\infty} \mathrm{D}_i \theta^i \right) \boldsymbol{x} = 0 \tag{4.26}$$

Assuming a power series expansion of $\frac{\partial V}{\partial \boldsymbol{x}} = \sum_{i=0}^{\infty} \mathrm{T}_i(\boldsymbol{x}, \theta) \theta^i \boldsymbol{x}$, the optimal control becomes:

$$\boldsymbol{u} = -\mathrm{R}^{-1}\mathrm{B}^T \sum_{i=0}^{\infty} \mathrm{T}_i(\boldsymbol{x}, \theta) \theta^i \boldsymbol{x} \tag{4.27}$$

where $\mathrm{T}_i(\boldsymbol{x}, \theta)$ $(i = 0, \cdots, n, \cdots)$ is a symmetric matrix and is solved recursively by the following algorithm (4.28), which is obtained by substituting $\frac{\partial V}{\partial \boldsymbol{x}} = \sum_{i=0}^{\infty} \mathrm{T}_i(\boldsymbol{x}, \theta) \theta^i \boldsymbol{x}$ in the perturbed HJB equation (4.26) and equating the coefficients of θ^i to zero:

$$\mathrm{T}_0\mathrm{A}_0 + \mathrm{A}_0^T\mathrm{T}_0 - \mathrm{T}_0\mathrm{B}\mathrm{R}^{-1}\mathrm{B}^T\mathrm{T}_0 + \mathrm{Q} = 0 \tag{4.28a}$$

$$\mathrm{T}_1(\mathrm{A}_0 - \mathrm{B}\mathrm{R}^{-1}\mathrm{B}^T\mathrm{T}_0) + (\mathrm{A}_0^T - \mathrm{T}_0\mathrm{B}\mathrm{R}^{-1}\mathrm{B}^T)\mathrm{T}_1 = -\frac{\mathrm{T}_0\mathrm{A}(\boldsymbol{x})}{\theta} - \frac{\mathrm{A}^T(\boldsymbol{x})\mathrm{T}_0}{\theta} - \mathrm{D}_1 \tag{4.28b}$$

$$\mathrm{T}_2(\mathrm{A}_0 - \mathrm{B}\mathrm{R}^{-1}\mathrm{B}^T\mathrm{T}_0) + (\mathrm{A}_0^T - \mathrm{T}_0\mathrm{B}\mathrm{R}^{-1}\mathrm{B}^T)\mathrm{T}_2 = -\frac{\mathrm{T}_1\mathrm{A}(\boldsymbol{x})}{\theta} - \frac{\mathrm{A}^T(\boldsymbol{x})\mathrm{T}_1}{\theta} + \mathrm{T}_1\mathrm{B}\mathrm{R}^{-1}\mathrm{B}^T\mathrm{T}_1 - \mathrm{D}_2 \tag{4.28c}$$

…

$$T_n(A_0 - BR^{-1}B^T T_0) + (A_0{}^T - T_0 BR^{-1}B^T)T_n = -\frac{T_{n-1}A(\boldsymbol{x})}{\theta} - \frac{A^T(\boldsymbol{x})T_{n-1}}{\theta} + \sum_{j=1}^{n-1} T_j BR^{-1}BT_{n-j} - D_n \tag{4.28d}$$

Note that (4.28a) is an algebraic Riccati equation and the rest of equations are Lyapunov equations that are *linear* in terms of T_i $(i = 1, \cdots, n)$.

Steps of applying the θ-D algorithm to solve T_i recursively are summarized as follows [78]:

1) Solve the algebraic Riccati equation (4.28a) to obtain T_0 once A_0, B, Q and R are determined. Note that the resulting T_0 is a positive definite constant matrix under the controllability and observability conditions.

2) Solve the Lyapunov equation (4.28b) to obtain $T_1(\boldsymbol{x}, \theta)$. Note that this is a linear algebraic equation in terms of $T_1(\boldsymbol{x}, \theta)$. A unique property of this equation is that the coefficient matrices $A_0 - BR^{-1}B^T T_0$ and $A_0^T - T_0 BR^{-1}B^T$ are constant matrices.

   Assume that $A_{c_0} = A_0 - BR^{-1}B^T T_0$. Through some linear algebra, equation (4.28b) can be brought into the form of $\hat{A}_0 \mathrm{vec}[T_1(\boldsymbol{x}, \theta)] = \mathrm{vec}[M_1(\boldsymbol{x}, \theta, t)]$ where $\hat{A}_0 = I_n \otimes A_{c_0}^T + A_{c_0} \otimes I_n$ is a constant matrix and the symbol $\otimes$ denotes Kronecker product. $M_1(\boldsymbol{x}, \theta, t)$ includes all the terms on the right-hand side of the equation (4.28b); $\mathrm{vec}[M_1(\boldsymbol{x}, \theta, t)]$ denotes stacking the elements of the matrix $M_1(\boldsymbol{x}, \theta, t)$ by rows in a vector form. Thus, the solution of $T_1(\boldsymbol{x}, \theta)$ can be written in a closed-form expression $\mathrm{vec}[T_1(\boldsymbol{x}, \theta)] = \hat{A}_0^{-1} \mathrm{vec}[M_1(\boldsymbol{x}, \theta, t)]$.

3) Solve (4.28c) and (4.28d) for $T_2, \cdots, T_n$ by following the similar procedure in 2).

Since all the coefficients of $\mathrm{T}_i, i=1,\cdots n$ on the left-hand side of the equations (4.28b-4.28d) are the same constant matrices, i.e. $\mathrm{A}_0 - \mathrm{B}\mathrm{R}^{-1}\mathrm{B}^T\mathrm{T}_0$ and $\mathrm{A}_0^T - \mathrm{T}_0\mathrm{B}\mathrm{R}^{-1}\mathrm{B}^T$, closed-form solution for $\mathrm{T}_i(\boldsymbol{x},\theta)$ can be easily obtained with only one matrix inverse operation, i.e. $\hat{\mathrm{A}}_0^{-1}$.

The perturbation matrix $\mathrm{D}_i, i=1,\cdots n$ is constructed as follows:

$$\mathrm{D}_1 = k_1 e^{-l_1 t}\left[-\frac{\mathrm{T}_0\mathrm{A}(\boldsymbol{x})}{\theta} - \frac{\mathrm{A}^T(\boldsymbol{x})\mathrm{T}_0}{\theta}\right] \tag{4.29a}$$

$$\mathrm{D}_2 = k_2 e^{-l_2 t}\left[-\frac{\mathrm{T}_1\mathrm{A}(\boldsymbol{x})}{\theta} - \frac{\mathrm{A}^T(\boldsymbol{x})\mathrm{T}_1}{\theta} + \mathrm{T}_1\mathrm{B}\mathrm{R}^{-1}\mathrm{B}^T\mathrm{T}_1\right] \tag{4.29b}$$

…

$$\mathrm{D}_n = k_n e^{-l_n t}\left\{-\frac{\mathrm{T}_{n-1}\mathrm{A}(\boldsymbol{x})}{\theta} - \frac{\mathrm{A}^T(\boldsymbol{x})\mathrm{T}_{n-1}}{\theta} + \sum_{j=1}^{n-1}\mathrm{T}_j\mathrm{B}\mathrm{R}^{-1}\mathrm{B}^T\mathrm{T}_{n-j}\right\} \tag{4.29c}$$

where k_i and $l_i > 0, i=1,\ldots,n$ are adjustable design parameters.

The D_i ($i=1,\cdots n$) are chosen such that:

$$\begin{aligned} -\frac{\mathrm{T}_{i-1}\mathrm{A}(\boldsymbol{x})}{\theta} - \frac{\mathrm{A}^T(\boldsymbol{x})\mathrm{T}_{i-1}}{\theta} + \sum_{j=1}^{i-1}\mathrm{T}_j\mathrm{B}\mathrm{R}^{-1}\mathrm{B}^T\mathrm{T}_{i-j} - \mathrm{D}_i \\ = \varepsilon_i(t)\left\{-\frac{\mathrm{T}_{i-1}\mathrm{A}(\boldsymbol{x})}{\theta} - \frac{\mathrm{A}^T(\boldsymbol{x})\mathrm{T}_{i-1}}{\theta} + \sum_{j=1}^{i-1}\mathrm{T}_j\mathrm{B}\mathrm{R}^{-1}\mathrm{B}^T\mathrm{T}_{i-j}\right\} \end{aligned} \tag{4.30}$$

where
$$\varepsilon_i(t) = 1 - k_i e^{-l_i t} \tag{4.31}$$

ε_i is chosen to be a small number to overcome the initial large control gain problem because the state dependent term $\mathrm{A}(\boldsymbol{x})$ on the right-hand side of (4.28b)-(4.28d) may cause a large magnitude of $\mathrm{T}_i(\boldsymbol{x},\theta)$ if the initial states are large. To illustrate it, let us suppose there is no ε_i or D_i in (4.28). For example, in (4.28b), if there exists a cubic

term in A($\boldsymbol{x}$) and the initial $\boldsymbol{x}$ is large, this large value will be reflected in the solution of T_1. Since T_1 and A($\boldsymbol{x}$) will be used in solving for T_2 in the ensuing (4.28c), this large value will be propagated and amplified. As a result, it causes the large control gain or even instability. Therefore, the small number ε_i is used to suppress this large value from propagating in (4.28b)-(4.28d).

ε_i is also required in the proof of convergence and stability of the above algorithm [78]. The exponential term $e^{-l_i t}$ in D_i lets the perturbation terms in the cost function (4.24) diminish as time evolves.

Remark 3.2: k_i and l_i are design parameters used to modulate system transient responses. Selection of k_i and l_i can be done systematically [78] by applying the least-squares curve-fitting of the maximum singular value of the θ-D solution with that of the state-dependent Riccati equation solution.

Remark 3.3: θ is merely an intermediate variable. The introduction of θ is for the convenience of power series expansion, and it is cancelled when $T_i(\boldsymbol{x},\theta)$ times θ^i in the final control calculations, i.e., equation (4.27). Note that in every θ^i equation (4.28) and D_i expression (4.29), $\frac{1}{\theta^i}$ factor appears linearly on the right-hand side of the equations. Consequently, $\frac{1}{\theta^i}$ will appear linearly in the solution of T_i, i.e. $T_i = \frac{\hat{T}_i}{\theta^i}$ where $\hat{T}_i$ is the solution without $\frac{1}{\theta^i}$. When T_i is multiplied by θ^i in the control (4.27), θ^i gets cancelled.

In the θ-D algorithm, retaining the first three terms, T_0, T_1 and T_2, in the control equation (4.27) has been sufficient to achieve satisfactory performance in the problems

that have been solved [78, 152, 153]. Theoretical results concerning the convergence of series $\sum_{i=0}^{\infty} \mathrm{T}_i(\boldsymbol{x}, \theta)\theta^i$, closed-loop stability, and optimality of truncating the series can be referred to [78].

CHAPTER V

INTEGRATED INDIRECT ROBUST CONTROL DESIGN FOR SPACECRAFT PROXIMITY OPERATION

Theorem 4.1 has shown the equivalency of the robust control problem and the optimal control problem. In this section, we will design the robust controller for spacecraft proximity operation using the indirect robust control scheme and the θ-D optimal control method,

First, the translational dynamic equations need to be expressed in the state-space representations. The relative translational equation of motion (3.3-3.5) can be rewritten as:

$$\frac{d}{dt}x = \dot{x} \tag{5.1a}$$

$$\frac{d}{dt}y = \dot{y} \tag{5.1b}$$

$$\frac{d}{dt}z = \dot{z} \tag{5.1c}$$

$$\frac{d}{dt}\dot{x} = 2\dot{\nu}\dot{y} + \ddot{\nu}y + \dot{\nu}^2 x - \frac{\mu x}{((\overline{r}+x)^2 + y^2 + z^2)^{\frac{3}{2}}} - \frac{\mu\overline{r}}{((\overline{r}+x)^2 + y^2 + z^2)^{\frac{3}{2}}} + \frac{\mu}{\overline{r}^2} + a_x \tag{5.1d}$$

$$\frac{d}{dt}\dot{y} = -2\dot{\nu}\dot{x} - \ddot{\nu}x + \dot{\nu}^2 y - \frac{\mu}{((\overline{r}+x)^2 + y^2 + z^2)^{\frac{3}{2}}}y + a_y \tag{5.1e}$$

$$\frac{d}{dt}\dot{z} = -\frac{\mu}{((\overline{r}+x)^2 + y^2 + z^2)^{\frac{3}{2}}}z + a_z \tag{5.1f}$$

In order to apply the θ-D method, $\boldsymbol{f}(\mathbf{0})=\mathbf{0}$ needs to be satisfied. If there are terms that make $\boldsymbol{f}(\mathbf{0}) \neq 0$, they prevent a direct C^1 factorization of $\boldsymbol{f}(\boldsymbol{x})$. These terms are called biased terms. For example, terms such as $-\dfrac{\mu\bar{r}}{((\bar{r}+x)^2+y^2+z^2)^{\frac{3}{2}}}$ and $\dfrac{\mu}{\bar{r}^2}$ are biased terms because they do not go to zero when the states become zero. One of the ways [79, 145, 146, 148-150] to handle this problem is to augment the system with a stable state ' s_a ' satisfying:

$$\dot{s}_a = -\lambda_a s_a \tag{5.2}$$

in which λ_a is a positive number. With the augmented state ' s_a ', the biased terms can then be factorized as

$$-\frac{\mu\bar{r}}{((\bar{r}+x)^2+y^2+z^2)^{\frac{3}{2}}} = \left[-\frac{\mu\bar{r}}{((\bar{r}+x)^2+y^2+z^2)^{\frac{3}{2}} s_a}\right] s_a \tag{5.3a}$$

$$\frac{\mu}{\bar{r}^2} = \left[\frac{\mu}{\bar{r}^2 s_a}\right] s_a \tag{5.3b}$$

The introduction of ' s_a ' does not change the actual spacecraft dynamics. Each time through the controller, the initial value $s_a(0)$ is used in the state-dependent coefficient matrix and in calculating the control. Usually we set $s_a(0)=1$.

Thus, the state variables for the translational motion are:

$$[\mathbf{r}_L^T \quad \mathbf{v}_L^T \quad s_a]^T = [x \quad y \quad z \quad \dot{x} \quad \dot{y} \quad \dot{z} \quad s_a]^T \tag{5.4}$$

The state-space representations of the coupled attitude dynamics and flexible motion from the previous model in Chapter 3 are repeated here:

$$\dot{\boldsymbol{\omega}}_s = M_0^{-1}(\delta^T C - \tilde{\omega}_s \delta^T)\dot{\boldsymbol{\eta}} + M_0^{-1}\delta^{\mathrm{T}} K\boldsymbol{\eta} - M_0^{-1}\tilde{\omega}_s J_s \boldsymbol{\omega}_s + M_0^{-1}\boldsymbol{\Gamma}_s + \mathrm{P}_1\dot{\boldsymbol{\eta}} + \mathrm{P}_2\boldsymbol{\eta} + \mathrm{P}_3\boldsymbol{\omega}_s + \mathrm{P}_4\boldsymbol{\Gamma}_s \tag{5.5}$$

$$\ddot{\boldsymbol{\eta}} = [-\delta M_0^{-1}(\delta^T C - \tilde{\omega}_s \delta^T) - C]\dot{\boldsymbol{\eta}} + (-\delta M_0^{-1}\delta^T K - K)\boldsymbol{\eta} + \delta M_0^{-1}\tilde{\omega}_s J_s \boldsymbol{\omega}_s - \delta M_0^{-1}\boldsymbol{\Gamma}_s + \mathrm{P}_5\dot{\boldsymbol{\eta}} + \mathrm{P}_6\boldsymbol{\eta} + \mathrm{P}_7\boldsymbol{\omega}_s + \mathrm{P}_8\boldsymbol{\Gamma}_s \tag{5.6}$$

Note that (5.5) and (5.6) are expressed in the form of nominal dynamics plus parametric uncertainties. Define $\boldsymbol{s}_1 = \boldsymbol{\eta}, \boldsymbol{s}_2 = \dot{\boldsymbol{\eta}}$, (5.5) can be rewritten as:

$$\dot{\boldsymbol{s}}_1 = \boldsymbol{s}_2 \tag{5.7a}$$

$$\begin{aligned}\dot{\boldsymbol{s}}_2 = {} & [-\delta M_0^{-1}(\delta^T C - \tilde{\omega}_s \delta^T) - C]\boldsymbol{s}_2 + (-\delta M_0^{-1}\delta^T K - K)\boldsymbol{s}_1 + \delta M_0^{-1}\tilde{\omega}_s J_s \boldsymbol{\omega}_s - \delta M_0^{-1}\boldsymbol{\Gamma}_s \\ & + \mathrm{P}_5\boldsymbol{s}_2 + \mathrm{P}_6\boldsymbol{s}_1 + \mathrm{P}_7\boldsymbol{\omega}_s + \mathrm{P}_8\boldsymbol{\Gamma}_s\end{aligned} \tag{5.7b}$$

The relative attitude kinematics can be described in terms of quaternion error $\boldsymbol{q}_e$ and angular velocity error $\boldsymbol{\omega}_e$ [142]:

$$\dot{\boldsymbol{q}}_e = \frac{1}{2}\begin{bmatrix} q_{0e}\varepsilon_{\omega t} - q_{1e}\omega_{ex} - q_{2e}\omega_{ey} - q_{3e}\omega_{ez} \\ q_{0e}\omega_{ex} + q_{1e}\varepsilon_{\omega t} + q_{2e}\omega_{ez} - q_{3e}\omega_{ey} \\ q_{0e}\omega_{ey} - q_{1e}\omega_{ez} + q_{2e}\varepsilon_{\omega t} + q_{3e}\omega_{ex} \\ q_{0e}\omega_{ez} + q_{1e}\omega_{ey} - q_{2e}\omega_{ex} + q_{3e}\varepsilon_{\omega t} \end{bmatrix} \tag{5.8}$$

where ω_{ex}, ω_{ey}, and ω_{ez} are the angular velocity tracking errors expressed in the spacecraft body frame $\{\boldsymbol{B}_s\}$, which are defined in (3.20); $\varepsilon_{\omega t} = -0.0001$ is added to the quaternion error kinematics in order for the Riccati equation (4.28a) to have a stable solution. Note that (5.8) is only used for the control design. When the attitude quaternion kinematics is propagated (or integrated), the true kinematics equation is used without $\varepsilon_{\omega t}$.

Let $\boldsymbol{\xi} = T_{\boldsymbol{I}}^{\boldsymbol{B}_s} T_{\boldsymbol{B}_d}^{\boldsymbol{I}} \boldsymbol{\omega}_d^{\boldsymbol{B}_d}$. Referring to (3.20), the angular velocity tracking error can be written as:

$$\omega_{ex} = \omega_{sx} - \begin{bmatrix}1 & 0 & 0\end{bmatrix}\boldsymbol{\xi}; \quad \omega_{ey} = \omega_{sy} - \begin{bmatrix}0 & 1 & 0\end{bmatrix}\boldsymbol{\xi}; \quad \omega_{ez} = \omega_{sz} - \begin{bmatrix}0 & 0 & 1\end{bmatrix}\boldsymbol{\xi}$$

Thus, the attitude error kinematics (5.8) can be rewritten in a linear form:

$$\dot{\boldsymbol{q}}_e = \frac{1}{2}\begin{bmatrix} \varepsilon_{\omega t} & a\xi & b\xi & c\xi \\ -a\xi & \varepsilon_{\omega t} & -c\xi & b\xi \\ -b\xi & c\xi & \varepsilon_{\omega t} & -a\xi \\ -c\xi & -b\xi & a\xi & \varepsilon_{\omega t} \end{bmatrix}\boldsymbol{q}_e + \frac{1}{2}\begin{bmatrix} -q_{1e} & -q_{2e} & -q_{3e} \\ q_{0e} & -q_{3e} & q_{2e} \\ q_{3e} & q_{0e} & -q_{1e} \\ -q_{2e} & q_{1e} & q_{0e} \end{bmatrix}\boldsymbol{\omega}_s = \frac{1}{2}Q_1 \cdot \boldsymbol{q}_e + \frac{1}{2}Q_2 \cdot \boldsymbol{\omega}_s \quad (5.9)$$

where $a = [1 \quad 0 \quad 0], b = [0 \quad 1 \quad 0], c = [0 \quad 0 \quad 1]$, and Q_1 and Q_2 are the corresponding coefficient matrices.

In order to improve the relative position tracking performance, an integral of the relative position vector $\boldsymbol{r}_L$ is augmented into the state space, i.e.

$$\dot{\boldsymbol{r}}_{LI} = \boldsymbol{r}_L \quad (5.10)$$

The state variables for the entire integrated control system are chosen to be:

$$\boldsymbol{X} = \begin{bmatrix} \boldsymbol{r}_L^T & \mathbf{v}_L^T & s_a & \boldsymbol{q}_e^T & \boldsymbol{\omega}_s^T & \boldsymbol{r}_{LI}^T & \boldsymbol{s}_1^T & \boldsymbol{s}_2^T \end{bmatrix}^T \quad (5.11)$$

and control variables are defined as:

$$\boldsymbol{u} = [a_x \quad a_y \quad a_z \quad \Gamma_{s_x} \quad \Gamma_{s_y} \quad \Gamma_{s_z}]^T \quad (5.12)$$

$\boldsymbol{r}_L$ and $\mathbf{v}_L$ are defined in (3.1). Their dynamics are governed by (5.1). s_a is the augmented state to absorb the biased terms and satisfies (5.2). The attitude error quaternion $\boldsymbol{q}_e$, pursuer's angular velocity $\boldsymbol{\omega}_s$, and coupling flexible motion states $\boldsymbol{s}_1$ and $\boldsymbol{s}_2$ are governed by (5.9), (5.5), and (5.7), respectively. In this dissertation, the number of significant elastic modes is 3. It has been shown to be a good approximation for spacecraft applications [110, 144]. So each of the states $\boldsymbol{s}_1$ and $\boldsymbol{s}_2$ becomes a 4×1 vector. The state-space in (5.11) has the dimension of 25.

In addition to the parametric uncertainty, we also consider the control input uncertainty due to actuators. The input matrix uncertainty $h(\boldsymbol{X})$ and its bound $H_{\max}(\boldsymbol{X})$

satisfy the condition (4.5). In order to use *Theorem* 4.1, the nonlinear state-space equation for the spacecraft control problem is rewritten as:

$$\dot{\boldsymbol{X}} = \boldsymbol{f}_n(\boldsymbol{X}) + \mathrm{B}_n(\boldsymbol{X})\boldsymbol{u} + \mathrm{B}_n(\boldsymbol{X})h(\boldsymbol{X})\boldsymbol{u} + \boldsymbol{d}_n(\boldsymbol{X}) \tag{5.13}$$

where:

$$\boldsymbol{f}_n(\boldsymbol{X}) = \mathrm{F}(\boldsymbol{X})\boldsymbol{X}$$

$$= \begin{bmatrix} A_1 & 0_{7\times4} & 0_{7\times3} & 0_{7\times3} & 0_{7\times4} & 0_{7\times4} \\ 0_{4\times7} & \frac{1}{2}Q_1 & \frac{1}{2}Q_2 & 0_{4\times3} & 0_{4\times4} & 0_{4\times4} \\ 0_{3\times7} & 0_{3\times4} & -M_0^{-1}\tilde{\omega}_s J_s & 0_{3\times3} & M_0^{-1}\delta^T K & M_0^{-1}(\delta^T C - \tilde{\omega}_s\delta^T) \\ \begin{bmatrix} I_{3\times3} & 0_{3\times4} \end{bmatrix} & 0_{3\times4} & 0_{3\times3} & 0_{3\times3} & 0_{3\times4} & 0_{3\times4} \\ 0_{4\times7} & 0_{4\times4} & 0_{4\times3} & 0_{4\times3} & 0_{4\times4} & I_{4\times4} \\ 0_{4\times7} & 0_{4\times4} & \delta M_0^{-1}\tilde{\omega}_s J_s & 0_{4\times3} & -\delta M_0^{-1}\delta^T K - K & -\delta M_0^{-1}(\delta^T C - \tilde{\omega}_s\delta^T) - C \end{bmatrix} \boldsymbol{X} \tag{5.14}$$

A_1 corresponds to the translational dynamics (5.1) and the dynamics of the biased absorbing state s_a

$$A_1 = \begin{bmatrix} 0 & 0 & 0 & 1 & 0 & 0 & 0 \\ 0 & 0 & 0 & 0 & 1 & 0 & 0 \\ 0 & 0 & 0 & 0 & 0 & 1 & 0 \\ \dot{v}^2 - coeff & \ddot{v} & 0 & 0 & 2\dot{v} & 0 & bias/s_a \\ -\ddot{v} & \dot{v}^2 - coeff & 0 & -2\dot{v} & 0 & 0 & 0 \\ 0 & 0 & -coeff & 0 & 0 & 0 & 0 \\ 0 & 0 & 0 & 0 & 0 & 0 & -\lambda_a \end{bmatrix} \tag{5.15}$$

where $coeff = \dfrac{\mu}{((\bar{r}+x)^2 + y^2 + z^2)^{\frac{3}{2}}}, bias = -coeff \bullet \bar{r} + \dfrac{\mu}{\bar{r}^2}$

The input matrix $\mathrm{B}_n(\boldsymbol{X})$ is:

$$\mathrm{B}_n(\boldsymbol{X}) = \begin{bmatrix} B_1 & 0_{7\times3} \\ 0_{4\times3} & 0_{4\times3} \\ 0_{3\times3} & M_0^{-1} \\ 0_{3\times3} & 0_{3\times3} \\ 0_{4\times3} & 0_{4\times3} \\ 0_{4\times3} & -\delta M_0^{-1} \end{bmatrix} \tag{5.16}$$

where B_1 is the control coefficient matrix corresponding to the translational dynamics (5.1), i.e.

$$B_1 = \begin{bmatrix} 0_{3\times3} \\ I_{3\times3} \\ 0_{1\times3} \end{bmatrix} \tag{5.17}$$

Note that $\mathrm{B}_n(\boldsymbol{X})$ is a constant matrix in this spacecraft control problem.

The disturbance term $\boldsymbol{d}_n(\boldsymbol{X})$ is derived from Eqs (5.5) and (5.6):

$$\boldsymbol{d}_n(\boldsymbol{X}) = \begin{bmatrix} 0_{3\times1} \\ 0_{3\times1} \\ 0_{1\times1} \\ 0_{4\times1} \\ \mathrm{P}_1\dot{\boldsymbol{\eta}} + \mathrm{P}_2\boldsymbol{\eta} + \mathrm{P}_3\boldsymbol{\omega}_\mathrm{s} + \mathrm{P}_4\boldsymbol{\Gamma}_\mathrm{s} \\ 0_{3\times1} \\ 0_{4\times1} \\ \mathrm{P}_5\dot{\boldsymbol{\eta}} + \mathrm{P}_6\boldsymbol{\eta} + \mathrm{P}_7\boldsymbol{\omega}_\mathrm{s} + \mathrm{P}_8\boldsymbol{\Gamma}_\mathrm{s} \end{bmatrix} \tag{5.18}$$

In order to use *Theorem* 4.1, the uncertainty bounds $g_{\max}(\boldsymbol{X})$ and $H_{\max}(\boldsymbol{X})$ need to be determined. Rewrite $\boldsymbol{d}_n(\boldsymbol{X})$ as:

$$\boldsymbol{d}_n(\boldsymbol{X}) = \begin{bmatrix} 0_{11\times14} \\ \mathrm{P}_3 \quad \mathrm{P}_2 \quad \mathrm{P}_1 \quad \mathrm{P}_4 \\ 0_{7\times14} \\ \mathrm{P}_7 \quad \mathrm{P}_6 \quad \mathrm{P}_5 \quad \mathrm{P}_8 \end{bmatrix} \begin{bmatrix} \boldsymbol{\omega}_s \\ \boldsymbol{\eta} \\ \dot{\boldsymbol{\eta}} \\ \boldsymbol{\Gamma}_s \end{bmatrix} \tag{5.19}$$

then $\left\|\boldsymbol{d}_n(\boldsymbol{X})\right\|^2 = \begin{bmatrix}\boldsymbol{\omega}_s^T & \boldsymbol{\eta}^T & \dot{\boldsymbol{\eta}}^T & \boldsymbol{\Gamma}_s^T\end{bmatrix}\begin{bmatrix} & 0_{11\times 14} & \\ \mathrm{P}_3 & \mathrm{P}_2 & \mathrm{P}_1 & \mathrm{P}_4 \\ & 0_{7\times 14} & \\ \mathrm{P}_7 & \mathrm{P}_6 & \mathrm{P}_5 & \mathrm{P}_8 \end{bmatrix}^T \begin{bmatrix} & 0_{11\times 14} & \\ \mathrm{P}_3 & \mathrm{P}_2 & \mathrm{P}_1 & \mathrm{P}_4 \\ & 0_{7\times 14} & \\ \mathrm{P}_7 & \mathrm{P}_6 & \mathrm{P}_5 & \mathrm{P}_8 \end{bmatrix}\begin{bmatrix}\boldsymbol{\omega}_s \\ \boldsymbol{\eta} \\ \dot{\boldsymbol{\eta}} \\ \boldsymbol{\Gamma}_s\end{bmatrix}$

If we consider the detail formulation of ΔJ bound and $\Delta\delta$ bound, then the bound for each $\mathrm{P}_1, \mathrm{P}_2, ..., \mathrm{P}_8$ will be very complicated and hard to determine. In this dissertation, the bound for $\left\|\boldsymbol{d}_n(\boldsymbol{X})\right\|$ is chosen to be a quadratic form in terms of the rotational states such that the θ-D method can be easily applied, i.e.

$$\left\|\boldsymbol{d}_n(\boldsymbol{X})\right\|^2 \le \begin{bmatrix}\boldsymbol{\omega}_s \\ \boldsymbol{\eta} \\ \dot{\boldsymbol{\eta}}\end{bmatrix}^T \sigma \begin{bmatrix}\boldsymbol{\omega}_s \\ \boldsymbol{\eta} \\ \dot{\boldsymbol{\eta}}\end{bmatrix} \tag{5.20}$$

where $\sigma = \begin{bmatrix}\sigma_1 & & \\ & \sigma_2 & \\ & & \sigma_3\end{bmatrix}$ is a positive definite diagonal matrix. We can estimate the σ value and use it as a tunable design parameter. Then for the condition (4.4) $\left\|\boldsymbol{d}_n(\boldsymbol{X})\right\|^2 \le g_{\max}^2(\boldsymbol{X})$, we can select $g_{\max}^2(\boldsymbol{X}) = \begin{bmatrix}\boldsymbol{\omega}_s \\ \boldsymbol{\eta} \\ \dot{\boldsymbol{\eta}}\end{bmatrix}^T \sigma \begin{bmatrix}\boldsymbol{\omega}_s \\ \boldsymbol{\eta} \\ \dot{\boldsymbol{\eta}}\end{bmatrix} = (C_0\boldsymbol{X})^T \sigma (C_0\boldsymbol{X})$. The constant matrix C_0 is defined as: $C_0 = \begin{bmatrix} 0_{3\times 11} & I_{3\times 3} & 0_{3\times 11} \\ 0_{4\times 17} & I_{4\times 4} & 0_{4\times 4} \\ 0_{4\times 21} & I_{4\times 4} & \end{bmatrix}$

Consider the condition (4.5), $4\left\|\tilde{R}h(\boldsymbol{X})\boldsymbol{u}\right\|^2 \le H_{\max}^2(\boldsymbol{X})$. Suppose the control input uncertainty is bounded by $\left\|h(\boldsymbol{X})\boldsymbol{u}\right\|^2 \le \left\|\beta\boldsymbol{X}\right\|^2$, where β is a predefined constant number, then $H_{\max}(\boldsymbol{X})$ can be selected as $H_{\max}^2(\boldsymbol{X}) = 4\beta^2\left\|\tilde{R}\right\|^2 \boldsymbol{X}^T\boldsymbol{X}$.

Regarding the condition (4.6):

$$2\rho^2 \|\mathbf{v}\|^2 + 4\left\|\tilde{R}\mathrm{B}_n(\boldsymbol{x})^+\right\|^2 g_{\max}^2(\boldsymbol{x}) < \gamma'^2 \|\boldsymbol{x}\|^2$$

notice that

$$\left\|\tilde{R}\mathrm{B}_n(\boldsymbol{X})^+\right\|^2 g_{\max}^2(\boldsymbol{X}) \le \left\|\tilde{R}\mathrm{B}_n(\boldsymbol{X})^+\right\|^2 (C_0\boldsymbol{X})^T \sigma C_0\boldsymbol{X} = \left\|\tilde{R}\mathrm{B}_n(\boldsymbol{X})^+\right\|^2 \boldsymbol{X}^T C_0^T \sigma C_0\boldsymbol{X} \qquad (5.21)$$

This provides a condition on choosing a proper weight matrix $\tilde{Q}$ since γ'^2 can be selected as large as $\lambda_{\min}(\tilde{Q})$. With a careful selection of ρ, σ, and $\tilde{Q}$, the condition (4.6) can be satisfied.

According to *Theorem* 4.1, we can formulate the following optimal control problem with the system equation:

$$\dot{\boldsymbol{X}} = \boldsymbol{f}_n(\boldsymbol{X}) + \mathrm{B}_n(\boldsymbol{X})\boldsymbol{u} + (I - \mathrm{B}_n(\boldsymbol{X})\mathrm{B}_n(\boldsymbol{X})^+)\mathbf{v} = \mathrm{F}(\boldsymbol{X})\boldsymbol{X} + \mathrm{B}(\boldsymbol{X})\begin{bmatrix}\boldsymbol{u}\\ \mathbf{v}\end{bmatrix} \qquad (5.22)$$

where $\mathrm{B}(\boldsymbol{X}) = [\mathrm{B}_n(\boldsymbol{X}) \quad (I - \mathrm{B}_n(\boldsymbol{X})\mathrm{B}_n(\boldsymbol{X})^+)]$ is a constant matrix, and with the cost function:

$$\int_0^\infty [H_{\max}^2(\boldsymbol{X}) + \rho^2 g_{\max}(\boldsymbol{X})^2 + \boldsymbol{X}^T\tilde{Q}\boldsymbol{X} + 2\boldsymbol{u}^T\tilde{R}^T\tilde{R}\boldsymbol{u} + \rho^2\|\mathbf{v}\|^2]dt$$

where $\|g_{\max}(\boldsymbol{X})\|^2 = \boldsymbol{X}^T C_0^T \sigma C_0\boldsymbol{X}$, $H_{\max}^2(\boldsymbol{X}) = 4\beta^2\left\|\tilde{R}\right\|^2 \boldsymbol{X}^T\boldsymbol{X}$, The cost function can be rewritten in a quadratic form:

$$\int_0^\infty \left\{\boldsymbol{X}^T[4\beta^2\left\|\tilde{R}\right\|^2 I + \rho^2 C_0^T\sigma C_0 + \tilde{Q}]\boldsymbol{X} + \begin{bmatrix}\boldsymbol{u} & \mathbf{v}\end{bmatrix}\begin{bmatrix}2\tilde{R}^T\tilde{R} & \\ & \rho^2 I\end{bmatrix}\begin{bmatrix}\boldsymbol{u}\\ \mathbf{v}\end{bmatrix}\right\} dt \qquad (5.23)$$

so that the θ-D technique can be applied to design the optimal controller.

Comparing (5.22) with the θ-D formulation (4.25):

$$\dot{\boldsymbol{X}} = \mathrm{F}(\boldsymbol{X})\boldsymbol{X} + \mathrm{B}(\boldsymbol{X})\begin{bmatrix}\boldsymbol{u}\\ \mathbf{v}\end{bmatrix} = \left\{\mathrm{A}_0 + \theta\left[\frac{\mathrm{A}(\boldsymbol{X})}{\theta}\right]\right\}\boldsymbol{X} + \mathrm{B}(\boldsymbol{X})\begin{bmatrix}\boldsymbol{u}\\ \mathbf{v}\end{bmatrix} \tag{5.24}$$

we can choose $\mathrm{A}_0 = \mathrm{F}(\boldsymbol{X}_0)$, $\mathrm{A}(\boldsymbol{X}) = \mathrm{F}(\boldsymbol{X}) - \mathrm{A}_0$ where $\boldsymbol{X}_0$ is the initial state, and choose

$\mathrm{Q} = 2(4\beta^2 \left\|\tilde{R}\right\|^2 I + \rho^2 C_0^T \sigma C_0 + \tilde{Q})$, $\mathrm{R} = \begin{bmatrix} 2\tilde{R}^T\tilde{R} & \\ & \rho^2 I \end{bmatrix}$.

The first three terms in the control law (4.27) have been found to be good enough to achieve satisfactory performance. So the optimal control can be written as [78, 145, 146, 148]:

$$\begin{bmatrix}\boldsymbol{u}\\ \mathbf{v}\end{bmatrix} = -\mathrm{R}^{-1}\mathrm{B}^T(\boldsymbol{X})[\mathrm{T}_0 + \mathrm{T}_1(\boldsymbol{X},\theta) + \mathrm{T}_2(\boldsymbol{X},\theta)]\cdot \\ \left[(\boldsymbol{r}_L - \boldsymbol{r}_c)^T \quad (\mathbf{v}_L - \mathbf{v}_c)^T \quad 0 \quad (\boldsymbol{q}_e - \boldsymbol{q}_e^d)^T \quad \boldsymbol{\omega}_e^T \quad (\boldsymbol{r}_{LI} - \int \boldsymbol{r}_c dt)^T \quad \boldsymbol{s}_1^T \quad \boldsymbol{s}_2^T\right]^T \tag{5.25}$$

where $\mathrm{T}_0, \mathrm{T}_1(\boldsymbol{X},\theta), \text{and } \mathrm{T}_2(\boldsymbol{X},\theta)$ are solved from the θ-D algorithm (4.28)-(4.30). Note that only the $\boldsymbol{u}$ component in (5.25) is applied to the actual spacecraft control and $\mathbf{v}$ is just an auxiliary control variable.

The control law (5.25) is implemented as a servomechanism [78, 145]. $\boldsymbol{r}_c$ is the desired relative position expressed in the LVLH frame. The pursuer is required to be positioned at a safe distance of r_d along the target body $\hat{\boldsymbol{b}}_{tx}$ axis that is the outward normal direction of its docking port. Thus, $\begin{bmatrix} r_d & 0 & 0\end{bmatrix}^T$ is a desired relative position vector expressed in the target body frame. The desired relative position vector expressed in the LVLH frame, i.e. $\boldsymbol{r}_c$, can be obtained by:

$$\boldsymbol{r}_c = T_{\boldsymbol{B}_t}^{\boldsymbol{L}} \cdot r_d \hat{\boldsymbol{b}}_{tx} = T_{\boldsymbol{B}_t}^{\boldsymbol{L}} \cdot \begin{bmatrix} r_d & 0 & 0\end{bmatrix}^T = T_{\boldsymbol{I}}^{\boldsymbol{L}} T_{\boldsymbol{B}_t}^{\boldsymbol{I}} \cdot \begin{bmatrix} r_d & 0 & 0\end{bmatrix}^T \tag{5.26}$$

where $T_{B_t}^{L}$ is the target body-to-LVLH coordinate transformation matrix; $T_{B_t}^{I}$ is the target body-to-inertial coordinate transformation matrix and can be computed from the target quaternion $\boldsymbol{q}_t$; T_{I}^{L} is the inertial-to-LVLH coordinate transformation matrix and can be computed from the target orbital elements [154]: right ascension of ascending node, Ω_t, inclination i_t, argument of latitude u_t, etc.

The desired relative velocity $\mathbf{v}_c$ can be computed from $\boldsymbol{r}_c$ by differentiating $\boldsymbol{r}_c$ in the LVLH frame and expressing the result in the LVLH frame, i.e.

$$\mathbf{v}_c = \frac{d\boldsymbol{r}_c}{dt} = T_{B_t}^{L}(\boldsymbol{\omega}_{B_t/L}^{B_t} \times \begin{bmatrix} r_d & 0 & 0 \end{bmatrix}^T) \tag{5.27}$$

where $\boldsymbol{\omega}_{B_t/L}^{B_t}$ is the angular velocity of the target body frame with respect to the LVLH frame expressed in the target body frame. It can be computed from:

$$\boldsymbol{\omega}_{B_t/L}^{B_t} = \boldsymbol{\omega}_{B_t/I}^{B_t} - \boldsymbol{\omega}_{L/I}^{B_t} = \boldsymbol{\omega}_{B_t/I}^{B_t} - T_{I}^{B_t} \cdot \boldsymbol{\omega}_{L/I}^{I} \tag{5.28}$$

where $\boldsymbol{\omega}_{B_t/I}^{B_t} = \boldsymbol{\omega}_t$ is the target angular velocity with respect to the inertial frame expressed in the target body frame; $\boldsymbol{\omega}_{L/I}^{B_t}$ and $\boldsymbol{\omega}_{L/I}^{I}$ are the angular velocity of the LVLH frame with respect to the inertial frame expressed in the target body frame and the inertial frame respectively. These values can be calculated from the orbital elements [154].

The desired quaternion error $\boldsymbol{q}_e^d$ in (5.25) is $\begin{bmatrix} 1 & 0 & 0 & 0 \end{bmatrix}^T$, which implies the attitude of the pursuer is synchronized with the target attitude.

The perturbation coefficient matrices D_i are chosen to be:

$$\mathrm{D}_1 = e^{-0.01t}\left[-\frac{\mathrm{T}_0 \mathrm{A}(\boldsymbol{X})}{\theta} - \frac{\mathrm{A}^T(\boldsymbol{X})\mathrm{T}_0}{\theta} \right] \tag{5.29a}$$

$$D_2 = e^{-0.01t}\left[-\frac{T_1 A(\boldsymbol{X})}{\theta} - \frac{A^T(\boldsymbol{X})T_1}{\theta} + T_1 B R^{-1} B^T T_1\right] \tag{5.29b}$$

Note that we are designing an optimal controller for this highly nonlinear dynamical system with 25 state variables. Conventional optimal control methods are difficult to handle the control problem related with this nonlinear, complex and coupled spacecraft dynamic system. However, the θ-D optimal control technique is particularly useful here since the integrated controller (5.25) can be obtained in a closed-form by virtue of the θ-D algorithm. This closed-form controller facilitates the real-time implementation because it does not demand intensive and iterative computations.

CHAPTER VI

INVERSE OPTIMAL ADAPTIVE CONTROL DESIGN FOR SPACECRAFT PROXIMITY OPERATION

In this chapter, we will redesign the controller by combining an adaptive control approach with an inverse optimal control approach, which is named as the inverse optimal adaptive control (IOAC) method. A controller with analytical form and certain optimality will be derived. Theorem 4.1 will be applied to extend this approach to cases where disturbances and uncertainties are present. The purpose of using the IOAC is to evaluate the indirect robust control method against the adaptive control approach.

6.1 Motivation

When designing the integrated indirect robust control in Chapter 5, the conditions (4.4)-(4.6) on disturbance bounds must be satisfied. Since these conditions are based on the uncertainty bounds, the resultant robust control design may be conservative if these bounds cannot be estimated accurately.

As discussed in the literature review in Section 2.1.2, conventional methods to deal with unknown parametric uncertainties are usually based on adaptive control methods. Adaptive control is different from robust control in that it does not need prior information about the bounds on these uncertain or time-varying parameters. Robust control guarantees that if the changes are within given bounds, the control need not change, while adaptive control adjusts its control gains by updating the knowledge about

the uncertain parameters. Certain update laws for the unknown parameters are designed to explicitly deal with the parametric uncertainties.

In order to alleviate the conservativeness of the indirect robust control method, we propose a new method called the indirect optimal adaptive control (IOAC). The IOAC design combines the advantages of adaptive control, robust control and optimal control. By using the Lyapunov direct method, a parameter estimation update law and a corresponding controller of a special formulation are designed to stabilize the system with parametric uncertainties. Then a modified dynamic feedback control law, together with the original update law, is proved to be capable of minimizing a derived meaningful cost function that penalizes the parameter estimation error and keeps system performance optimal [57, 58, 102]. When the IOAC is combined with the indirect robust control, the IOAC method can be enhanced with robustness to the unknown disturbances.

The IOAC method can circumvent the difficulty of directly solving the Hamilton-Jacobi-Bellman equation since it handles the problem of optimal adaptive control as "adaptive control made optimal" [61]. In other words, the adaptive controller is truly a minimizer of a meaningful cost function but is designed before constructing the performance index. The overall system optimality and stability can be ensured simultaneously.

Comparing with integrated indirect robust control method, the IOAC method shares certain similarities since the indirect robust control also penalizes the disturbance and uncertainties in the performance index.

To evaluate the effect of the conservative bounds and test the performance of the indirect robust control method, we redesign the spacecraft proximity motion controller by IOAC in this chapter. For the spacecraft proximity operations, the system is a relatively

high-dimensional system with coupled nonlinearities and uncertainties. Here we separate the translational motion control and rotational motion control. We use IOAC to design the attitude tracking controller since uncertainties mainly exist in the attitude dynamics, while the indirect robust control method will be applied in the translational controller design.

It is worth noting that this separate design is for the convenience of comparison. No requirement is placed on the convergence order of the translational or attitude motion synchronization.

6.2 Attitude control design

In order to compare the IOAC result with the one from the indirect robust control, we assume that the moment of inertia matrix of the pursuer spacecraft, J_s, is unknown, and the pursuer is under the influence of flexible structure deformation and other un-modeled disturbances when undergoing large angular maneuvers.

Since it is required to have the pursuer spacecraft's docking port face the one on the target, virtual target frame is again used as the reference attitude and the control objective is to synchronize the pursuer's rotational motion with the one of the virtual target. How to generate such a virtual frame from the target frame has been described in Chapter 4. The state vector is chosen to be the same as the one in the previous chapter:

$$\boldsymbol{X} = \left[\boldsymbol{r}_L;\quad \mathbf{v}_L;\quad s_a;\quad \boldsymbol{q}_e;\quad \boldsymbol{\omega}_s;\quad \boldsymbol{r}_{LI};\quad \boldsymbol{s}_1;\quad \boldsymbol{s}_2\right] \tag{6.1}$$

The quaternion error $\boldsymbol{q}_e$, pursuer angular velocity $\boldsymbol{\omega}_s$, and generalized deformation modal coordinate vector $\boldsymbol{\eta} = \boldsymbol{s}_1$ and its time derivative $\dot{\boldsymbol{\eta}} = \boldsymbol{s}_2$ are the spacecraft rotational motion state variables. When external disturbance torque is present, the coupled rotational dynamics are given below as in (5.8), (3.10) and (3.11):

$$\dot{\boldsymbol{q}}_e = \frac{1}{2}\begin{bmatrix} q_{0e}\varepsilon_{\omega t} - q_{1e}\omega_{e_x} - q_{2e}\omega_{e_y} - q_{3e}\omega_{e_z} \\ q_{0e}\omega_{e_x} + q_{1e}\varepsilon_{\omega t} + q_{2e}\omega_{e_z} - q_{3e}\omega_{e_y} \\ q_{0e}\omega_{e_y} - q_{1e}\omega_{e_z} + q_{2e}\varepsilon_{\omega_t} + q_{3e}\omega_{e_x} \\ q_{0e}\omega_{e_z} + q_{1e}\omega_{e_y} - q_{2e}\omega_{e_x} + q_{3e}\varepsilon_{\omega t} \end{bmatrix} \tag{6.2a}$$

$$J_s\dot{\boldsymbol{\omega}}_s + \delta^T\ddot{\boldsymbol{\eta}} = -\boldsymbol{\omega}_s^{\times}J_s\boldsymbol{\omega}_s - \boldsymbol{\omega}_s^{\times}\delta^T\dot{\boldsymbol{\eta}} + \boldsymbol{\Gamma}_s + \boldsymbol{d} \tag{6.2b}$$

$$\ddot{\boldsymbol{\eta}} + C\dot{\boldsymbol{\eta}} + K\boldsymbol{\eta} = -\delta\dot{\boldsymbol{\omega}}_s \tag{6.2c}$$

where $\boldsymbol{d}$ is the external disturbance torque, $\boldsymbol{\omega}_d$ is the virtual target angular velocity, $\boldsymbol{\omega}_e = [\omega_{e_x}\ \omega_{e_y}\ \omega_{e_z}]^T = \boldsymbol{\omega}_s - T_{B_d}^{B_s}\boldsymbol{\omega}_d$ is the angular velocity tracking error, C and K are defined as in (3.13).

For the quaternion kinematics, we separate the quaternion vector part and quaternion scalar part. If we denote $\boldsymbol{q}_e = [q_{e_0}, q_{e_1}, q_{e_2}, q_{e_3}]^T = q_{e_0} + q_{e_1}\boldsymbol{i} + q_{e_2}\boldsymbol{j} + q_{e_3}\boldsymbol{k} = q_{e_s} + \boldsymbol{q}_{e_v}$ where $q_{e_s} = q_{e_0}$ is the scalar part and $\boldsymbol{q}_{e_v}$ is the vector part. Rewrite (6.2a) as:

$$\dot{q}_{e_s} = -\frac{1}{2}\boldsymbol{q}_{e_v}^T\boldsymbol{\omega}_e, \quad \dot{\boldsymbol{q}}_{e_v} = \frac{1}{2}[q_{e_s}I_{3\times 3} + \boldsymbol{q}_{e_v}^{\times}]\boldsymbol{\omega}_e \tag{6.3}$$

In (6.3), $\boldsymbol{q}_{e_v}^{\times}$ is the cross product matrix. As (3.12), for any 3 by 1 vector $\boldsymbol{a} = [a_1, a_2, a_3]^T$, its cross product matrix can be given by:

$$\boldsymbol{a}^{\times} = \begin{bmatrix} 0 & -a_3 & a_2 \\ a_3 & 0 & -a_1 \\ -a_2 & a_1 & 0 \end{bmatrix}$$

The dynamics of the angular velocity tracking error $\boldsymbol{\omega}_e = \boldsymbol{\omega}_s - T_{B_d}^{B_s}\boldsymbol{\omega}_d$ can be derived from Eq. (6.2b):

$$J_s\dot{\boldsymbol{\omega}}_e = -(\boldsymbol{\omega}_e + T_{B_d}^{B_s}\boldsymbol{\omega}_d)^{\times}J_s(\boldsymbol{\omega}_e + T_{B_d}^{B_s}\boldsymbol{\omega}_d) + J_s(\boldsymbol{\omega}_e^{\times}T_{B_d}^{B_s}\boldsymbol{\omega}_d - T_{B_d}^{B_s}\dot{\boldsymbol{\omega}}_d) - \boldsymbol{\omega}_s^{\times}\delta^T\dot{\boldsymbol{\eta}} - \delta^T\ddot{\boldsymbol{\eta}} + \boldsymbol{\Gamma}_s + \boldsymbol{d} \tag{6.4}$$

The transformation matrix $T_{B_d}^{B_s}$ represents attitude transformation from virtual target body frame to the pursuer spacecraft body frame, and can be calculated from the quaternion error:

$$T_{B_d}^{B_s} = 2\boldsymbol{q}_{e_v}\boldsymbol{q}_{e_v}^T - 2q_{e_s}\boldsymbol{q}_{e_v}^{\times} + (q_{e_s}^2 - \boldsymbol{q}_{e_v}^T\boldsymbol{q}_{e_v})I_{3\times 3} \tag{6.5}$$

As discussed in the introduction section, flexible deformation can be suppressed actively by extra actuators on the flexible structure, or can be suppressed by the overall attitude control torque. Here we treat the flexible deformation as the disturbance. If the flexible deformation is too large to keep the system stability, we can adopt the active suppression method reviewed in Chapter 2.

Rewrite (6.4) as:

$$J_s\dot{\boldsymbol{\omega}}_e = -(\boldsymbol{\omega}_e + T_{B_d}^{B_s}\boldsymbol{\omega}_d)^{\times}J_s(\boldsymbol{\omega}_e + T_{B_d}^{B_s}\boldsymbol{\omega}_d) + J_s(\boldsymbol{\omega}_e^{\times}T_{B_d}^{B_s}\boldsymbol{\omega}_d - T_{B_d}^{B_s}\dot{\boldsymbol{\omega}}_d) + \boldsymbol{\Gamma}_s + \boldsymbol{d}_n \tag{6.6}$$

where $\boldsymbol{d}_n = \boldsymbol{d} - \boldsymbol{\omega}_s^{\times}\delta^T\dot{\boldsymbol{\eta}} - \delta^T\ddot{\boldsymbol{\eta}}$ is the lumped uncertainty term.

Combine equations (6.3) and (6.6), we now have the rotational system dynamics:

$$\dot{q}_{e_s} = -\frac{1}{2}\boldsymbol{q}_{e_v}^T\boldsymbol{\omega}_e \tag{6.7a}$$

$$\dot{\boldsymbol{q}}_{e_v} = \frac{1}{2}[q_{e_s}\boldsymbol{I}_{3\times 3} + \boldsymbol{q}_{e_v}^{\times}]\boldsymbol{\omega}_e \tag{6.7b}$$

$$J_s\dot{\boldsymbol{\omega}}_e = -(\boldsymbol{\omega}_e + T_{B_d}^{B_s}\boldsymbol{\omega}_d)^{\times}J_s(\boldsymbol{\omega}_e + T_{B_d}^{B_s}\boldsymbol{\omega}_d) + J_s(\boldsymbol{\omega}_e^{\times}T_{B_d}^{B_s}\boldsymbol{\omega}_d - T_{B_d}^{B_s}\dot{\boldsymbol{\omega}}_d) + \boldsymbol{\Gamma}_s + \boldsymbol{d}_n \tag{6.7c}$$

First, we will follow the steps of the IOAC scheme [59] to find the stabilizing controller for the system with the moment of inertia uncertainty. Then we will prove using the indirect robust control method that this controller is also robust to the disturbance of $\boldsymbol{d}_n$.

Error quaternion dynamic system (6.7) is a typical cascaded system in which the quaternion kinematics can be considered as a subsystem with $\boldsymbol{\omega}_e$ as the control input. The typical backstepping procedure can be applied in the next two sections to find the required stabilizing controller for the system (6.7).

6.2.1 Quaternion kinematic subsystem

For the quaternion kinematics, if we treat $\boldsymbol{\omega}_e$ as a virtual control $\boldsymbol{\omega}_v$ for the subsystem (6.7a) and (6.7b), we can prove that if $\boldsymbol{\omega}_v = -K_n \boldsymbol{q}_{e_v}$, where K_n is any positive definite matrix, the system quaternion will converges to $\boldsymbol{q}_{e_0} = [1,0,0,0]^T$ asymptotically.

To justify this, first we will show that by using $\boldsymbol{\omega}_v = -K_n \boldsymbol{q}_{e_v}$ as virtual control, $\boldsymbol{q}_{e_s}$ goes to 1 as t goes to ∞ whenever $q_{e_s}(0) \neq -1$. Let k_1 and k_2 be the minimum and maximum eigenvalue of K_n, respectively. When $\boldsymbol{\omega}_e = \boldsymbol{\omega}_v = -K_n \boldsymbol{q}_{e_v}$, it is obvious that:

$$\frac{1}{2}k_1(1-q_{e_s}^2) \leq \dot{q}_{e_s} = \frac{1}{2}\boldsymbol{q}_{e_v}^T K_n \boldsymbol{q}_{e_v} \leq \frac{1}{2}k_2(1-q_{e_s}^2)$$

From the comparison principle [155]:

$$1-\frac{2[1-q_{e_s}(0)]e^{-k_1 t}}{1+q_{e_s}(0)+[1-q_{e_s}(0)]e^{-k_1 t}} \leq q_{e_s}(t) \leq 1-\frac{2[1-q_{e_s}(0)]e^{-k_2 t}}{1+q_{e_s}(0)+[1-q_{e_s}(0)]e^{-k_2 t}}\ , \text{ for all } t \geq 0\,.$$

Hence $q_{e_s}(t) = -1$ for all t if $q_{e_s}(0) = -1$. In addition, we have $q_{e_s}(t) > 0$ for all t that satisfies $t \geq \max\{0, k_1^{-1}\ln[(1-q_{e_s}(0))/(1+q_{e_s}(0))]\}$ with $\lim_{t\to\infty} q_{e_s}(t) = 1$. Now, we have $\lim_{t\to\infty} q_{e_s}(t) = 1, \forall q_{e_s}(0) \neq -1$. We also can derive $\lim_{t\to\infty} \boldsymbol{q}_{e_v}(t) = 0_{3\times 1}$. Notice that $[-1,0,0,0]^T$ represents the same attitude as $\boldsymbol{q}_{e_0} = [1,0,0,0]^T$

Furthermore, using the direct Lyapunov method, we can prove that the error quaternion $\boldsymbol{q}_{e_0} = [1,0,0,0]^T$ is globally asymptotic stable when $\boldsymbol{\omega}_e = \boldsymbol{\omega}_v = -K_n \boldsymbol{q}_{e_v}$. Select the Lyapunov function:

$$V_q = \boldsymbol{q}_{e_v}^T \boldsymbol{q}_{e_v} + (1 - q_{e_s})^2$$

Its time derivative under $\boldsymbol{\omega}_v$ is:

$$\dot{V}_q = \boldsymbol{q}_{e_v}^T \boldsymbol{\omega}_e = -\boldsymbol{q}_{e_v}^T K_n \boldsymbol{q}_{e_v} \leq 0$$

Thus the global asymptotical stability of $\boldsymbol{q}_{e_0} = [1,0,0,0]^T$ is ensured when $\boldsymbol{\omega}_e = \boldsymbol{\omega}_v = -K_n \boldsymbol{q}_{e_v}$.

6.2.2 Adaptive attitude control using the IOAC

We first consider attitude control system with the moment of inertia uncertainty. The lumped disturbance will be added in the next section.

The unknown pursuer spacecraft moment of inertia is a symmetric matrix:

$$J_s = \begin{bmatrix} J_s(1,1) & J_s(1,2) & J_s(1,3) \\ J_s(1,2) & J_s(2,2) & J_s(2,3) \\ J_s(1,3) & J_s(2,3) & J_s(3,3) \end{bmatrix}$$

Rewrite the element of J_s into a vector form:

$$\boldsymbol{P} = [J_s(1,1), J_s(2,2), J_s(3,3), J_s(2,3), J_s(1,3), J_s(1,2)]^T$$

Denote the function L that satisfies:

$$J_s \boldsymbol{a} = L(\boldsymbol{a})\boldsymbol{P}, \quad L(\boldsymbol{a}) = \begin{bmatrix} a_1 & 0 & 0 & 0 & a_3 & a_2 \\ 0 & a_2 & 0 & a_3 & 0 & a_1 \\ 0 & 0 & a_3 & a_2 & a_1 & 0 \end{bmatrix}$$

where $\boldsymbol{a}$ is any 3 by 1 vector $\boldsymbol{a} = [a_1, a_2, a_3]^T$. Based on the above relationship, we may get the value of J_s if we have the value of $\boldsymbol{P}$.

Let $\hat{\boldsymbol{P}}$ denote the estimated value for $\boldsymbol{P}$, $\hat{J}_s$ denote the estimated value for J_s, and $\tilde{\boldsymbol{P}}$ and $\tilde{J}_s$ be the estimation error, i.e. $\tilde{\boldsymbol{P}} = \boldsymbol{P} - \hat{\boldsymbol{P}}, \tilde{J}_s = J_s - \hat{J}_s$. We make the following transformations:

$$\boldsymbol{z} = \boldsymbol{\omega}_e - \boldsymbol{\omega}_v = \boldsymbol{\omega}_e + K_n \boldsymbol{q}_{e_v}, \quad \boldsymbol{\Gamma}_e = \boldsymbol{\Gamma}_s + (-\boldsymbol{\omega}_d^{\times} L(\boldsymbol{\omega}_d) - L(\dot{\boldsymbol{\omega}}_d))\hat{\boldsymbol{P}} \tag{6.8}$$

where K_n is any positive definite matrix, $\boldsymbol{\omega}_v$ is the stabilizing virtual control as in the Section 6.1.1.

Rewrite (6.7c) into the following form:

$$J_s \dot{\boldsymbol{z}} = [F(q_{e_s}, \boldsymbol{q}_{e_v}, \boldsymbol{\omega}_e, \boldsymbol{\omega}_d, \dot{\boldsymbol{\omega}}_d) + G(q_{e_s}, \boldsymbol{q}_{e_v}, \boldsymbol{\omega}_e)]\boldsymbol{P} + H(\boldsymbol{\omega}_d, \dot{\boldsymbol{\omega}}_d)\tilde{\boldsymbol{P}} + \boldsymbol{\Gamma}_e \tag{6.9}$$

where:

$$\begin{aligned} F(q_{e_s}, \boldsymbol{q}_{e_v}, \boldsymbol{\omega}_e, \boldsymbol{\omega}_d, \dot{\boldsymbol{\omega}}_d) = {} & L(\boldsymbol{\omega}_e^{\times} T\boldsymbol{\omega}_d) - (\boldsymbol{\omega}_e + T\boldsymbol{\omega}_d)^{\times} L(\boldsymbol{\omega}_e) - (\boldsymbol{\omega}_e + T_1\boldsymbol{\omega}_d) \times L(T\boldsymbol{\omega}_d) \\ & - \boldsymbol{\omega}_d^{\times} L(T_1\boldsymbol{\omega}_d) - L(T_1\dot{\boldsymbol{\omega}}_d) \end{aligned} \tag{6.10a}$$

$$G(q_{e_s}, \boldsymbol{q}_{e_v}, \boldsymbol{\omega}_e) = \frac{1}{2} L(K_n(q_{e_s} I_{3\times 3} + \boldsymbol{q}_{e_v}^{\times})\boldsymbol{\omega}_e) \tag{6.10b}$$

$$H(\boldsymbol{\omega}_d, \dot{\boldsymbol{\omega}}_d) = -\boldsymbol{\omega}_d^{\times} L(\boldsymbol{\omega}_d) - L(\dot{\boldsymbol{\omega}}_d) \tag{6.10c}$$

and $T = T_{B_d}^{B_s}, T_1 = T - I_{3\times 3} = 2\boldsymbol{q}_{e_v}\boldsymbol{q}_{e_v}^T - 2q_{e_s}\boldsymbol{q}_{e_v}^{\times} - 2\boldsymbol{q}_{e_v}^T\boldsymbol{q}_{e_v} I_{3\times 3}$.

By these equations, we transfer the attitude synchronization problem (6.7a), (6.7b) and (6.9) to the stabilization problem:

$$\dot{q}_{e_s} = -\frac{1}{2}\boldsymbol{q}_{e_v}^T \boldsymbol{\omega}_e \tag{6.11a}$$

$$\dot{\boldsymbol{q}}_{e_v} = \frac{1}{2}[q_{e_s} I_{3\times 3} + \boldsymbol{q}_{e_v}^{\times}]\boldsymbol{\omega}_e \tag{6.11b}$$

$$J_s \dot{\boldsymbol{z}} = [F(q_{e_s}, \boldsymbol{q}_{e_v}, \boldsymbol{\omega}_e, \boldsymbol{\omega}_d, \dot{\boldsymbol{\omega}}_d) + G(q_{e_s}, \boldsymbol{q}_{e_v}, \boldsymbol{\omega}_e)]\boldsymbol{P} + H(\boldsymbol{\omega}_d, \dot{\boldsymbol{\omega}}_d)\tilde{\boldsymbol{P}} + \boldsymbol{\Gamma}_e \tag{6.11c}$$

The system state vector is defined as $\boldsymbol{x}_r \triangleq [q_{e_s} \ \boldsymbol{q}_{e_v}^T \ \boldsymbol{z}^T]^T$.

We also need to make a reasonable assumption on the target angular velocity:

Assumption 6.1: The desired angular velocity $\boldsymbol{\omega}_d$ and its time derivative $\dot{\boldsymbol{\omega}}_d$ are bounded for all $t \geq 0$.

The following theorem gives the adaptive control law:

Theorem 6.1: For the unperturbed rotational system (6.11), $\boldsymbol{d}_n = \mathbf{0}$, under the assumption 6.1, the system can be stabilized asymptotically with the feedback control law:

$$\boldsymbol{\Gamma}_e = -R_{rot}(q_{e_s}, \boldsymbol{q}_{e_v}, \boldsymbol{\omega}_e, \hat{\boldsymbol{P}}, \boldsymbol{\omega}_d, \dot{\boldsymbol{\omega}}_d)^{-1}(\boldsymbol{\omega}_e + K_n \boldsymbol{q}_{e_v}) \tag{6.12}$$

and update law:

$$\dot{\hat{\boldsymbol{P}}} = \gamma \times [F(q_{e_s}, \boldsymbol{q}_{e_v}, \boldsymbol{\omega}_e, \boldsymbol{\omega}_d, \dot{\boldsymbol{\omega}}_d) + G(q_{e_s}, \boldsymbol{q}_{e_v}, \boldsymbol{\omega}_e) + H(\boldsymbol{\omega}_d, \dot{\boldsymbol{\omega}}_d)]^T (\boldsymbol{\omega}_e + K_n \boldsymbol{q}_{e_v}) \tag{6.13}$$

where matrices *F*, *G* and *H* are given in (6.10)

$$R_{rot}^{-1} = K_1 + \frac{\Psi_1^T \Psi_1}{2} + \frac{\Psi_2^T K_1^{-1} \Psi_2}{2} \tag{6.14a}$$

$$\begin{aligned} \Psi_1 = c^{-1/2} K^{1/2} [&(\boldsymbol{\omega}_e + T\boldsymbol{\omega}_d)^{\times} \hat{J}_s + \hat{J}_s (T\boldsymbol{\omega}_d)^{\times} - (\hat{J}_s T\boldsymbol{\omega}_d)^{\times} - 0.5 \hat{J}_s K (q_{e_s} I_{3\times 3} + \boldsymbol{q}_{e_v}^{\times}) + cK^{-1} \\ &+ (\hat{J}_s T\boldsymbol{\omega}_d)^{\times} T_2 K^{-1} - \boldsymbol{\omega}_d^{\times} \hat{J}_s T_2 K^{-1} - \hat{J}_s T_3 K^{-1}]^T \end{aligned} \tag{6.14b}$$

$$\Psi_2 = \frac{1}{2} \hat{J}_s K (q_{e_s} I_{3\times 3} + \boldsymbol{q}_{e_v}^{\times}) - \boldsymbol{\omega}_e^{\times} \hat{J}_s \tag{6.14c}$$

$$T_2 = 2\boldsymbol{q}_{e_v}^T \boldsymbol{\omega}_d I_{3\times 3} - 2\boldsymbol{\omega}_d \boldsymbol{q}_{e_v}^T + 2q_{e_s} \boldsymbol{\omega}_d^{\times} \tag{6.14d}$$

$$T_3 = 2\boldsymbol{q}_{e_v}^T \dot{\boldsymbol{\omega}}_d I_{3\times 3} - 2\dot{\boldsymbol{\omega}}_d \boldsymbol{q}_{e_v}^T + 2q_{e_s} \dot{\boldsymbol{\omega}}_d^{\times} \tag{6.14e}$$

K_n, K_1 , and γ are positive definite and constant matrices, and $c > 0$.

Proof:

To validate that the controller (6.12) with the update law (6.13) can stabilize the rotational system (6.11), we propose the following control Lyapunov function candidate:

$$V = c\boldsymbol{q}_{e_v}^T \boldsymbol{q}_{e_v} + c(1 - q_{e_s})^2 + \frac{1}{2} \boldsymbol{z}^T J_s \boldsymbol{z} + \frac{1}{2} \tilde{\boldsymbol{P}}^T \gamma^{-1} \tilde{\boldsymbol{P}} \tag{6.15}$$

Its time derivative can be calculated by:

$$\begin{aligned}\dot{V} &= 2c\boldsymbol{q}_{e_v}^T\dot{\boldsymbol{q}}_{e_v} - 2c(1-q_{e_s})\dot{q}_{e_s} + \boldsymbol{z}^T J_s\dot{\boldsymbol{z}} + \tilde{\boldsymbol{P}}^T\gamma^{-1}\dot{\tilde{\boldsymbol{P}}} \\ &= c\boldsymbol{q}_{e_v}^T(\boldsymbol{z} - K_n\boldsymbol{q}_{e_v}) + \boldsymbol{z}^T[\boldsymbol{\Gamma}_e + (F+G)\hat{\boldsymbol{P}}] + \boldsymbol{z}^T[H\tilde{\boldsymbol{P}} + (F+G)\tilde{\boldsymbol{P}}] - \boldsymbol{z}^T(F+G+H)\tilde{\boldsymbol{P}} \\ &= -c\boldsymbol{q}_{e_v}^T K\boldsymbol{q}_{e_v} + \boldsymbol{z}^T[c\boldsymbol{q}_{e_v} + \boldsymbol{\Gamma}_e + (F+G)\hat{\boldsymbol{P}}]\end{aligned} \tag{6.16}$$

We may choose $\boldsymbol{\Gamma}_e$ to cancel all the nonlinearities in the $\dot{V}$ so that $\dot{V} \le 0$, but as stated in Chapter 2, controllers based on nonlinearity cancellation are in general non-optimal. Here in our derivation, to achieve inverse optimality, the preferred controller $\boldsymbol{\Gamma}_e$ is required to have certain mathematical formulation as (6.12). To design such controller, we rewrite (6.16) and complete the square.

Apply (6.10) to (6.16), we have:

$$\begin{aligned}\dot{V} &= -c\boldsymbol{q}_{e_v}^T K_n\boldsymbol{q}_{e_v} + \boldsymbol{z}^T[c\boldsymbol{q}_{e_v} + \boldsymbol{\Gamma}_e - (\boldsymbol{\omega}_e + T\boldsymbol{q}_{e_v})^\times\hat{J}_s(\boldsymbol{z} - K_n\boldsymbol{q}_{e_v}) + (\hat{J}_s T\boldsymbol{\omega}_d)^\times(\boldsymbol{z} - K_n\boldsymbol{q}_{e_v}) - \hat{J}_s T_1\dot{\boldsymbol{\omega}}_d \\ &\quad -\hat{J}_s(T\boldsymbol{\omega}_d)^\times(\boldsymbol{z} - K_n\boldsymbol{q}_{e_v}) + \frac{1}{2}\hat{J}_s K_n(q_{e_s}I_{3\times3} + \boldsymbol{q}_{e_v}^\times)(\boldsymbol{z} - K_n\boldsymbol{q}_{e_v}) - \boldsymbol{\omega}_d^\times\hat{J}_s T_1\boldsymbol{\omega}_d + (\hat{J}_s T\boldsymbol{\omega}_d)^\times T_1\boldsymbol{\omega}_d] \\ &= \boldsymbol{z}^T\boldsymbol{\Gamma}_e - c\boldsymbol{q}_{e_v}^T K\boldsymbol{q}_{e_v} \\ &\quad +\boldsymbol{z}^T[cK^{-1} + (\boldsymbol{\omega}_e + T\boldsymbol{q}_{e_v})^\times\hat{J}_s - (\hat{J}_s T\boldsymbol{\omega}_d)^\times - \frac{1}{2}\hat{J}_s K_n(q_{e_s}I_{3\times3} + \boldsymbol{q}_{e_v}^\times) + \hat{J}_s(T\boldsymbol{\omega}_d)^\times]K_n\boldsymbol{q}_{e_v} \\ &\quad +\boldsymbol{z}^T[\frac{1}{2}\hat{J}_s K_n(q_{e_s}I_{3\times3} + \boldsymbol{q}_{e_v}^\times) - \boldsymbol{\omega}_e^\times\hat{J}_s]\boldsymbol{z} + \boldsymbol{z}^T[(\hat{J}_s\boldsymbol{\omega}_d)^\times - (T\boldsymbol{\omega}_d)^\times\hat{J}_s - \hat{J}_s(T\boldsymbol{\omega}_d)^\times]\boldsymbol{z} \\ &\quad +\boldsymbol{z}^T[-\boldsymbol{\omega}_d^\times\hat{J}_s + (\hat{J}_s T\boldsymbol{\omega}_d)^\times]T_1\boldsymbol{\omega}_d - \boldsymbol{z}^T\hat{J}_s T_1\dot{\boldsymbol{\omega}}_d\end{aligned} \tag{6.17}$$

Note that it is easy to verify that $[(\hat{J}_s\boldsymbol{\omega}_d)^\times - (T\boldsymbol{\omega}_d)^\times\hat{J}_s - \hat{J}_s(T\boldsymbol{\omega}_d)^\times]$ is a skew-symmetric matrix. Thus term $\boldsymbol{z}^T[(\hat{J}_s\boldsymbol{\omega}_d)^\times - (T\boldsymbol{\omega}_d)^\times\hat{J}_s - \hat{J}_s(T\boldsymbol{\omega}_d)^\times]\boldsymbol{z} = 0$.

Inspecting the terms in (6.17), we can regroup the RHS into several groups: $\boldsymbol{q}_{e_v}^T(\bullet)\boldsymbol{q}_{e_v}$, $\boldsymbol{z}^T(\bullet)\boldsymbol{q}_{e_v}$, $\boldsymbol{z}^T(\bullet)\boldsymbol{z}$, $\boldsymbol{z}^T\boldsymbol{\Gamma}_e$, $\boldsymbol{z}^T(\bullet)\boldsymbol{\omega}_d$, and $\boldsymbol{z}^T(\bullet)\dot{\boldsymbol{\omega}}_d$. Here $(\bullet)$ represents the omitted matrices in these terms. Using (6.14d) and (6.14e), we have:

$$T_1\boldsymbol{\omega}_d = T_2\boldsymbol{q}_{e_v}, \quad T_1\dot{\boldsymbol{\omega}}_d = T_3\boldsymbol{q}_{e_v} \tag{6.18}$$

so that terms $\boldsymbol{z}^T(\bullet)\boldsymbol{\omega}_d$ and $\boldsymbol{z}^T(\bullet)\dot{\boldsymbol{\omega}}_d$ can be transformed to $\boldsymbol{z}^T(\bullet)\boldsymbol{q}_{e_v}$.

Using (6.18) into the corresponding terms in (6.17) and after a series of manipulations, we can get:

$$\begin{aligned}\dot{V} &= \boldsymbol{z}^T\boldsymbol{\Gamma}_e - c\boldsymbol{q}_{e_v}^T K_n \boldsymbol{q}_{e_v} \\ &+\boldsymbol{z}^T[cK_n^{-1} + (\boldsymbol{\omega}_e + T\boldsymbol{q}_{e_v})^{\times}\hat{J}_s - (\hat{J}_s T\boldsymbol{\omega}_d)^{\times} - \frac{1}{2}\hat{J}_s K_n(q_{e_s} I_{3\times 3} + \boldsymbol{q}_{e_v}^{\times}) + \hat{J}_s(T\boldsymbol{\omega}_d)^{\times} \\ &-\boldsymbol{\omega}_d^{\times}\hat{J}_s T_2 K_n^{-1} + (\hat{J}_s T\boldsymbol{\omega}_d)^{\times} T_2 K_n^{-1} - \hat{J}_s T_3 K_n^{-1}]K_n\boldsymbol{q}_{e_v} \\ &+\boldsymbol{z}^T[\frac{1}{2}\hat{J}_s K_n(q_{e_s} I_{3\times 3} + \boldsymbol{q}_{e_v}^{\times}) - \boldsymbol{\omega}_e^{\times}\hat{J}_s]\boldsymbol{z}\end{aligned}$$

Now using Ψ_1 and Ψ_2 defined in (6.14b) and (6.14c) into the above equation leads to:

$$\dot{V} = \boldsymbol{z}^T\boldsymbol{\Gamma}_e - c\boldsymbol{q}_{e_v}^T K_n \boldsymbol{q}_{e_v} + c^{1/2}\boldsymbol{z}^T\Psi_1^T K_n^{1/2}\boldsymbol{q}_{e_v} + \boldsymbol{z}^T\Psi_2\boldsymbol{z} \tag{6.19}$$

Then utilizing (6.12) and (6.14a), we can complete the square:

$$\begin{aligned}\dot{V} &= -\frac{c}{2}\boldsymbol{q}_{e_v}^T K_n \boldsymbol{q}_{e_v} - \frac{1}{2}\boldsymbol{z}^T K_1 \boldsymbol{z} - \frac{1}{2}\left\| c^{1/2}K_n^{1/2}\boldsymbol{q}_{e_v} - \Psi_1\boldsymbol{z}\right\|^2 - \frac{1}{2}\boldsymbol{z}^T(K_1 - \Psi_2)^T K_1^{-1}(K_1 - \Psi_2)\boldsymbol{z} \\ &\le -\frac{c}{2}\boldsymbol{q}_{e_v}^T K_n \boldsymbol{q}_{e_v} - \frac{1}{2}\boldsymbol{z}^T K_1 \boldsymbol{z}\end{aligned} \tag{6.20}$$

Thus, we can conclude that function $\dot{V}$ is negative semi-definite, K_1 is a positive definite matrix and symmetric. Besides, the control Lyapunov function $V(x)$ is bounded below by $V(q_{e_s}, \boldsymbol{q}_{e_v}, \boldsymbol{z}, \hat{\boldsymbol{P}}, t) \le V(q_{e_s}, \boldsymbol{q}_{e_v}, \boldsymbol{z}, \hat{\boldsymbol{P}}, 0)$ for all $t > 0$.

Using Barbalat's Lemma[156], we can conclude that $\dot{V} \to 0$ as $t \to \infty$. Based on (6.20), we have $\boldsymbol{q}_{e_v} \to \boldsymbol{0}$ and $\boldsymbol{z} \to \boldsymbol{0}$ as $t \to \infty$. It is easy to derive $\boldsymbol{\omega}_e \to \boldsymbol{0}$ and $q_{e_s} \to 1$. Thus the dynamic feedback control law (6.12) with update law (6.13) stabilized the rotational system. Besides, based on (6.13), parameter estimation error $\hat{\boldsymbol{P}} \to \boldsymbol{0}$ as $t \to 0$. □

Based on *Theorem* 6.1 and inverse optimal adaptive control theory, we may construct a meaningful optimal performance index and a modified controller so that the modified controller will possess both stability and optimality for the original attitude control system.

To demonstrate the optimality, we propose the following theorem:

Theorem 6.2: For the unperturbed system with Assumption 6.1, the feedback control law:

$$\boldsymbol{\Gamma}_e^{'} = \beta_n \boldsymbol{\Gamma}_e = -\beta_n R_{rot}(q_{e_s}, \boldsymbol{q}_{e_v}, \boldsymbol{\omega}_e, \hat{\boldsymbol{P}}, \boldsymbol{\omega}_d, \dot{\boldsymbol{\omega}}_d)^{-1}(\boldsymbol{\omega}_e + K_n \boldsymbol{q}_{e_v}) \tag{6.21}$$

with the same update law as (6.13):

$$\dot{\hat{\boldsymbol{P}}} = \gamma \times [F(q_{e_s}, \boldsymbol{q}_{e_v}, \boldsymbol{\omega}_e, \boldsymbol{\omega}_d, \dot{\boldsymbol{\omega}}_d) + G(q_{e_s}, \boldsymbol{q}_{e_v}, \boldsymbol{\omega}_e) + H(\boldsymbol{\omega}_d, \dot{\boldsymbol{\omega}}_d)]^T (\boldsymbol{\omega}_e + K_n \boldsymbol{q}_{e_v}) \tag{6.22}$$

where $\beta_n \geq 2$, stabilizes the attitude system (6.11) and at the same time, minimizes the cost function:

$$J_a = \lim_{t\to\infty}\left\{ \beta_n \left\| \tilde{\boldsymbol{P}}(t) \right\|_{\gamma^{-1}}^2 + 4\beta_n c[1 - q_{e_s}(t)] + \int_0^t (l(q_{e_s}, \boldsymbol{q}_{e_v}, \boldsymbol{\omega}_e, \hat{\boldsymbol{P}}, \boldsymbol{\omega}_d, \dot{\boldsymbol{\omega}}_d) + \boldsymbol{\Gamma}_e^{'T} R_{rot} \boldsymbol{\Gamma}_e^{'}) dt \right\} \tag{6.23a}$$

where:

$$\begin{aligned} l(q_{e_s}, \boldsymbol{q}_{e_v}, \boldsymbol{\omega}_e, \hat{\boldsymbol{P}}, \boldsymbol{\omega}_d, \dot{\boldsymbol{\omega}}_d) = & -2\beta_n [c \boldsymbol{q}_{e_v}^T \boldsymbol{\omega}_e + (\boldsymbol{\omega}_e + K_n \boldsymbol{q}_{e_v})^T (F + G) \hat{\boldsymbol{P}}] \\ & + \beta_n^2 (\boldsymbol{\omega}_e + K_n \boldsymbol{q}_{e_v})^T R_{rot}^{-1} (\boldsymbol{\omega}_e + K_n \boldsymbol{q}_{e_v}) \end{aligned} \tag{6.23b}$$

c is any positive constant number, R_{rot} is defined in (6.14). As in (6.13), γ is a selected positive definite matrix.

Proof:

To prove that the controller can stabilize the nominal system, we use the same control Lyapunov candidate (6.15) as in *Theorem* 6.1. When we replace (6.12) with (6.21), the time derivative of (6.19) can be rewritten as:

$$\begin{aligned}\dot{V} &= \boldsymbol{z}^T\boldsymbol{\Gamma}_e' - c\boldsymbol{q}_{e_v}^T K\boldsymbol{q}_{e_v} + c^{1/2}\boldsymbol{z}^T\Psi_1^T K^{1/2}\boldsymbol{q}_{e_v} + \boldsymbol{z}^T\Psi_2\boldsymbol{z} \\ &= (\beta_n - 1)\boldsymbol{z}^T\boldsymbol{\Gamma}_e + \boldsymbol{z}^T\boldsymbol{\Gamma}_e - c\boldsymbol{q}_{e_v}^T K\boldsymbol{q}_{e_v} + c^{1/2}\boldsymbol{z}^T\Psi_1^T K^{1/2}\boldsymbol{q}_{e_v} + \boldsymbol{z}^T\Psi_2\boldsymbol{z}\end{aligned}$$

Note that $(\beta_n - 1)\boldsymbol{z}^T\boldsymbol{\Gamma}_e = -(\beta_n - 1)\boldsymbol{z}^T R_{rot}^{-1}\boldsymbol{z}$. The remaining term is proven to be less than or equal to $-\frac{c}{2}\boldsymbol{q}_{e_v}^T K\boldsymbol{q}_{e_v} - \frac{1}{2}\boldsymbol{z}^T K_1\boldsymbol{z}$ in (6.20). Following the same procedure in *Theorem* 6.1, we can see that the feedback control law (6.21) is able to stabilize the nominal system (6.11) and thus, $\boldsymbol{z} \to \boldsymbol{0}, \boldsymbol{q}_{e_v} \to 0$ as $t \to \infty$.

To prove the optimality, first we will prove that the cost function (6.23) is meaningful. From the proof of *Theorem* 6.1, we use the equation (6.16) and transform it to:

$$\begin{aligned}\dot{V} &= -c\boldsymbol{q}_{e_v}^T K\boldsymbol{q}_{e_v} + \boldsymbol{z}^T[c\boldsymbol{q}_{e_v} + \boldsymbol{\Gamma}_e + (F+G)\hat{\boldsymbol{P}}] \\ &= -c\boldsymbol{q}_{e_v}^T K\boldsymbol{q}_{e_v} + c\boldsymbol{q}_{e_v}^T\boldsymbol{z} - \boldsymbol{z}^T R_{rot}^{-1}\boldsymbol{z} + \boldsymbol{z}^T(F+G)\hat{\boldsymbol{P}} \\ &= c\boldsymbol{q}_{e_v}^T\boldsymbol{\omega}_e + \boldsymbol{z}^T[(F+G)\hat{\boldsymbol{P}} - R^{-1}\boldsymbol{z}]\end{aligned}$$

Here we still use $\boldsymbol{\Gamma}_e$ rather than $\boldsymbol{\Gamma}_e'$ since all we need is the inequality (6.20): $\dot{V} \le -k_0\left\|[\boldsymbol{q}_{e_v}, \boldsymbol{z}]\right\|^2 \le -W(\boldsymbol{x}_r)$, where $W(\boldsymbol{x}_r)$ is a positive definite function.

Thus we have:

$$c\boldsymbol{q}_{e_v}^T\boldsymbol{\omega}_e + \boldsymbol{z}^T[(F+G)\hat{\boldsymbol{P}} - R_{rot}^{-1}\boldsymbol{z}] \le -W(\boldsymbol{x}_r) \tag{6.24}$$

Comparing (6.24) with *l* in (6.23b) and using $\beta_n \ge 2$, we can get:

$$l(q_{e_s}, \boldsymbol{q}_{e_v}, \boldsymbol{\omega}_e, \hat{\boldsymbol{P}}, \boldsymbol{\omega}_d, \dot{\boldsymbol{\omega}}_d) \ge 2\beta_n W(\boldsymbol{x}_r) + \beta_n(\beta - 2)(\boldsymbol{\omega}_e + K_n\boldsymbol{q}_{e_v})^T R_{rot}^{-1}(\boldsymbol{\omega}_e + K_n\boldsymbol{q}_{e_v}) \tag{6.25}$$

The right-hand-side is a positive value. Therefore, the cost function J_a (6.22a) is a meaningful performance index.

To prove that the controller (6.21) minimizes the performance index (6.23), we denote the error controller as:

$$\boldsymbol{\Gamma}_0 = \boldsymbol{\Gamma}'_e - [-\beta_n R_{rot}^{-1}(\boldsymbol{\omega}_e + K_n \boldsymbol{q}_{e_v})] = \boldsymbol{\Gamma}'_e + \beta_n R_{rot}^{-1}(\boldsymbol{\omega}_e + K_n \boldsymbol{q}_{e_v})$$

If the controller can get minimum performance index value at $\boldsymbol{\Gamma}_0 = \mathbf{0}$, *Theorem* 6.2 can be proved.

Replace $\boldsymbol{\Gamma}_0$ with corresponding term in (6.23):

$$J_a = \lim_{t\to\infty}\left\{\beta_n \left\|\tilde{\boldsymbol{P}}(t)\right\|^2_{\gamma^{-1}} + 4\beta_n c[1-q_{e_s}(t)] + \int_0^t (l + \boldsymbol{\Gamma}'^T_e R_{rot} \boldsymbol{\Gamma}'_e)dt\right\}$$

$$= \lim_{t\to\infty}\left\{\begin{array}{l}\beta_n \left\|\tilde{\boldsymbol{P}}(t)\right\|^2_{\gamma^{-1}} + 4\beta_n c[1-q_{e_s}(t)] \\ \qquad + \int_0^t [-2\beta_n (c\boldsymbol{q}^T_{e_v}\boldsymbol{\omega}_e + \boldsymbol{z}^T(F+G)\hat{\boldsymbol{P}}) + \beta_n^2 \boldsymbol{z}^T R_{rot}^{-1}\boldsymbol{z} + \boldsymbol{\Gamma}'^T_e R_{rot}\boldsymbol{\Gamma}'_e]dt\end{array}\right\}$$

Inspect the terms inside the integration part:

$$\begin{aligned}
&-2\beta_n(c\boldsymbol{q}^T_{e_v}\boldsymbol{\omega}_e + \boldsymbol{z}^T(F+G)\hat{\boldsymbol{P}}) + \beta_n^2 \boldsymbol{z}^T R_{rot}^{-1}\boldsymbol{z} + \boldsymbol{\Gamma}'^T_e R_{rot}\boldsymbol{\Gamma}' \\
&\quad = -2\beta_n(c\boldsymbol{q}^T_{e_v}\boldsymbol{\omega}_e + \boldsymbol{z}^T(F+G)\hat{\boldsymbol{P}}) + \beta_n^2 \boldsymbol{z}^T R_{rot}^{-1}\boldsymbol{z} + (\boldsymbol{\Gamma}_0 - \beta_n R_{rot}^{-1}\boldsymbol{z})^T R_{rot}(\boldsymbol{\Gamma}_0 - \beta_n R_{rot}^{-1}\boldsymbol{z}) \\
&\quad = -\beta_n[\boldsymbol{z}^T(\boldsymbol{\Gamma}_0 - \beta_n R_{rot}^{-1}\boldsymbol{z}) + \beta_n \boldsymbol{z}^T R_{rot}^{-1}\boldsymbol{z} - \boldsymbol{\Gamma}_0^T \boldsymbol{z}] \\
&\qquad -2\beta_n[c\boldsymbol{q}^T_{e_v}\boldsymbol{\omega}_e + \boldsymbol{z}^T[(F+G)\boldsymbol{P} + H\tilde{\boldsymbol{P}} + \boldsymbol{\Gamma}'_e] - \boldsymbol{z}^T(F+G+H)\tilde{\boldsymbol{P}}] + \boldsymbol{\Gamma}_0^T R_{rot}\boldsymbol{\Gamma}_0 \\
&\quad = -2\beta_n \frac{d}{dt}\left(c(1-q_{e_s})^2 + c\boldsymbol{q}^T_{e_v}\boldsymbol{q}_{e_v} + \frac{1}{2}\boldsymbol{z}^T J_s \boldsymbol{z}\right) - \beta_n \frac{d}{dt}(\tilde{\boldsymbol{P}}^T\gamma^{-1}\tilde{\boldsymbol{P}}) + \boldsymbol{\Gamma}_0^T R_{rot}\boldsymbol{\Gamma}_0
\end{aligned}$$

Using the above equation in J_a and rearranging the terms lead to:

$$J_a = \beta_n[\tilde{\boldsymbol{P}}^T\gamma^{-1}\tilde{\boldsymbol{P}}]\Big|_{t=0} + 4\beta_n c[1-q_{es}(0)] + \beta_n[\boldsymbol{z}^T J_s \boldsymbol{z}]\Big|_{t=0} - \beta_n[\boldsymbol{z}^T J_s \boldsymbol{z}]\Big|_{t\to\infty} + \int_0^\infty \boldsymbol{\Gamma}_0^T R_{rot}\boldsymbol{\Gamma}_0 dt$$

We have proved that (6.21) stabilizes the nominal system and $\beta_n[\boldsymbol{z}^T J_s \boldsymbol{z}]\Big|_{t\to\infty} = 0$. Hence the minimum value of J_a is only reached when $\boldsymbol{\Gamma}_0 = \mathbf{0}$, or $\boldsymbol{\Gamma}'_e = \beta_n \boldsymbol{\Gamma}_e$. *Theorem* 6.2 is thus proved. □

6.2.3 Perturbed attitude control

Before the lumped disturbance is introduced, we write *Theorem* 6.2 into the state space representation so that the following derivation can be simplified.

In Section 6.2.2, it has been shown that controller $\boldsymbol{\Gamma}_e = -R_{rot}(q_{e_s}, \boldsymbol{q}_{e_v}, \boldsymbol{\omega}_e, \hat{\boldsymbol{P}}, \boldsymbol{\omega}_d, \dot{\boldsymbol{\omega}}_d)^{-1}$ $(\boldsymbol{\omega}_e + K\boldsymbol{q}_{e_v})$ stabilizes the nominal system (6.11) with state space:

$$\dot{\boldsymbol{x}}_r = A_n(\boldsymbol{x}_r) + B_n\boldsymbol{\Gamma}_e$$

where:

$$A_n(\boldsymbol{x}_r) = \begin{bmatrix} -\frac{1}{2}\boldsymbol{q}_{e_v}^T\boldsymbol{\omega}_e \\ \frac{1}{2}[q_{e_s}I_{3\times 3} + \boldsymbol{q}_{e_v}^{\times}]\boldsymbol{\omega}_e \\ J_s^{-1}[F(q_{e_s}, \boldsymbol{q}_{e_v}, \boldsymbol{\omega}_e, \boldsymbol{\omega}_d, \dot{\boldsymbol{\omega}}_d) + G(q_{e_s}, \boldsymbol{q}_{e_v}, \boldsymbol{\omega}_e)]\boldsymbol{P} + J_s^{-1}H(\boldsymbol{\omega}_d, \dot{\boldsymbol{\omega}}_d)\tilde{\boldsymbol{P}} \end{bmatrix}$$

$$B_n = [0_{3\times 3} \quad 0_{3\times 3} \quad J_s^{-T}]^T, \boldsymbol{x}_r = [q_{e_s} \ \boldsymbol{q}_{e_v}^T \ \boldsymbol{z}^T]^T$$

and at the same time minimizes the performance index (6.23):

$$J_a = \lim_{t\to\infty}\left\{\beta_n \left\|\tilde{\boldsymbol{P}}(t)\right\|_{\gamma^{-1}}^2 + 4\beta_n c[1-q_{e_s}(t)] + \int_0^t (l(q_{e_s}, \boldsymbol{q}_{e_v}, \boldsymbol{\omega}_e, \hat{\boldsymbol{P}}, \boldsymbol{\omega}_d, \dot{\boldsymbol{\omega}}_d) + \boldsymbol{\Gamma}_e^T R_{rot}\boldsymbol{\Gamma}_e)dt\right\}$$

Using the expressions of $F(q_{e_s}, \boldsymbol{q}_{e_v}, \boldsymbol{\omega}_e, \boldsymbol{\omega}_d, \dot{\boldsymbol{\omega}}_d)$, $G(q_{e_s}, \boldsymbol{q}_{e_v}, \boldsymbol{\omega}_e)$ and $H(\boldsymbol{\omega}_d, \dot{\boldsymbol{\omega}}_d)$ in (6.10), we can rewrite l as:

$$\begin{aligned} l(q_{e_s}, \boldsymbol{q}_{e_v}, \boldsymbol{\omega}_e, \hat{\boldsymbol{P}}, \boldsymbol{\omega}_d, \dot{\boldsymbol{\omega}}_d) &= -2\beta_n[c\boldsymbol{q}_{e_v}^T\boldsymbol{\omega}_e + (\boldsymbol{\omega}_e + K\boldsymbol{q}_{e_v})^T(F+G)\hat{\boldsymbol{P}}] \\ &\quad + \beta_n^2(\boldsymbol{\omega}_e + K\boldsymbol{q}_{e_v})^T R_{rot}^{-1}(\boldsymbol{\omega}_e + K\boldsymbol{q}_{e_v}) \\ &= \beta_n \boldsymbol{x}_r^T Q_1 \boldsymbol{x}_r + \beta_n^2 \boldsymbol{z}^T R_{rot}^{-1}\boldsymbol{z} \\ &\triangleq \beta_n \boldsymbol{x}_r^T Q_2 \boldsymbol{x}_r \end{aligned} \tag{6.26}$$

where Q_1 is selected to satisfy $\boldsymbol{x}_r^T Q_1 \boldsymbol{x}_r = -2[c\boldsymbol{q}_{e_v}^T\boldsymbol{\omega}_e + (\boldsymbol{\omega}_e + K\boldsymbol{q}_{e_v})^T(F+G)\hat{\boldsymbol{P}}]$. In (6.25), l is proved to be a positive number, and $\beta \geq 2$, thus Q_2 is a positive definite matrix.

Based on (6.26), we rewrite the performance index as:

$$J_a = \lim_{t\to\infty}\left\{\beta_n \left\|\tilde{\boldsymbol{P}}(t)\right\|^2_{\gamma^{-1}} + 4\beta_n c[1-q_{e_s}(t)] + \int_0^t (l(q_{e_s}, \boldsymbol{q}_{e_v}, \boldsymbol{\omega}_e, \hat{\boldsymbol{P}}, \boldsymbol{\omega}_d, \dot{\boldsymbol{\omega}}_d) + \boldsymbol{\Gamma}'^T_e R_{rot} \boldsymbol{\Gamma}'_e)dt\right\}$$
$$= \lim_{t\to\infty}\left\{D(\boldsymbol{x}_r(t)) + \int_0^t (\beta_n \boldsymbol{x}_r^T Q_2 \boldsymbol{x}_r + \boldsymbol{\Gamma}'^T_e R_{rot} \boldsymbol{\Gamma}'_e)dt\right\} \tag{6.27}$$

where $D(\boldsymbol{x}_r(t)) = \beta_n \left\|\tilde{\boldsymbol{P}}(t)\right\|^2_{\gamma^{-1}} + 4\beta_n c[1-q_{es}(t)]$. We can now state the result in *Theorem* 6.2 in another way:

Theorem 6.3: For the system without perturbation and defined under the assumption 6.1, the feedback control law:

$$\boldsymbol{\Gamma}_e = -\beta_n R_{rot}(q_{e_s}, \boldsymbol{q}_{e_v}, \boldsymbol{\omega}_e, \hat{\boldsymbol{P}}, \boldsymbol{\omega}_d, \dot{\boldsymbol{\omega}}_d)^{-1}(\boldsymbol{\omega}_e + K\boldsymbol{q}_{e_v}) \tag{6.28}$$

with the same update law as (6.13):

$$\dot{\hat{\boldsymbol{P}}} = \gamma \times [F(q_{e_s}, \boldsymbol{q}_{e_v}, \boldsymbol{\omega}_e, \boldsymbol{\omega}_d, \dot{\boldsymbol{\omega}}_d) + G(q_{e_s}, \boldsymbol{q}_{e_v}, \boldsymbol{\omega}_e) + H(\boldsymbol{\omega}_d, \dot{\boldsymbol{\omega}}_d)]^T (\boldsymbol{\omega}_e + K\boldsymbol{q}_{e_v}) \tag{6.29}$$

where $\beta_n \geq 2$, stabilizes the nominal attitude control system:

$$\dot{\boldsymbol{x}}_r = A_n(\boldsymbol{x}_r) + B_n \boldsymbol{\Gamma}_e \tag{6.30}$$

and minimizes the cost function:

$$J_a = D(\boldsymbol{x}_r(t))\big|_{t\to\infty} + \int_0^\infty (\beta_n \boldsymbol{x}_r^T Q_2 \boldsymbol{x}_r + \boldsymbol{\Gamma}'^T_e R_{rot} \boldsymbol{\Gamma}'_e) \tag{6.31}$$

Now we return to the perturbed case when lumped disturbance $\boldsymbol{d}_n$ in (6.6) is introduced. The system (6.11) can be formulated as:

$$\dot{q}_{e_s} = -\frac{1}{2}\boldsymbol{q}_{e_v}^T \boldsymbol{\omega}_e \tag{6.32a}$$

$$\dot{\boldsymbol{q}}_{e_v} = \frac{1}{2}[q_{e_s} I_{3\times 3} + \boldsymbol{q}_{e_v}^{\times}]\boldsymbol{\omega}_e \tag{6.32b}$$

$$J_s \dot{\boldsymbol{z}} = [F(q_{e_s}, \boldsymbol{q}_{e_v}, \boldsymbol{\omega}_e, \boldsymbol{\omega}_d, \dot{\boldsymbol{\omega}}_d) + G(q_{e_s}, \boldsymbol{q}_{e_v}, \boldsymbol{\omega}_e)]\boldsymbol{P} + H(\boldsymbol{\omega}_d, \dot{\boldsymbol{\omega}}_d)\tilde{\boldsymbol{P}} + \boldsymbol{\Gamma}_e + \boldsymbol{d}_n \tag{6.32c}$$

To stabilize the above perturbed system, we first rewrite it into the state space formulation with the system state vector $\boldsymbol{x}_r = [q_{e_s} \ \boldsymbol{q}_{e_v}^T \ \boldsymbol{z}^T]^T$:

$$\dot{\boldsymbol{x}}_r = A_n(\boldsymbol{x}_r) + B_n \boldsymbol{\Gamma}_e + B_n \boldsymbol{d}_n \tag{6.33}$$

where $A_n(\boldsymbol{x}_r) = \begin{bmatrix} -0.5\boldsymbol{q}_{e_v}^T \boldsymbol{\omega}_e \\ 0.5[q_{e_s} I_{3\times 3} + \boldsymbol{q}_{e_v}^{\times}]\boldsymbol{\omega}_e \\ J_s^{-1}[F+G]\boldsymbol{P} + J_s^{-1} H \tilde{\boldsymbol{P}} \end{bmatrix}$, $B_n = \begin{bmatrix} 0 \\ 0 \\ J_s^{-1} \end{bmatrix}$.

Based on *Theorem* 6.3 and the indirect robust control *Theorem* 4.1, we have the following theorem:

Theorem 6.4: Consider the perturbed attitude control system:

$$\dot{\boldsymbol{x}}_r = A_n(\boldsymbol{x}_r) + B_n \boldsymbol{\Gamma}_e(\boldsymbol{x}_r) + B_n \boldsymbol{d}_n(\boldsymbol{x}_r) \tag{6.34}$$

If the lumped perturbation $\boldsymbol{d}_n$ satisfies:

$$\left\| \tilde{R}_{rot} \boldsymbol{d}_n(\boldsymbol{x}_r) \right\|^2 \le \beta_n \boldsymbol{x}_r^T Q_0 \boldsymbol{x}_r < \beta_n \boldsymbol{x}_r^T Q_2 \boldsymbol{x}_r \tag{6.35}$$

where $\beta_n \ge 2$; R_{rot} satisfies (6.14a) with $\tilde{R}_{rot}^T \tilde{R}_{rot} = R_{rot}$; Q_0 is a positive definite matrix and Q_2 satisfies (6.26), the system (6.34) is asymptotically stable with the control law $\boldsymbol{\Gamma}_e$ given in *Theorem* 6.3.

Proof:

This theorem is an application of the *Theorem* 4.1 and can be proved using the similar procedure:

For the optimal control problem, if $\boldsymbol{\Gamma}_e$ stabilizes (6.30) and at the same time minimizes (6.31), it must satisfy the following Hamilton-Jacobi-Bellman equation:

$$\beta_n \boldsymbol{x}_r^T Q_2 \boldsymbol{x}_r + \boldsymbol{\Gamma}_e^T R_{rot} \boldsymbol{\Gamma}_e + \bar{V}_{x_r}^T [A_n(\boldsymbol{x}_r) + B_n(\boldsymbol{x}_r)\boldsymbol{\Gamma}_e] = -\bar{V}_t \tag{6.36}$$

where $\bar{V}(\boldsymbol{x}_r(t)) = \min_{\boldsymbol{\Gamma}_e} J_a(t)$, and $\bar{V}_{x_r}, \bar{V}_t$ represent the partial derivative of $\bar{V}$ with respect to $\boldsymbol{x}_r$ and t, respectively. When $t \to \infty$, based on *Theorem* 6.3, (6.30) is stabilized,

and $\boldsymbol{q}_{ev} \to 0, \boldsymbol{z} \to 0$. Consequently, $\boldsymbol{\omega}_e \to 0, \dot{\tilde{\boldsymbol{P}}} \to \boldsymbol{0}$. It can be proved that when $t \to \infty$, the system is stabilized, and $\bar{V}_t \to 0$.

From (6.36), the steady state stationary condition becomes:

$$2\boldsymbol{\Gamma}_e^T \tilde{R}_{rot}^T \tilde{R}_{rot} + \bar{V}_{x_r}^T B_n(\boldsymbol{x}_r) = \boldsymbol{0} \tag{6.37}$$

Equation (6.36) and (6.37) will be used to prove that $\bar{V}(\boldsymbol{x}_r)$ is a Lyapunov function for the perturbed robust control problem (6.34).

$$\begin{aligned}\dot{\bar{V}} = \bar{V}_{x_r}^T \dot{\boldsymbol{x}}_r &= \bar{V}_{x_r}^T [A_n(\boldsymbol{x}_r) + B_n(\boldsymbol{x}_r)\boldsymbol{\Gamma}_e + B_n(\boldsymbol{x}_r)\boldsymbol{d}_n(\boldsymbol{x}_r)] \\ &= \bar{V}_{x_r}^T [A_n(\boldsymbol{x}_r) + B_n(\boldsymbol{x}_r)\boldsymbol{\Gamma}_e] + \bar{V}_{x_r}^T B_n(\boldsymbol{x}_r)\boldsymbol{d}_n(\boldsymbol{x}_r) \\ &= -\beta_n \boldsymbol{x}_r^T Q_2 \boldsymbol{x}_r - \boldsymbol{\Gamma}_e^T R_{rot} \boldsymbol{\Gamma}_e + \bar{V}_{x_r}^T B_n(\boldsymbol{x}_r)\boldsymbol{d}_n(\boldsymbol{x}_r)\end{aligned}$$

Here we applied (6.36). Recall $R_{rot} = \tilde{R}_{rot}^T \tilde{R}_{rot}$ and use (6.37), the above equation can be written as:

$$\dot{\bar{V}} = \bar{V}_{x_r}^T \dot{\boldsymbol{x}}_r = -\beta_n \boldsymbol{x}_r^T Q_2 \boldsymbol{x}_r - \boldsymbol{\Gamma}_e^T \tilde{R}_{rot}^T \tilde{R}_{rot} \boldsymbol{\Gamma}_e - 2\boldsymbol{\Gamma}_e^T \tilde{R}_{rot}^T \tilde{R}_{rot} \boldsymbol{d}_n(\boldsymbol{x}_r)$$

Using $-2\boldsymbol{\Gamma}_e^T \tilde{R}_{rot}^T \tilde{R}_{rot} \boldsymbol{d}_n(\boldsymbol{x}_r) \le \left\| \tilde{R}_{rot} \boldsymbol{d}_n(\boldsymbol{x}_r) \right\|^2 + \left\| \tilde{R}_{rot} \boldsymbol{\Gamma}_e \right\|^2 \le \left\| \tilde{R}_{rot} \boldsymbol{\Gamma}_e \right\|^2 + \beta_n \boldsymbol{x}_r^T Q_0 \boldsymbol{x}_r$ leads to:

$$\begin{aligned}\dot{\bar{V}} = \bar{V}_{x_r}^T \dot{\boldsymbol{x}}_r &= -\beta_n \boldsymbol{x}_r^T Q_2 \boldsymbol{x}_r - \boldsymbol{\Gamma}_e^T \tilde{R}_{rot}^T \tilde{R}_{rot} \boldsymbol{\Gamma}_e + \left\| \tilde{R}_{rot} \boldsymbol{\Gamma}_e \right\|^2 + \beta_n \boldsymbol{x}_r^T Q_0 \boldsymbol{x}_r = -\beta_n \left\| \boldsymbol{x}_r \right\|_{Q_2 - Q_0}^2 \\ &\le -\beta_n \lambda_{\min}(Q_2 - Q_0) \left\| \boldsymbol{x}_r \right\|^2\end{aligned}$$

where $\lambda_{\min}(Q_2 - Q_0)$ is the minimum eigenvalue of the matrix $Q_2 - Q_0$, which is positive definite using the condition (6.35). Thus, $V \le -W(\boldsymbol{x}_r)$ where $W(\boldsymbol{x}_r)$ is a positive number.

According to the Lyapunov stability theorem, there exists a neighborhood of 0, $N_n = \left\{ \boldsymbol{x}_r : \left\| \boldsymbol{x}_r \right\| < n_h \right\}$ for some $n_h > 0$ such that if $\boldsymbol{x}_r$ enters N_n, then $\boldsymbol{x}_r \to \boldsymbol{0}$ as $t \to \infty$.

Furthermore, $\boldsymbol{x}_r$ cannot always stay outside N_n. If $\left\| \boldsymbol{x}_r \right\| \ge n_h$ for all $t > 0$, then:

$$\begin{aligned}\bar{V}(t) - \bar{V}(0) = \int_0^t \dot{\bar{V}}(t) d\tau &\le \int_0^t -\lambda_{\min}(Q_2 - Q_0) \left\| \boldsymbol{x}_r \right\|^2 d\tau \\ &\le -\int_0^t \lambda_{\min}(Q_2 - Q_0) n_h^2 d\tau \le -\lambda_{\min}(Q_2 - Q_0) n_h^2 t\end{aligned}$$

When $t \to \infty$, the Lyapunov function $\bar{V}$ will go to negative, which contradicts the assumption that $\bar{V}$ is always positive for the system (6.34) at all time. Therefore $\boldsymbol{x}_r$ cannot always stay outside N_n. Once it enters N_n, it will converge to 0 as t evolves. □

Remark 6.1: In *Theorem* 6.4, the lumped disturbance is formulated inside the performance index. Since the controller (6.28) not only stabilizes the unperturbed system but also possesses certain optimality, we use its optimality to extend it to the disturbed system control. Parameter β_n can be chosen to be any positive value no less than 2, and at the same time is required to satisfy the condition (6.35), which provides certain degree of freedom for the designer. In the following simulation section, we can design a relatively large β_n to handle both flexible structure induced disturbance and input uncertainty.

Combining *Theorem* 6.2 and *Theorem* 6.4, we have successfully designed the adaptive controller (6.21) with the update law (6.22), which can stabilize not only the unperturbed nominal system (6.11) with certain optimality (6.23), but also the perturbed system (6.7). Other tunable parameters include $c \in \mathbb{R}^1$, $K \in \mathbb{R}^{3\times3}$, $K_1 \in \mathbb{R}^{3\times3}$, and $\gamma \in \mathbb{R}^{6\times6}$. These parameters are required to be positive definite and symmetric.

6.3 Translational control law design:

For the translational motion control, we use the indirect robust control method. As discussed in Chapter 3, the translational dynamic equations can be written in the state space representation (Eq. 5.1):

$$\frac{d}{dt}x = \dot{x} \tag{6.40a}$$

$$\frac{d}{dt}y = \dot{y} \tag{6.40b}$$

$$\frac{d}{dt}z = \dot{z} \tag{6.40c}$$

$$\frac{d}{dt}\dot{x} = 2\dot{\nu}\dot{y} + \ddot{\nu}y + \dot{\nu}^2 x - \frac{\mu x}{((\bar{r}+x)^2 + y^2 + z^2)^{\frac{3}{2}}} - \frac{\mu\bar{r}}{((\bar{r}+x)^2 + y^2 + z^2)^{\frac{3}{2}}} + \frac{\mu}{\bar{r}^2} + a_x \tag{6.40d}$$

$$\frac{d}{dt}\dot{y} = -2\dot{\nu}\dot{x} - \ddot{\nu}x + \dot{\nu}^2 y - \frac{\mu}{((\bar{r}+x)^2 + y^2 + z^2)^{\frac{3}{2}}}y + a_y \tag{6.40e}$$

$$\frac{d}{dt}\dot{z} = -\frac{\mu}{((\bar{r}+x)^2 + y^2 + z^2)^{\frac{3}{2}}}z + a_z \tag{6.40f}$$

Recall that we introduced an augmented state s_a as in (5.2) to absorb the biased terms. Then the state variables for the translational motion are chosen to be:

$$\boldsymbol{x} = \begin{bmatrix} \boldsymbol{r}_L^T & \boldsymbol{v}_L^T & s_a & \boldsymbol{r}_{LI}^T \end{bmatrix}^T \tag{6.41}$$

where $\boldsymbol{r}_{LI}$ is the integral of the relative position vector $\boldsymbol{r}_L$ as in (5.10). The controller is defined as gas jet acceleration: $\boldsymbol{u} = [a_x \quad a_y \quad a_z]^T$.

The nominal nonlinear state-space equation for the spacecraft translational problem is written as:

$$\dot{\boldsymbol{x}} = A_n(\boldsymbol{x})\boldsymbol{x} + B_n(\boldsymbol{x})\boldsymbol{u} \tag{6.42}$$

where

$$A_n = \begin{bmatrix} 0_{3\times3} & I_{3\times3} & 0_{3\times1} & 0_{3\times3} \\ A_1 & A_2 & A_3 & 0_{3\times3} \\ 0_{1\times3} & 0_{1\times3} & -\lambda_a & 0_{1\times3} \\ I_{3\times3} & 0_{3\times3} & 0_{3\times1} & 0_{3\times3} \end{bmatrix},$$

$$A_1 = \begin{bmatrix} \dot{v}^2 - coeff & \ddot{v} & 0 \\ -\ddot{v} & \dot{v}^2 - coeff & 0 \\ 0 & 0 & -coeff \end{bmatrix}, A_2 = \begin{bmatrix} 0 & 2\dot{v} & 0 \\ -2\dot{v} & 0 & 0 \\ 0 & 0 & 0 \end{bmatrix}, A_3 = \begin{bmatrix} bias / s_a \\ 0 \\ 0 \end{bmatrix}$$

and $coeff = \dfrac{\mu}{((\overline{r}+x)^2 + y^2 + z^2)^{\frac{3}{2}}}, bias = -coeff \bullet \overline{r} + \dfrac{\mu}{\overline{r}^2}$

The input matrix $B_n = [0_{3\times3}, I_{3\times3}, 0_{3\times1}, 0_{3\times3}]^T$.

In the presence of the input matrix uncertainty $h(\boldsymbol{x})$, the perturbed system becomes:

$$\dot{\boldsymbol{x}} = A_n(\boldsymbol{x})\boldsymbol{x} + B_n(\boldsymbol{x})\boldsymbol{u} + B_n(\boldsymbol{x})h(\boldsymbol{x})\boldsymbol{u} \tag{6.43}$$

No disturbance vector $d_n(\boldsymbol{x})$ is included since in the indirect robust control design, the $d_n(\boldsymbol{x})$ only relates with rotational states. The indirect robust control theory as stated in *Theorem* 4.1 can be applied. Following the indirect robust control theorem, we can formulate an equivalent optimal control problem based on the perturbed system (6.43). For the nonlinear system

$$\dot{\boldsymbol{x}} = A_n(\boldsymbol{x})\boldsymbol{x} + B_n(\boldsymbol{x})\boldsymbol{u} + (I - B_n(\boldsymbol{x})B_n(\boldsymbol{x})^+)\mathbf{v} = A_n(\boldsymbol{x})\boldsymbol{x} + \mathrm{B}(\boldsymbol{x})\begin{bmatrix} \boldsymbol{u} \\ \mathbf{v} \end{bmatrix} \tag{6.44}$$

where $\mathrm{B}(\boldsymbol{x}) = [B_n(\boldsymbol{x}) \quad (I - B_n(\boldsymbol{x})B_n(\boldsymbol{x})^+)]$, find an optimal control law $[\boldsymbol{u}^T \quad \mathbf{v}^T]^T$ to minimize the cost function:

$$\int_0^\infty \left[H_{\max}^2(\boldsymbol{x}) + \boldsymbol{x}^T \tilde{Q}\boldsymbol{x} + 2\boldsymbol{u}^T \tilde{R}_{trans}^T \tilde{R}_{trans}\boldsymbol{u} + \rho^2 \|\mathbf{v}\|^2 \right] dt \tag{6.45}$$

where $\tilde{Q}_{trans}$ and $\tilde{R}_{trans}$ are the weighting matrices.

To use the indirect robust control method, the conditions (4.4-4.6) must be satisfied. We can choose

$$H_{\max}^2(\boldsymbol{x}) = 4\beta_0^2 \left\| \tilde{R}_{trans} \right\|^2 \boldsymbol{x}^T \boldsymbol{x}$$

where β_0 is a predefined tunable constant number.

Rewrite the performance index into a quadratic formulation:

$$\int_0^\infty \left\{ \boldsymbol{x}^T \left[4\beta_0^2 \left\| \tilde{R}_{trans} \right\|^2 I + \tilde{Q}_{trans} \right] \boldsymbol{x} + \begin{bmatrix} \boldsymbol{u} & \mathbf{v} \end{bmatrix} \begin{bmatrix} 2\tilde{R}_{trans}^T \tilde{R}_{trans} & \\ & \rho^2 I \end{bmatrix} \begin{bmatrix} \boldsymbol{u} \\ \mathbf{v} \end{bmatrix} \right\} dt \qquad (6.46)$$

We can then apply the θ-D technique by noting that

$\mathrm{Q}_{trans} = 2 \times \left[4\beta_0^2 \left\| \tilde{R}_{trans} \right\|^2 I + \tilde{Q}_{trans} \right]$ and $\mathrm{R}_{trans} = \begin{bmatrix} 2\tilde{R}_{trans}^T \tilde{R}_{trans} & \\ & \rho^2 I \end{bmatrix}$. The closed-form optimal controller is then calculated by:

$$\begin{bmatrix} \boldsymbol{u} \\ \mathbf{v} \end{bmatrix} = -\mathrm{R}_{trans}^{-1} \mathrm{B}^T(\boldsymbol{x}) [\mathrm{T}_0 + \mathrm{T}_1(\boldsymbol{x}, \theta) + \mathrm{T}_2(\boldsymbol{x}, \theta)] \bullet \left[(\boldsymbol{r}_L - \boldsymbol{r}_c)^T \quad (\mathbf{v}_L - \mathbf{v}_c)^T \quad 0 \quad (\boldsymbol{r}_{LI} - \int \boldsymbol{r}_c dt)^T \right]^T \qquad (6.47)$$

where $\mathrm{T}_0, \mathrm{T}_1(\boldsymbol{x}, \theta)$ and $\mathrm{T}_2(\boldsymbol{x}, \theta)$ are solved from the θ-D algorithm. Note that only the $\boldsymbol{u}$ component in (6.47) is applied to the spacecraft control and $\mathbf{v}$ is just an auxiliary control variable. $\boldsymbol{r}_c$ and $\mathbf{v}_c$ are desired relative position and relative velocity in the LVLH frame. We can refer to (5.26) and (5.27) to find their expressions.

CHAPTER VII

SIMULATION RESULTS AND ANALYSIS

In this chapter, the effectiveness of the indirect robust control approach will be demonstrated through simulation results. In the simulation scenario, the pursuer spacecraft will be controlled to approach a free tumbling target. The pursuer and the target are assumed to be in the same low earth orbit with 400km perigee altitude. Orbit inclination is set to 45 degrees. The eccentricity is 0.1375. The argument of perigee and the right ascension of ascending node are all set to 0 degree [108].

7.1 Integrated indirect robust control simulation results

First, we will design the controller by using the integrated indirect robust control method presented in Chapter 5. Initial conditions are given in Table 7.1 on the next page.

Four significant elastic modes are taken into account in the model for the flexible motion. Modal natural frequencies and damping coefficients are [40]:

$$\omega_{n_1} = 1.9 rad/s, \omega_{n_2} = 4.1 rad/s, \omega_{n_3} = 5.8 rad/s, \omega_{n_4} = 6 rad/s$$

$$\zeta_1 = 0.08, \zeta_2 = 0.30, \zeta_3 = 0.60, \zeta_4 = 0.75$$

Assume that the pursuer's nominal moment of inertia is [40]:

$$J_s = \begin{bmatrix} 800 & 12 & 5 \\ 12 & 400 & 1.5 \\ 5 & 1.5 & 600 \end{bmatrix} kg \cdot m^2$$

In the simulation, the actual parametric uncertainty on the moment of inertia is assumed to be:

$$\Delta J = \begin{bmatrix} 0.2\times r_1 J_s(1,1) & 0.3\times r_2 J_s(1,2) & 0.3\times r_3 J_s(1,3) \\ 0.3\times r_2 J_s(2,1) & 0.2\times r_4 J_s(2,2) & 0.3\times r_5 J_s(2,3) \\ 0.3\times r_3 J_s(3,1) & 0.3\times r_5 J_s(3,2) & 0.2\times r_6 J_s(3,3) \end{bmatrix}$$

where $r_1, r_2, \cdots, r_6$ are random numbers generated from standard normal distribution. When generating the random numbers, the actual pursuer moment of inertia, $J_s + \Delta J$, must be kept positive definite. The coupling matrix in (3.11) is [40]:

$$\delta = \begin{bmatrix} 10 & 0.5 & 0.2 \\ 0.5 & 2 & 0 \\ 0.1 & 10.9 & 0.8 \\ 1 & 0.5 & 0.5 \end{bmatrix}$$

Coupling matrix uncertainty $\Delta\delta$ is assumed to be 10% of the nominal value. The control input uncertainty is assumed to be 5% of the computed value.

Table 7.1 Initial conditions of the simulation scenario 7.1

Parameter Description	Pursuer Spacecraft	Target
Initial relative position $\boldsymbol{r}_{L_0}$ in $\{\boldsymbol{L}\}$	$\boldsymbol{r}_{L_0} = \begin{bmatrix} 50/\sqrt{2} & 0 & 50/\sqrt{2} \end{bmatrix}^T m$	
Initial relative velocity $\boldsymbol{v}_{L_0}$ in $\{\boldsymbol{L}\}$	$\boldsymbol{v}_{L_0} = \begin{bmatrix} -0.5 & -0.5 & 0.5 \end{bmatrix} m/s$	
Initial angular velocity represented in its own body frame	$\boldsymbol{\omega}_{s_0} = \begin{bmatrix} 3 & 3 & 3 \end{bmatrix}^T$ deg/ s	$\boldsymbol{\omega}_{t_0} = \begin{bmatrix} 3 & 3 & 3 \end{bmatrix}^T$ deg/ s
Initial attitude represented in Euler angles (3-1-3) $\Theta = \begin{bmatrix} \psi_1(0) & \phi(0) & \psi_2(0) \end{bmatrix}^T$	$\begin{bmatrix} 30^\circ & 30^\circ & 30^\circ \end{bmatrix}$	$\begin{bmatrix} 0 & 45^\circ & 0 \end{bmatrix}^T$
Initial Generalize Modal Coordinate $\boldsymbol{\eta}$	$\boldsymbol{\eta}_0 = \dot{\boldsymbol{\eta}}_0 = [0 \quad 0 \quad 0 \quad 0]^T$	N/A

To further demonstrate the robustness of the indirect robust control method, external torque due to the gravity gradient: $\boldsymbol{G} = \frac{3\mu}{\bar{r}_s^5}\boldsymbol{R}_s \times J_s \boldsymbol{R}_s$ is included in the system simulation, where μ is the gravitational constant, and $\bar{r}_s = \|\boldsymbol{R}_s\|$ is the norm of the distance vector from Earth center of mass to the spacecraft body.

The parameters in the uncertainty bounds are chosen to be $\beta = 0.01$, $\rho^2 = 2\times 10^4$, $\sigma = 10I$.

According to the condition (4.6), the matrices $\tilde{Q}$ and $\tilde{R}$ in the cost function (5.23) are selected to be:

$$\tilde{Q} = 0.5 \times diag\left(\begin{bmatrix} 5\times10^5 & 5\times10^5 & 5\times10^5 & 4\times10^5 & 4\times10^5 & 4\times10^5 & \cdots \\ 0 & \cdots & & & & & \\ 1 & 10^9 & 10^9 & 10^9 & \cdots & & \\ 5\times10^6 & 5\times10^6 & 5\times10^6 & \cdots & & & \\ 2\times10^4 & 2\times10^4 & 2\times10^4 & 6\times10^3 & 10^4 & 10^5 & \cdots \\ 2\times10^7 & 6\times10^3 & 1 & 1 & 9\times10^5 & & \end{bmatrix}\right)$$

$$\tilde{R} = diag\left(\left[100, 35, 100, 0.25, 0.25, 0.25\right]\right)$$

where the function $diag(\bullet)$ denotes the diagonal matrix.

Relative position and velocity expressed in the target body frame are shown in Fig. 7.1 and Fig. 7.2. The initial relative distance between the pursuer and the target is 50 meters. It is required that the pursuer is driven to a relative position of [5,0,0] meters in the target body frame. As can be seen, after about 80 seconds, the relative distance reaches the desired one with steady state error less than 10 cm, and the relative velocity converges to zero, which indicates there is no relative translational motion between the pursuer and the target. The attitude tracking in terms of quaternion error is shown in Fig. 7.3. Angular velocity tracking expressed in the virtual target body frame is shown in Fig.

7.4. These results demonstrate that the pursuer's attitude is synchronized with the virtual target's attitude with a good tracking performance. Recall that the desired attitude is the assumed virtual target's attitude obtained through rotating the actual target's body frame by 180 degrees about its body $\hat{\boldsymbol{b}}_{tz}$ axis in order to align the two vehicle's docking ports.

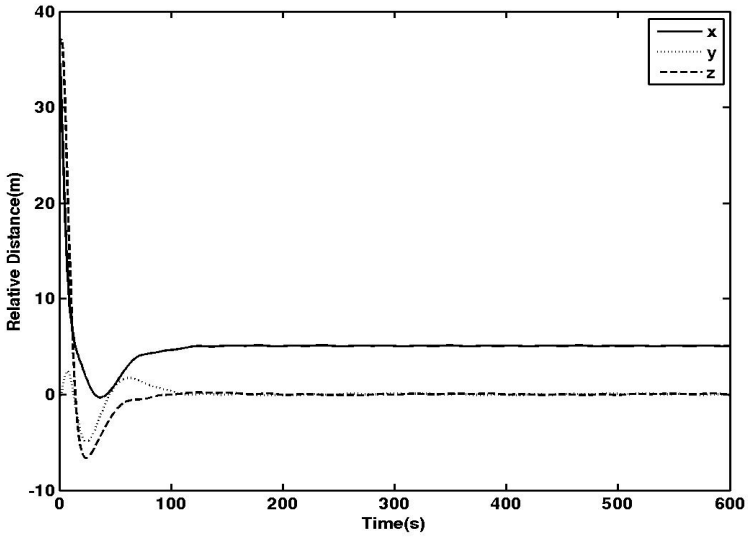

Figure 7.1 Relative position in target body frame (Indirect Robust Control method)

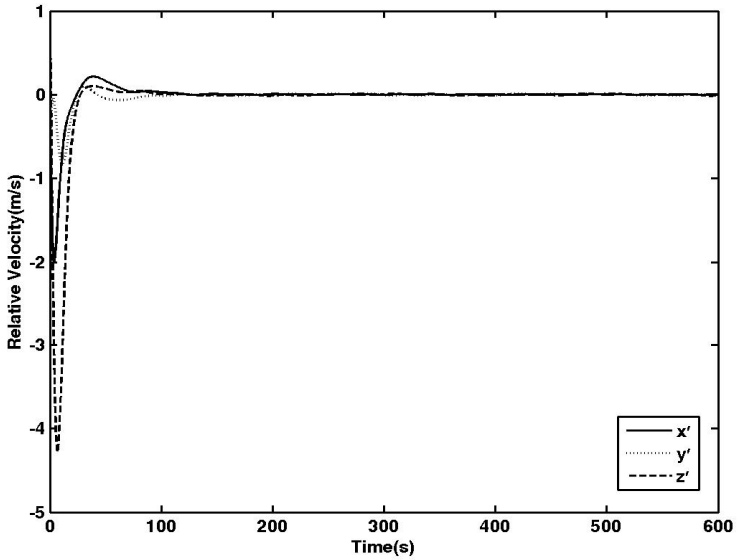

Figure 7.2 Relative velocity in target body frame (Indirect Robust Control method)

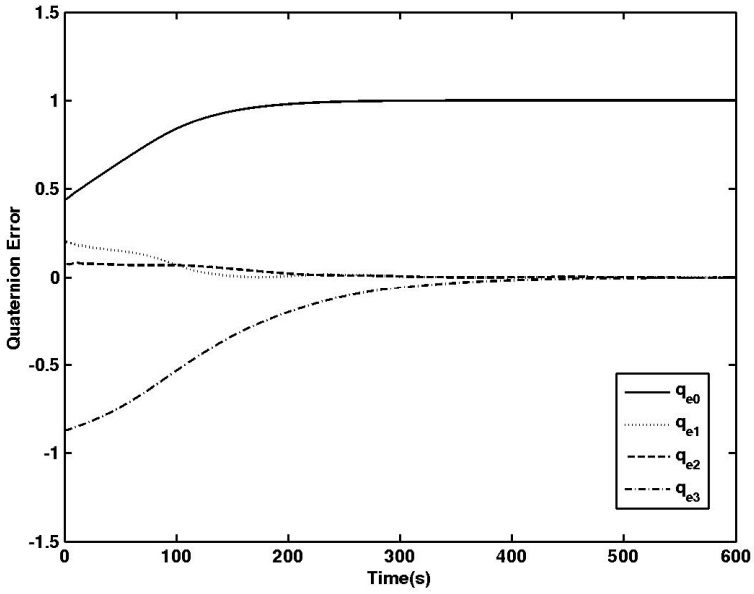

Figure 7.3 Quaternion error $\boldsymbol{q}_e$ (Indirect Robust Control method)

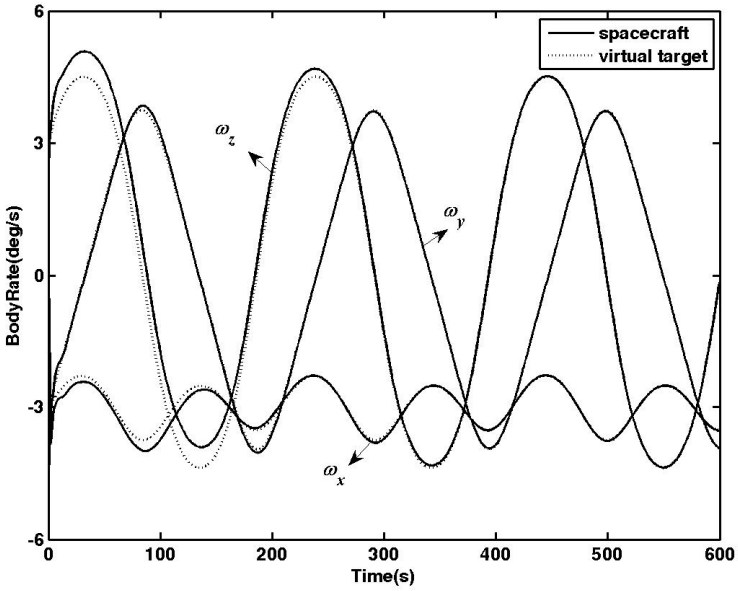

Figure 7.4 Angular velocity (Indirect Robust Control method)

As shown in Figs. 7.1-7.4, the spacecraft undergoes large and rapid translational and angular maneuvers. Without an effective control strategy, these maneuvers may incur flexible structure vibrations and deteriorate the attitude tracking performance.

Figure 7.5 shows the result of flexible vibration suppression using the indirect robust controller. Among the four modal coordinates, it is obvious that η_1 is the dominant one. Thus, a four-mode representation of the flexible motion is a good approximation. The vibration diminishes to a small level after about 150 seconds.

Figure 7.6 demonstrates the control accelerations and control torques. The initial control efforts are relatively large in order to drive the spacecraft to the desired position and attitude quickly. They decrease rapidly after the desired position and attitude are achieved. Small oscillating accelerations and torques are maintained as seen in Fig. 7.6 because tracking the tumbling target and suppressing flexible structure vibration require continuous control efforts.

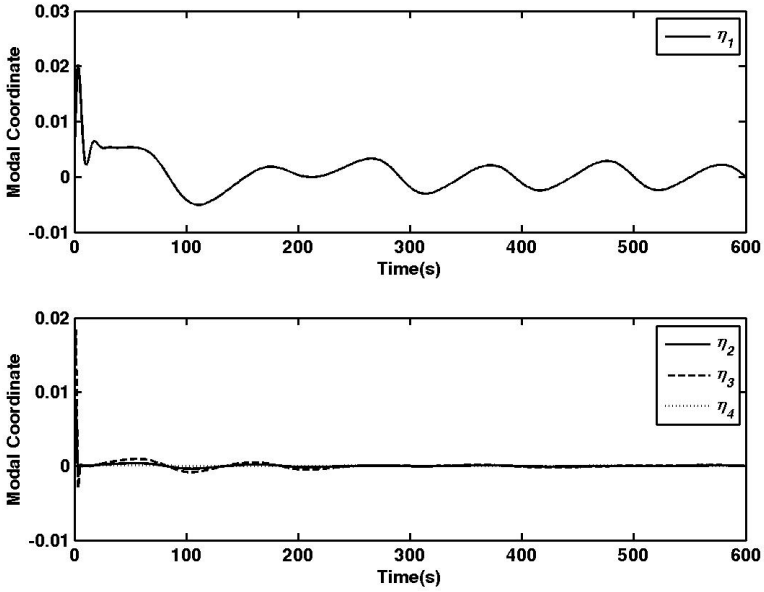

Figure 7.5 Generalized modal coordinates of flexible motion (Indirect Robust Control method)

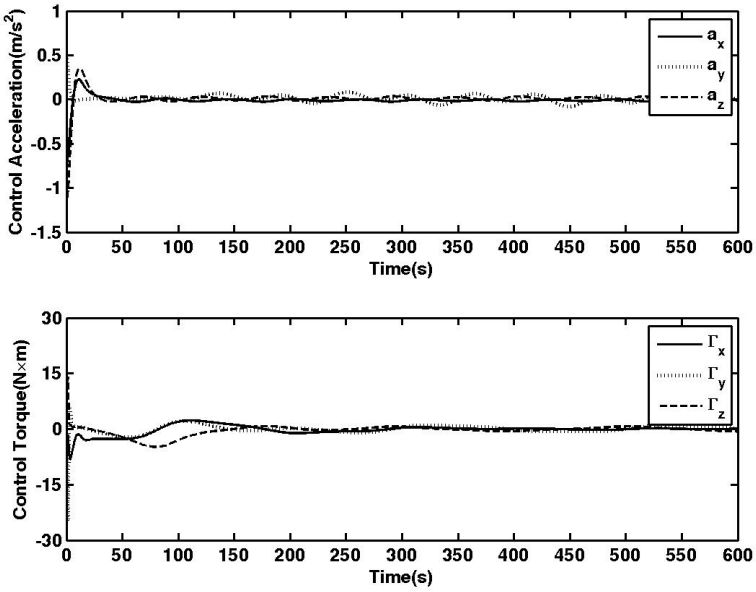

Figure 7.6 Control accelerations and control torques (Indirect Robust Control method)

7.2 Inverse optimal adaptive control simulation results

In this section, we employ the IOAC method combined with the indirect robust control method presented in Chapter 6, and compare its performance with respect to the indirect robust controller in Section 7.1.

Since the flexible deformation is considered as disturbance to the rotational motion, coupling matrix δ is not involved in the rotational motion controller design. The control input uncertainty is assumed to be 5% of the computed value. To make the result comparable with the ones in Section 7.1, gravity gradient disturbance torque is also added to the simulation.

During the rotational controller design, design parameters are: $K_n = 0.255 I_{3\times3}$, $K_1 = 200 I_{3\times3}$, $c = 24.6$, $\beta_n = 2$, $\gamma = 3\times10^5 I_{6\times6}$.

Initial moment of inertia estimation for the pursuer spacecraft is assumed to be:

$$\hat{J}_{s0} = \begin{bmatrix} 100 & 10 & 10 \\ 10 & 100 & 2 \\ 10 & 2 & 100 \end{bmatrix}$$

while the actual moment of inertia remains: $J_s = \begin{bmatrix} 800 & 12 & 5 \\ 12 & 400 & 1.5 \\ 5 & 1.5 & 600 \end{bmatrix} kg \cdot m^2$

In the translational controller design, since we follow the indirect robust control method, the same parameters are adapted: $\beta = 0.01$, $\rho^2 = 2 \times 10^4$. The weights which are put on the translational system parameters are the same as the ones used in the indirect robust control method:

$$\tilde{Q}_{trans} = 0.5 \times diag\left(\begin{bmatrix} 5\times10^5 & 5\times10^5 & 5\times10^5 & 4\times10^5 & 4\times10^5 & 4\times10^5 & \dots \\ 0 & 2\times10^4 & 2\times10^4 & 2\times10^4 & & & \end{bmatrix} \right)$$

$$\tilde{R}_{trans} = diag([100 \quad 35 \quad 100])$$

Since we are using the same scenario with the same system parameters, and the translational tracking control is based on the same indirect robust control law, the relative position and velocity tracking as shown in Fig. 7.7 and 7.8 are similar to the ones in Fig. 7.1 and Fig. 7.2. Negligible relative translational motion can be observed after 200 seconds of settling time. In Fig. 7.9, the control acceleration time history shows small oscillation during the steady state in order to maintain the position tracking since the target is a free tumbling one and the docking distance is not 0.

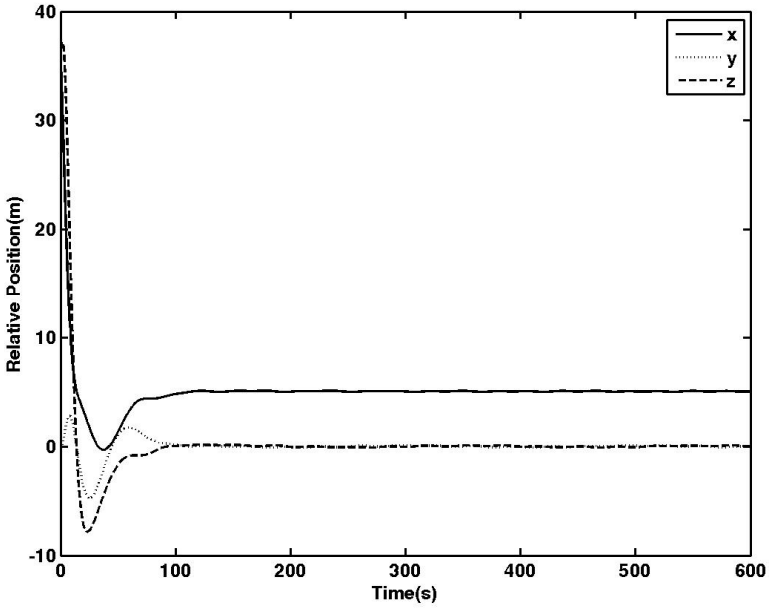

Figure 7.7 Relative position in target body frame (IOAC method)

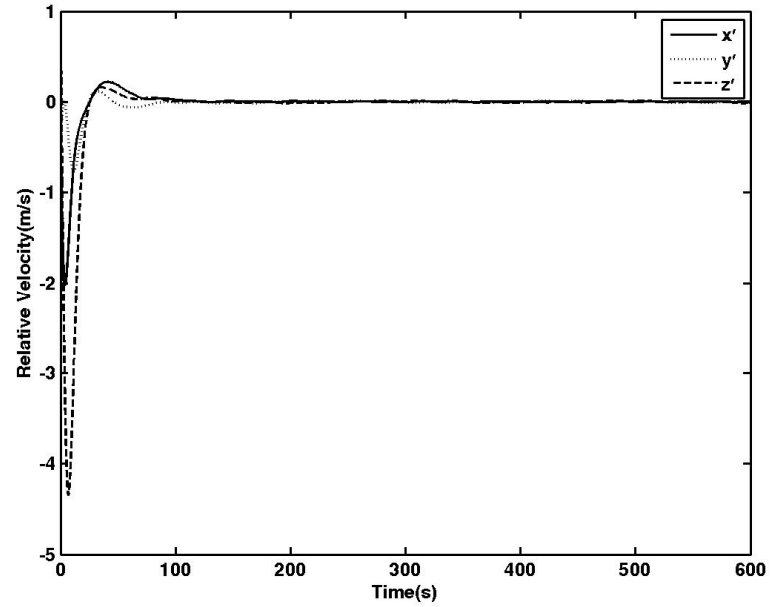

Figure 7.8 Relative velocity in target body frame (IOAC method)

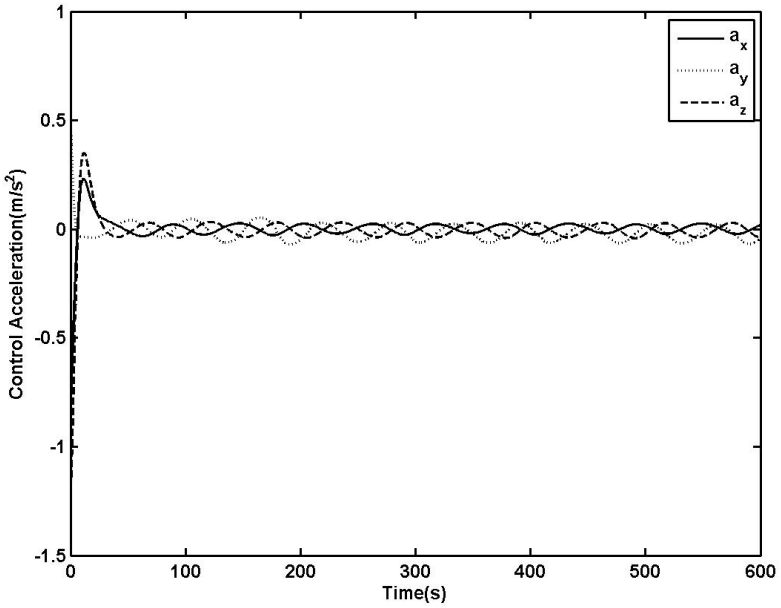

Figure 7.9 Control accelerations (IOAC method)

Attitude tracking in terms of quaternion error is shown in Fig. 7.10. Angular velocity tracking expressed in the virtual target body frame is shown in Fig. 7.11. These two figures illustrate that, by using conventional IOAC method, the pursuer and target attitude are synchronized more quickly than the results in Fig. 7.3 and Fig. 7.4.

However, fast attitude tracking excites the flexible deformation more significantly. The generalized modal coordinate time history is given in Fig. 7.12. Since the flexible deformation is not actively suppressed by formulating it into the state space and is considered as merely disturbance to the rigid spacecraft rotational system, its magnitude is almost 10 times larger than the one in Fig. 7.5. Attitude tracking control torque is shown in Fig. 7.13. Initial control torque is relatively large in order to drive the spacecraft to the desired attitude quickly, which can be seen from the quaternion error and angular velocity tracking. Compared with the results in Fig. 7.6, the trade-off for fast attitude tracking is the more oscillations in the control torque.

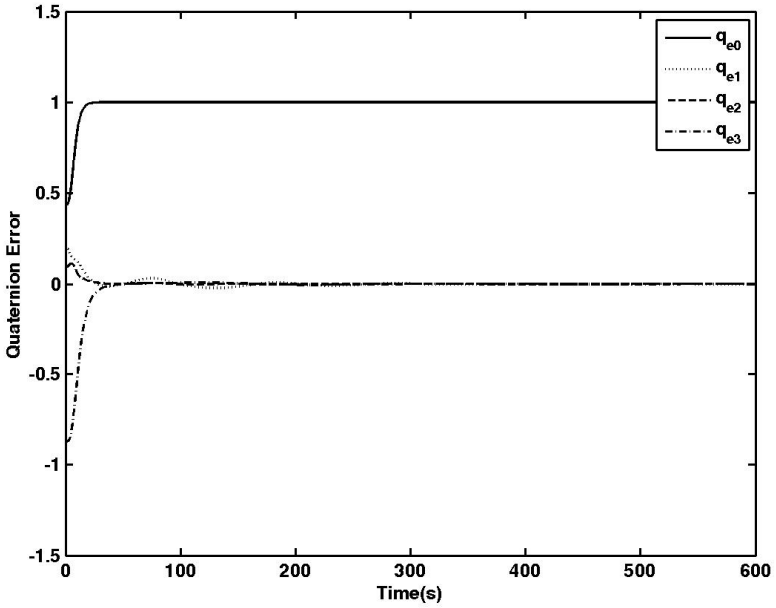

Figure 7.10 Quaternion error $\boldsymbol{q}_e$ (IOAC method)

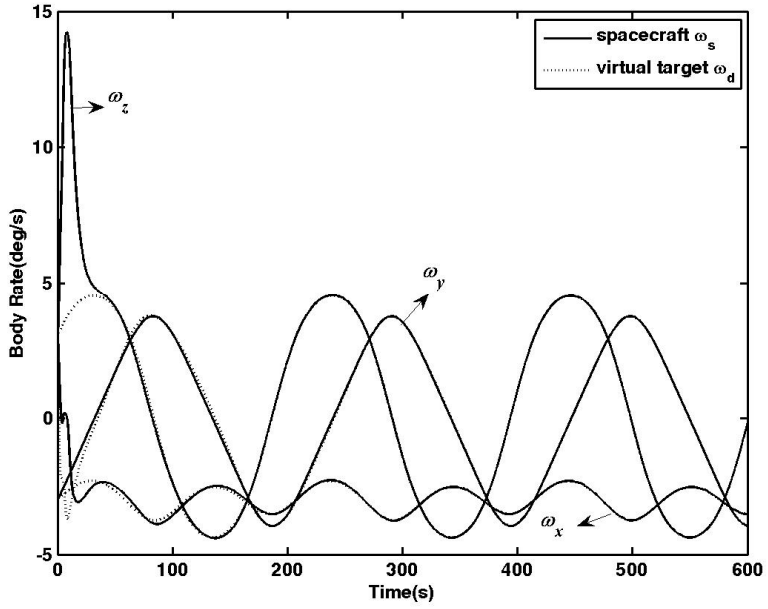

Figure 7.11 Angular velocity (IOAC method)

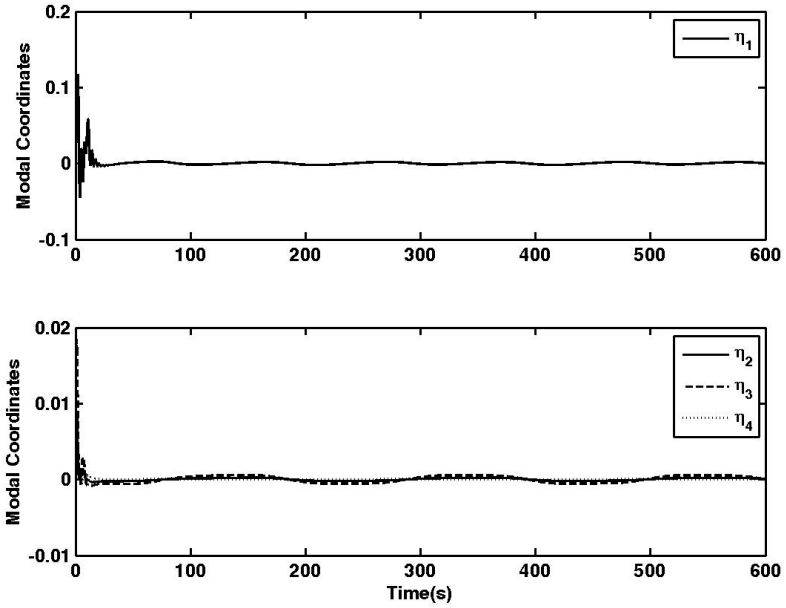

Figure 7.12 Generalized modal coordinates of flexible motion (IOAC method)

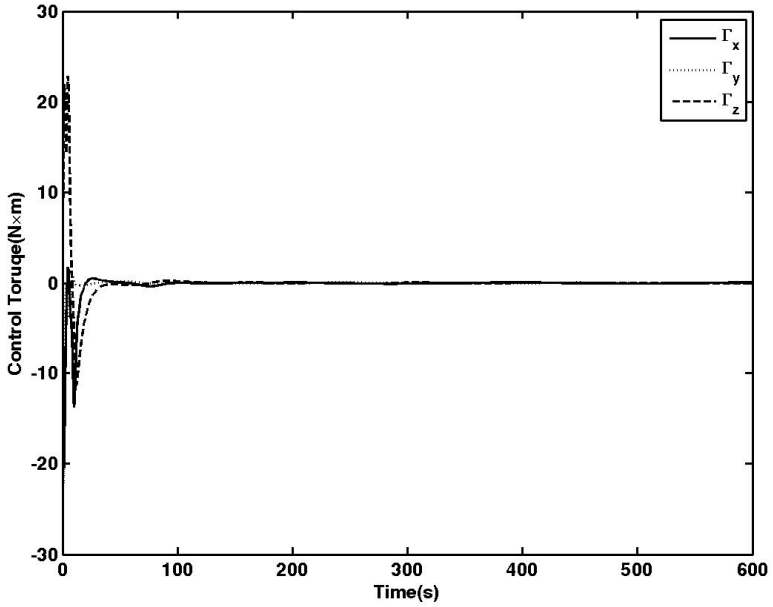

Figure 7.13 Control torque (IOAC method)

Figure 7.14 and Fig. 7.15 demonstrate the behavior of spacecraft moment of inertia estimation error $\tilde{J}_s = \hat{J}_s - J_s$. Simulation time is 1500 seconds. As stated in [42], in the case of lack of excitation, the convergence of the parameter estimate to a constant value is always achieved, but it does not need to converge to the actual parameter value. In our simulation, the steady state estimation error for the diagonal term does not converge to zero. Nevertheless, the system is still stabilized under the adaptive controller.

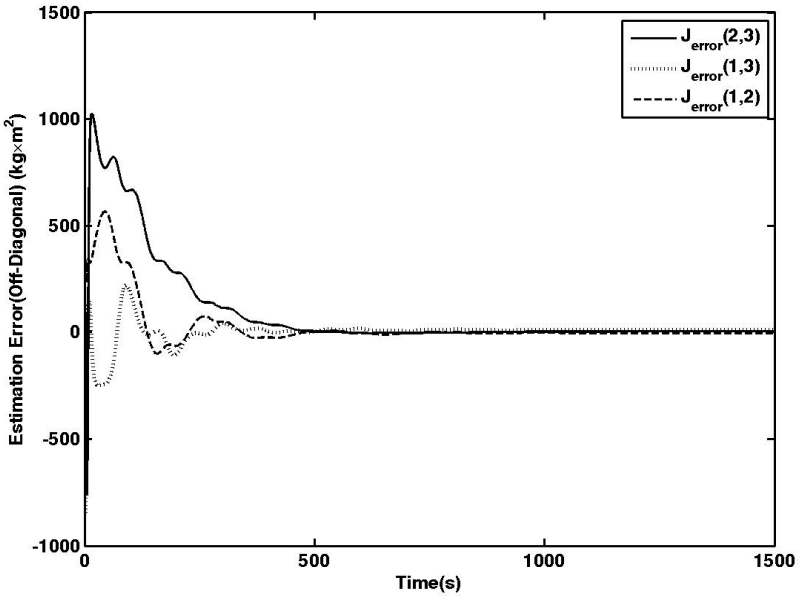

Figure 7.14 Moment of inertia estimation error (off-diagonal)

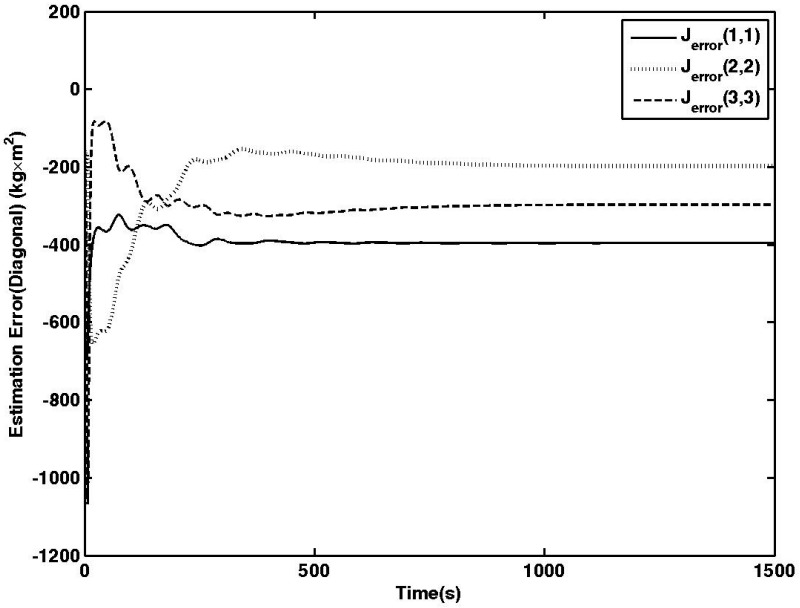

Figure 7.15 Moment of inertia estimation error (diagonal)

7.3 Integrated indirect robust control simulation with different initial conditions

To demonstrate the effectiveness of the integrated indirect robust control method, different initial conditions of the target and pursuer angular velocities are used in the simulation.

Table 7.2 Different initial conditions

Parameter Description	Pursuer Spacecraft	Target
Initial angular velocity represented in its own body frame	$\boldsymbol{\omega}_{s_0} = \begin{bmatrix} 1 & -5 & 1 \end{bmatrix}^T \text{ deg/ } s$	$\boldsymbol{\omega}_{t_0} = \begin{bmatrix} -2 & 4 & \sqrt{7} \end{bmatrix}^T \text{ deg/ } s$

No other initial values are changed. In order to compare the simulation results, we did not change any design parameters or any weighting matrices. Controller performance is demonstrated by the following figures.

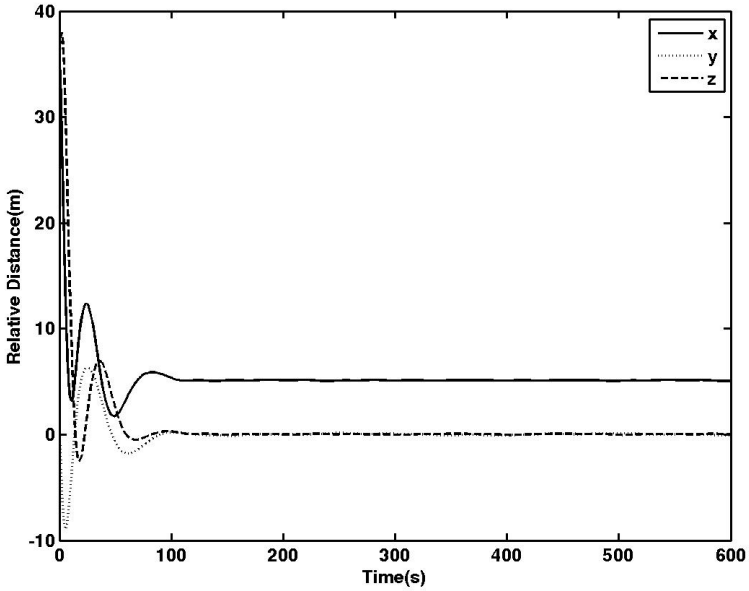

Figure 7.16 Relative position in target body frame (Indirect Robust Control method with different initial conditions)

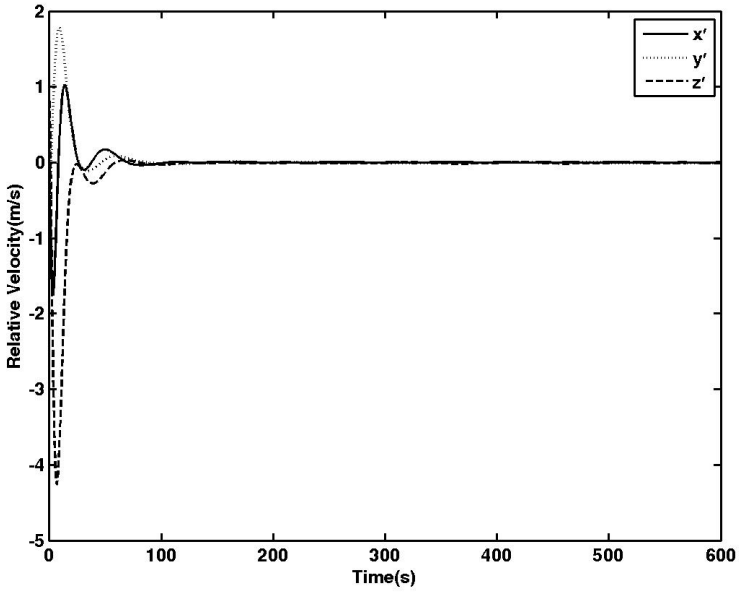

Figure 7.17 Relative velocity in target body frame (Indirect Robust Control method with different initial conditions)

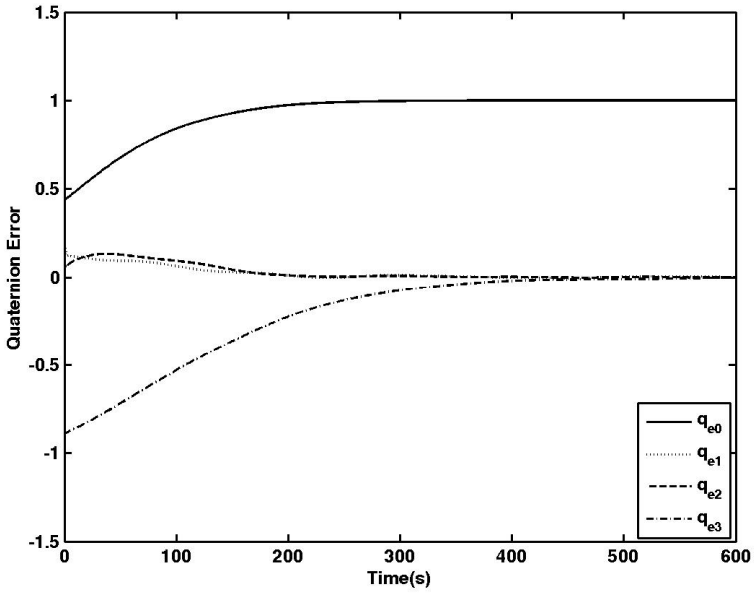

Figure 7.18 Quaternion error $\boldsymbol{q}_e$ (Indirect Robust Control method with different initial conditions)

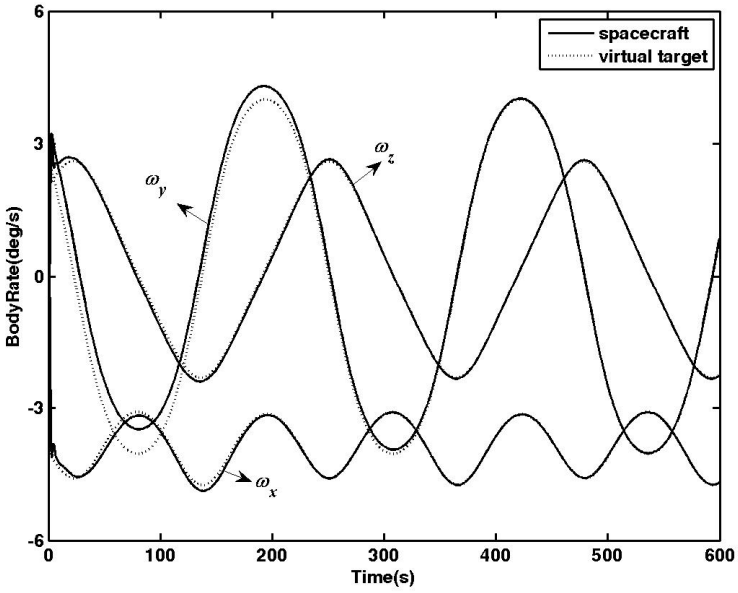

Figure 7.19 Angular velocities (Indirect Robust Control method with different initial conditions)

Compared with Fig. 7.1 and Fig. 7.2, the translational motion demonstrated in Fig. 7.16 and Fig. 7.17 changes greatly. Although coupling between the rotational motion and translational motion of the pursuer spacecraft is negligible, the change in the target angular velocity changes the desired position since the target is free tumbling and the docking distance is nonzero and results in different translational behavior. Translational motion converges to the steady state in about 100 seconds and steady state error is less than 10 centimeters.

As shown in Fig. 7.18 and Fig. 7.19, even though initial angular velocities are changed greatly, and angular maneuvers are relatively large and rapid, the rotational tracking performance is still satisfying.

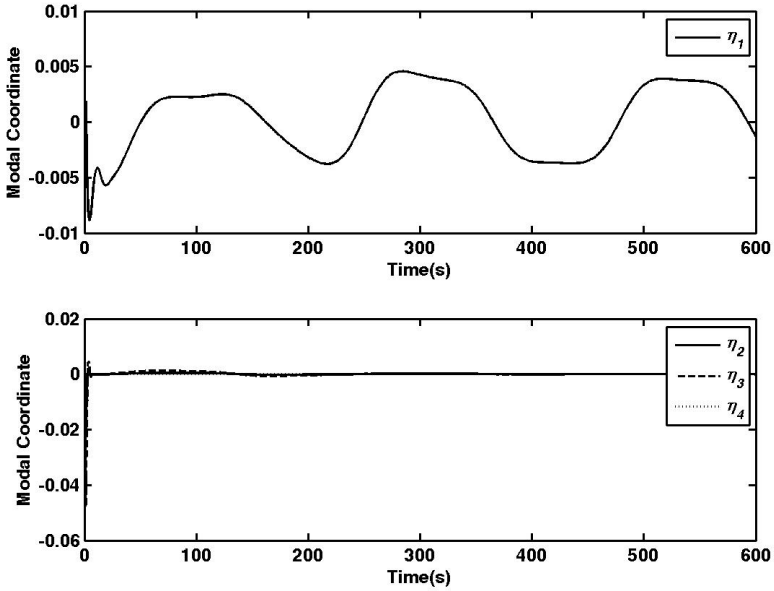

Figure 7.20 Generalized modal coordinates (Indirect Robust Control method with different initial conditions)

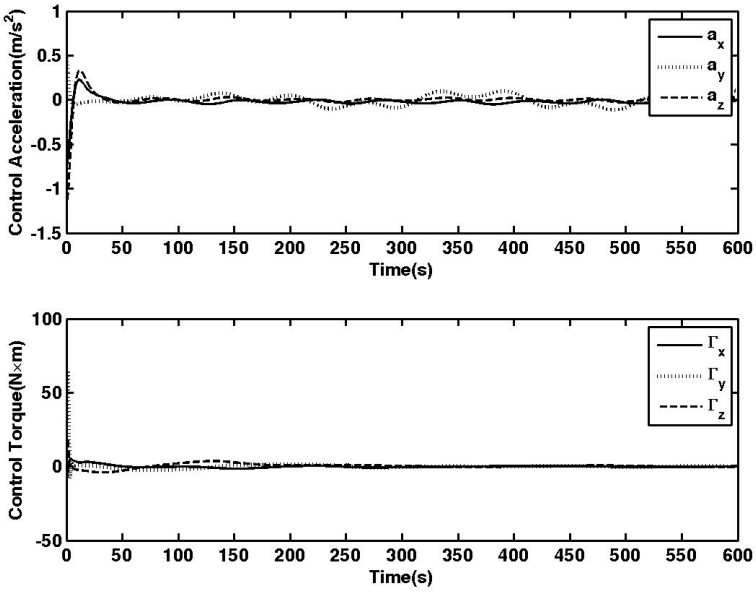

Figure 7.21 Control accelerations and control torques (Indirect Robust Control method with different initial conditions)

Figure 7.20 shows the flexible structure deformation suppression performance. As can be seen from the figure, the vibration diminishes quickly to small values after only a few seconds regardless of the large initial angular velocity error.

Figure 7.21 demonstrates the control accelerations and control torques. Compared with Fig. 7.6, the control torque is increased in Fig. 7.21 due to the change in the initial angular velocity error. Similar to the previous simulations, large initial control is applied to drive the system to the steady state quickly. Small oscillations are seen in the spacecraft control acceleration to maintain the desired relative position, while control torque converges to zero during the steady state.

7.4 Simulation results comparison and discussions

In Section 7.1, the controller design follows the indirect robust control method. In Section 7.2 the controller design is based on the inverse optimal adaptive control

technique. From the simulation results in Sections 7.1 and 7.2, the comparison between these two methods can be summarized in the following aspects:

1) Design strategy: the indirect robust control is designed via the combination of the robust control with the optimal control formulation such that both robust stability and optimality can be guaranteed. The uncertainty bounds are formulated into a modified cost function with a quadratic form such that the θ-D method can be applied to obtain a closed-form feedback control law. Since the robust control strategy and uncertainty bounds are used, the design may be conservative.

   To alleviate the conservative design, the inverse optimal adaptive control (IOAC) method is employed as the second strategy for comparison. In the IOAC method, the adaptive strategy is first used to design an adaptive controller and estimate the moment of inertia, which is the main uncertain parameter affecting the control accuracy. Then this adaptive controller can be shown to be robust to the bounded uncertainties, and to be the solution to an optimal control problem with a derived meaningful cost function.

   Both methods are based on the optimal control formulation. The indirect robust control method solves the robust control problem "indirectly" by solving a modified optimal control problem. But when dealing with the optimal control problem, a physically meaningful cost function is designed a priori, whereas the IOAC method indirectly derives a cost function from an adaptive control law and the physical meaning of the cost function is not explicit. The simulation results demonstrate each method's advantages and disadvantages.

2) Tracking error: both methods can guarantee the spacecraft to asymptotically approach the desired position and attitude.

3) Convergence speed: Since the translational part is the same in both these two simulations, we only compare convergence speed of the rotational motion. The settling time in Section 7.1 is around 300 seconds while the one in Section 7.2 is less than 100 seconds. But considering the average proximity operation time, both results are acceptable.

4) Required control torque: As analyzed in the previous two sections, the initial control acceleration and torque are relatively large in order to drive the system to the required position and attitude in a relatively short time. Required control torque in Section 7.1 is at the same magnitude as in Section 7.2.

5) Design Complexity:

On one hand, in Chapter 5, by using the indirect robust control design scheme, a sequential design procedure has been established. The control of translational motion, rotational motion, and flexible deformation are formulated in a unified framework, and the controller design is based on transforming robust control of the overall dynamic system into an equivalent optimal control problem. By using the θ-D optimal control method, a closed-form feedback solution can be obtained. On the other hand, in Chapter 6, due to the high design complexity of the inverse optimal adaptive control (IOAC) method, the translational control design and the rotational control design are separated. The IOAC method is used only in the rotational control part because the parameter uncertainty and disturbance mostly exist in the rotational motion. The IOAC design process is relatively more complicated because it involves the direct Lyapunov design process [56, 59, 102], and the proper Lyapunov function and controller with certain formulation need to be found. For systems with high nonlinearities, coupling dynamics, and high

dimensions, it is very difficult to do so.

The indirect robust control method modifies the original cost function by augmenting it with the uncertainty bounds and formulating it into a quadratic cost function, which makes the optimal control problem easier to solve. In addition, the θ-D method facilitates the closed-form feedback control design and design complexity is greatly reduced. But we have to realize that when dealing with parametric uncertainties, the indirect robust control method may be conservative by estimating the overall bounds of disturbance and uncertainty. No adaptive technique is utilized to actively deal with the parameter uncertainty.

As to the IOAC method, it follows the classical direct Lyapunov method to design the nominal adaptive control law, and then follows the inverse optimal control strategy to show optimality. By designing the parameter update law, it explicitly handles the parametric uncertainties and achieves both robustness for the disturbance and adaptiveness for the parametric uncertainty. The simulation results with IOAC also demonstrate better rotational motion control performance than the results using the indirect robust control method. As a trade-off, the parameter estimation or update law designs greatly increases the design complexity, and can be rather difficult in applying IOAC to more complex problems when flexible deformation is present.

CHAPTER VIII

CONCLUSION

Robust control of spacecraft proximity operation is investigated in this dissertation. The translational motion, rotational motion, and induced flexible deformation are all addressed in one unified optimal control framework. Two new control design schemes are proposed and tested by simulations. First, a novel design method named indirect robust control technique is introduced. By making use of the relationship between the stabilization and optimal control, both robustness and optimality can be achieved. Combining with the θ-D optimal control technique, the integrated indirect robust control method can be used to solve a wide range of highly nonlinear, high-dimensional robust control problems with approximate closed-form solution. Second, an inverse optimal adaptive control method is combined with the indirect robust control method to better handle parametric uncertainties using the adaptive control capability. Six degrees of freedom simulation results demonstrated the capability of these two control methods in spacecraft proximity operations. To summarize the dissertation, the following conclusions were drawn based upon the design processes:

1) By analyzing the spacecraft translational motion, rotational motion and flexible deformation caused by large maneuvers, a unified formulation of control of these spacecraft dynamic motions is shown to be effective in handling the coupling and simplifying the design process. However, the overall system dynamics are high-dimensional (containing 25 system states) and highly nonlinear, which makes the control design a challenging work. The two optimal control based robust and

adaptive control techniques are shown to be able to solve this challenging spacecraft control problem.

2) By exploring the inner relationship of the robust stabilization problem and the optimal control problem, i.e. the Lyapunov function guaranteeing closed-loop stability is in fact the solution to the steady-state HJB equation for the optimal-controlled nominal system with a modified cost function including uncertainty bounds, the robust control problem can be transformed into an equivalent optimal control problem. The greatest benefit is that both stabilization and performance can be both achieved.

3) To avoid the difficulty of directly solving the HJB equation in order to obtain the feedback solution to the transformed optimal control problem, the θ-D optimal control method is used along with the indirect robust control method to solve the high-dimensional and nonlinear spacecraft proximity control problem. Closed-form solution is obtained by virtue of a perturbation method. Compared with the traditional optimal control method, solving the HJB equation numerically is avoided. Thus, the new controller does not require intensive computational load and facilitates onboard implementation.

4) The inverse optimal adaptive control method is used to alleviate the conservativeness of the indirect robust control method based on direct estimation of unknown system parameters. When combined with the indirect robust control method, it achieves the robust, adaptive, and optimal characteristics. As a trade-off, since the inverse optimal adaptive control technique aims at finding an analytical solution, the design complexity is thus increased and the physical meaning of the derived cost function may not be straightforward.

5) Computer simulations are conducted to demonstrate the effectiveness of the proposed control techniques. A typical scenario in spacecraft proximity operation is investigated, where the pursuer spacecraft is required to synchronize its attitude and keep a constant relative docking distance with respect to a free tumbling non-cooperative target. Their docking ports are required to face each other during the simulation process. Controllers are designed with both the indirect robust control method and the inverse optimal adaptive control method. Simulation results show that both controllers demonstrate satisfying performance. While the indirect robust control method shows advantages in design simplicity and online implementation, the inverse optimal adaptive control method exhibits faster attitude control response in the presence of the moment of inertia uncertainty.

REFERENCES

[1] B. C. Hacker and J. M. Grimwood, "On the Shoulders of Titans: A History of Project Gemini," 1977.

[2] D. Chiarrappa, "Analysis and Design of Space Vehicle Flight Control Systems, Volume VIII Rendezvous and Docking," General Dynamics Corp.for the NASA-Marshall Space Flight Center, AL1967.

[3] J. A. Chamberlin and J. T. Rose, "Gemini Rendezvous Program," *Journal of Spacecraft and Rockets,* vol. 1, no. 1, pp. 13-18, 1964.

[4] M. Williamson, "Aiming for the Moon: the engineering challenge of Apollo," *Engineering Science and Education Journal,* vol. 11, no. 5, pp. 164 - 172, 2002.

[5] R. E. Stevenson, "From mercury to skylab: A decade of space oceanography," presented at the IEEE OCEAN 75 Conference, San Diego, CA, 1975.

[6] D. Zimpfer, P. Kachmar, and S. Tuohy, "Autonomous Rendezvous, Capture and In-Space Assembly: Past, Present and Future," in *1st Space Exploration Conference: Continuing the Voyage of Discovery*, Orlando, FL, 2005.

[7] T. Rumford, "Demonstration of Autonomous Rendezvous Technology (DART) Project Summary," *SPIE 5088,* vol. 10, pp. 10-19, 2003.

[8] NASA, "Overview of the DART Mishap Investigation Results," 2006.

[9] NASA, "Demonstration of Autonomous Rendezvous Technology Mishap Review Board," 2006.

[10] European Space Agency, "ATV Johannes Kepler Factsheet," Noodwijk, Netherlands, 2011.

[11] European Space Agency, "ATV Johannes Kepler Information Kit," Noodwijk, Netherlands, 2011.

[12] European Space Agency, "Autonomated Transfer Vehicle ATV: Servicing the International Space Station," 2010.

[13] J. Li, G. Tang, and H. Li, "Fuzzy/PID Hybrid Trajectory Control for Final Approach in Autonomous Rendezvous Mission," *Journal of Astronautics (Chinese),* vol. 31, no. 3, pp. 774-779, 2010.

[14] T. Oki, H. Nakanish, and K. Yoshida, "Whole-Body Motion Control for Capturing a Tumbling Target by a Free-floating Space Robot," in *International Conference on Intelligent Robots and Systems*, San Diego, CA, 2007, pp. 2256-2261.

[15] F. Aghili, "Optimal Control of a Space Manipulator for Detumbling of a Target Satellite," in *IEEE International Conference on Robotics and Automation*, Kobe, Japan, 2009, pp. 3019-3024.

[16] E. Carlson, S. Casali, D. Chambers, G. Geissler, A. Lalich, M. Leipold, R. Mach, J. Parry, and F. Weems, *Final Design of a Space Debris Removal System*, 1990.

[17] J. Pearson, E. Levin, and J. Oldson, "Electrodynamics Debris Eliminator (EDDE): Design Operation, and Ground Support," Star Technology and Research, Inc., Maui, HI2010.

[18] J. Pearson, J. Carroll, E. Levin, and J. Oldson, "EDDE: Electrodynamics Debris Eliminator for Active Debris Removal," *NASA-DARPA International Conference on Orbital Debris Removal,* pp. 1-14, 2009.

[19] S. I. Nishida and S. Kawamoto, "Strategy for Capturing of A Tumbling Space Debris," *Acta Astronautica,* vol. 68, pp. 113-120, 2011.

[20] S. I. Nishida, S. Kawamoto, Y. Okawa, F. Terui, and S. Kitamura, "Space Debris Removal System Using a Small Satellite," *Acta Astronautica,* vol. 65, pp. 95-102, 2009.

[21] S. I. Nishida and T. Yoshikawa, "Space Debris Capture by a Joint Compliance Controller Robot," in *IEEE/ASME International Conference on Advanced Intelligent Mechatronics*, 2003, pp. 496-502.

[22] S. I. Nishida and T. Yoshikawa, "A Robotic Small Satellite for Space Debris Capture," in *IEEE International Conference on Robotics and Biometics*, Bangkok, Thailand, 2008, pp. 1348-1353.

[23] S. I. Nishida and T. Yoshikawa, "Capture and Motion Braking of Space Debris by a Space Robot," in *International Conference on Control, Automation and Systems*, Seoul, Korea, 2007, pp. 706-711.

[24] I. Bekey, "Orion's Laser: Hunting Space Debris," *Aerospace America,* vol. 35, no. 5, pp. 38-44, 1997.

[25] M. D. Griffin and J. R. French, *Space Vehicle Design* vol. 2. Blacksburg, Virginia, 2004.

[26] A. E. Bryson, *Control of Spacecraft and Aircraft*. Princeton, NJ: Princeton University Press, 1994.

[27] J. R. Wertz, *Spacecraft Attitude Determination and Control* vol. 1. Torrance, CA: Microcosm Inc, 1999.

[28] D. Early, W. Haile, and M. Turczyn, "Thermal Creak Testing of the Hubble Space Telescope's New Solar Array 3," Goddard Space Flight Center2001.

[29] M. J. Sidi, *Spacecraft Dynamics and Control: A Practical Engineering Approach*. New York: Cambridge University Press, 1997.

[30] X. Yang, X. Luo, F. Sun, F. Wu, and H. Liu, "Dynamic Modeling and Tracking Control of Fuel Filled Space Robotics System with Flexible Manipulators," in *3rd International Symposium on Systems and Control in Aeronautics and Astronautics*, Harbin, China, 2010, pp. 1192-1197.

[31] C. Samson, C. English, A. Deslauriers, I. Christie, F. Blais, and F. Ferrie, "Neptec 3D Laser Camera System: From Space Mission STS-105 to Terrestrial Applications," *Canadian Aeronautics and Space Journal,* vol. 50, no. 2, pp. 115-123, 2004.

[32] F. K. Yeh, "Sliding-mode Adaptive Attitude Controller Design for Spacecraft with Thrusters," *IET-Control Theory and Applications,* vol. 4, no. 7, pp. 1254-1264, 2010.

[33] P. Tsiotras, "Further Passivity Results for the Attitude Control Problem," *IEEE Transactions on Automatic Control,* vol. 43, no. 11, pp. 1597-1600, 2002.

[34] H. Zhang, F. Wang, and P. Trivailo, "Spin-axis Stabilization of Undersaturated Rigid Spacecraft under Sinusoidal Disturbance," *International Journal of Control,* vol. 81, no. 12, pp. 1901-1909, 2008.

[35] Y. Tsuda and S. Nakasuka, "New Attitude Motion Following Control Algorithm for Capturing Tumbling Object in Space," *Acta Astronautica,* vol. 53, pp. 847-861, 2003.

[36] S. Tanygin, "Generalization of Adaptive Attitude Tracking," in *AIAA/AAS Astrodynamics Specialist Conference and Exhibit*, Monterey, CA, 2002, pp. 1-12.

[37] J. T. Wen and K. K. Delgado, "The Attitude Control Problem," *IEEE Transactions on Automatic Control,* vol. 36, no. 10, pp. 1148-1162, 1991.

[38] J. Ahmed, V. T. Coppola, and D. S. Bernstein, "Asymptotic Tracking of Spacecraft Attitude Motion with Inertia Matrix Identification," *Journal of Guidance, Control and Dynamics,* vol. 21, pp. 2471-2476, 1997/10// 1998.

[39] N. A. Chaturvedi, D. S. Bernstein, J. Ahmed, F. Bacconi, and N. H. McClamroch, "Globally Convergent Adaptive Tracking of Angular Velocity and Inertia Identification for a 3-DOF Rigid Body," *IEEE Transactions on Control System Technology,* vol. 14, no. 5, pp. 841-853, 2006.

[40] S. D. Gennaro, "Adaptive Robust Stabilization of Rigid Spacecraft in Presence of Disturbances," in *34th Conference on Decision and Control*, NO, LA, 1995, pp. 1147-1152.

[41] B. Yao, "High Performance Adaptive Robust Control of Nonlinear Systems: A General Framework and New Schemes," in *36th IEEE Conference on Decision and Control*, San Diego, CA, 1997, pp. 2489-2494.

[42] M. Krstic, "Invariant Manifolds and Asymptotic Properties of Adaptive Nonlinear Stabilizers," *IEEE Transactions on Automatic Control,* vol. 41, no. 6, pp. 817-829, 1996.

[43] N. A. Chaturvedi, A. K. Sanyal, M. Chellappa, J. L. Valk, N. H. McClamroch, and D. S. Bernstein, "Adaptive Tracking of Angular Velocity for a Planar Rigid Body with Unknown Models for Inertia and Input Nonlinearity," *IEEE Transactions on Control System Technology,* vol. 14, no. 4, pp. 613-627, 2006.

[44] Y. Jiang, Q. Hu, and G. Ma, "Adaptive Backstepping Fault-tolerant Control for Flexible Spacecraft with Unknown Bounded Disturbances and Actuator Failures," *ISA Transaction,* vol. 49, pp. 57-69, 2010.

[45] Q. Hu, L. Sun, and J. Hua, "Adaptive Integral Variable Structure Attitude Controller Design and Application to Flexible Spacecraft," in *7th World Congress on Intelligent Control and Automation*, Chongqing, China, 2008, pp. 2958-2963.

[46] H. Bang, C. Ha, and J. Kim, "Flexible Spacecraft Attitude Maneuver by Application of Sliding Mode Control," *Acta Astronautica,* vol. 57, pp. 841-850, 2005.

[47] C. Dong, L. Xu, Y. Chen, and Q. Wang, "Networked Flexible Spacecraft Attitude Maneuver Based on Adaptive Fuzzy Sliding Mode Control," *Acta Astronautica,* vol. 65, pp. 1564-1570, 2009.

[48] Q. Hu, B. Xiao, and Y. Zhang, "Robust Fault Tolerant Attitude Stabilization Control for Flexible Spacecraft under Partial Loss of Actuator Effectiveness," in *Conference on Control and Fault Tolerant Systems*, Nice, France, 2010, pp. 263-268.

[49] E. Jin and Z. Sun, "Robust Controllers Design with Finite Time Convergence for Rigid Spacecraft Attitude Tracking Control," *Aerospace Science and Technology,* vol. 12, pp. 324-330, 2008.

[50] Y. Jin, X. Liu, Q. Wei, and C. Hou, "Time-varying Sliding Mode Controls in Rigid Spacecraft Attitude Tracking," *Journal of Astronautics (Chinese),* vol. 21, pp. 352-360, 2008.

[51] J. Park, W. Chung, and Y. Youm, "Characteristics of Optimal Solutions in Kinematic Resolutions of Redundancy," *IEEE Transactions on Robotics and Automation,* vol. 12, no. 3, pp. 471-478, 1996.

[52] T. Ha, J. Lee, and J. Park, "Robust Control by Inverse Optimal PID Approach for Flexible Joint Robot Manipulator," in *International Conference on Robotics and Biometics*, Sanya, China, 2007, pp. 336-341.

[53] R. Bass and R. Webber, "Optimal Nonlinear Feedback Control Derived from Quartic and Higher-order performance Criteria," *IEEE Transactions on Automatic Control,* vol. 11, no. 3, pp. 448-454, 1966.

[54] B. Widrow and G. Plett, "Nonlinear Adaptive Inverse Control," in *Conference on Decision and Control*, San Diego, CA, 1997, pp. 1032-1037.

[55] N. T. Nguyen and A. K. Ishihara, "Robust Adaptive Optimal Control Modification with Large Adaptive Gain," in *American Control Conference*, St. Louis, MO, 2009, pp. 2581-2586.

[56] Z. Li and M. Krstic, "Optimal Design of Adaptive Tracking Controllers for Nonlinear Systems," *Automatica,* vol. 33, no. 8, pp. 1459-1473, 1997.

[57] M. Krstic and Z. Li, "Inverse Optimal Design of Input-to-State Stabilizing Nonlinear Controllers," *IEEE Transactions on Automatic Control,* vol. 43, no. 3, pp. 336-350, 1998.

[58] M. Krstic and P. Tsiotras, "Inverse Optimal Stabilization of a Rigid Spacecraft," *IEEE Transactions on Automatic Control,* vol. 44, no. 5, pp. 1042-1049, 1999.

[59] W. Luo, Y. Chu, and K. V. Ling, "Inverse Optimal Adaptive Control for Attitude Tracking of Spacecraft," *IEEE Transactions on Automatic Control,* vol. 50, no. 11, pp. 1639-1654, 2005.

[60] M. Krstic, "Optimal Adaptive Control-Contradiction in Terms or a Matter of Choosing the Right Cost Functional?," *IEEE Transactions on Automatic Control,* vol. 53, no. 8, pp. 1942-1947, 2008.

[61] M. Krstic, "Inverse Optimal Adaptive Control-The Interplay between Update Laws, Control Laws, and Lyapunov Functions," in *American Control Conference*, Saint Louis, MO, 2009, pp. 1250-1254.

[62] J. L. Fausz, V. S. Chellaboina, and W. M. Haddad, "Inverse Optimal Adaptive Control for Nonlinear Uncertain Systems with Exogenous Disturbances," in *36th IEEE Conference on Decision and Control*, San Diego, CA, 1997, pp. 2654-2659.

[63] W. M. Haddad and V. S. Chellaboina, "Robust Nonlinear Nonquadratic Feedback Control via Parameter Dependent Lyapunov Functions," *Nonlinear Analysis Theory, Methods and Applications,* vol. 30, no. 6, pp. 3725-3736, 1997.

[64] W. M. Haddad, V. S. Chellaboina, J. L. Fausz, and A. Leonessa, "Optimal Nonlinear Robust Control for Nonlinear Uncertain Cascade Systems," in *American Control Conference*, Albuquerque, NM, 1997, pp. 403-407.

[65] D. S. Bernstein, "Nonquadratic Cost and Nonlinear Feedback Control," *International Journal of Robust and Nonlinear Control,* vol. 3, pp. 211-229, 1993.

[66] C. J. Wan and D. S. Bernstein, "Nonlinear Feedback Control with Global Stabilization," *Dynamics and Control,* vol. 5, pp. 321-346, 1995.

[67] F. Lin, R. D. Brandt, and J. Sun, "Robust Control of Nonlinear Systems: Compensating for Uncertainty," *International Journal of Control,* vol. 56, no. 6, pp. 1453-1459, 1992.

[68] F. Lin and W. Zhang, "Robust Control of Nonlinear Systems without Matching Condition," in *32nd IEEE Conference on Decision and Control*, San Antonio, TX, 1993, pp. 2572-2577.

[69] F. Lin, "An Optimal Control Approach to Robust Control Design," *International Journal of Control,* vol. 73, no. 3, pp. 177-186, 2000.

[70] F. Lin, *Robust Control Design*, 1st ed. Chichester, England: John Wiley & Sons, Ltd, 2009.

[71] F. Lin and Robert D. Brandt, "An Optimal Control Approach to Robust Control of Robot Manipulators," *IEEE Transactions on Robotics and Automation,* vol. 14, no. 1, pp. 69-77, 1998.

[72] F. Lin, W. Zhang, and R. D. Brandt, "Robust Hovering Control of a PVTOL Aircraft," *IEEE Transactions on Control System Technology,* vol. 7, no. 3, pp. 343-351, 1999.

[73] P. Huang, J. Yan, J. Yuan, and Y. Xu, "Robust Control of Space Robot for Capturing Objects using Optimal Control Method," in *International Conference on Information Acquisition*, Seogwipo-si, Korea, 2007, pp. 397-402.

[74] J. R. Cloutier, C. N. D'Souza, and C. P. Mracek, "Nonlinear Regulation and Nonlinear H-inf Control via the State-Dependent Riccati Equation Technique," in *International Conference on Nonlinear Problems in Aviation and Aerospace*, Daytona Beach, FL, 1996, pp. 117-141.

[75] J. R. Cloutier and D. T. Stansbery, "The Capabilities and Art of State-Dependent Riccati Equation Based Design," in *American Control Conference*, Anchorage, AK, 2002, pp. 86-91.

[76] M. S. Naik and S. N. Singh, "State-Dependent Riccati Equation-Based Robust Dive Plane Control of AUV with Control Constraints," *Ocean Engineering,* vol. 34, pp. 1711-1723, 2007.

[77] Z. Ma, O. Ma, and B. N. Shashikanth, "Optimal Approach to and Alignment with a Rotating Rigid Body for Capture," *The Journal of the Astronautical Sciences,* vol. 55, no. 4, pp. 407-419, 2007.

[78] M. Xin and S. N. Balakrishnan, "A New Method for Suboptimal Control of a Class of Nonlinear Systems," *Optimal Control Applications and Methods,* vol. 26, pp. 55-83, 2005.

[79] M. Xin and S. N. Balakrishnan, "Missile Longitudinal Autopilot Design using a new Suboptimal Nonlinear Control Method," *IEEE Transactions on Control Theory and Application,* vol. 150, no. 6, pp. 577-584, 2003/01// 2003.

[80] W. H. Clohessy and R. S. Wiltshire, "Terminal Guidance System for Satellite Rendezvous," *Journal of the Astronautical Sciences,* vol. 27, no. 9, pp. 653-678, 1960.

[81] N. J. Kasdin, P. Gurfil, and E. Kolemen, "Canonical Modelling of Relative Spacecraft Motion via Epicyclic Orbital Elements," *Celestial Mechanics and Dynamical Astronomy,* vol. 92, pp. 337-370, 2005.

[82] H. Gao, X. Yang, and P. Shi, "Multi-objective Robust H-inf Control of Spacecraft Rendezvous," *IEEE Transactions on Control System Technology,* vol. 17, no. 4, pp. 794-802, 2009.

[83] X. Yang, Y. Bo, Y. Liu, Z. Ji, and H. Gao, "Output Tracking Control for Autonomous Spacecraft Rendezvous," in *48th IEEE Conference on Decision and Control*, Shanghai, China, 2010, pp. 5227-5232.

[84] G. Tang, Y. Luo, and H. Li, "Optimal Robust Linearized Impulsive Rendezvous," *Aerospace Science and Technology,* vol. 11, pp. 563-569, 2007.

[85] Y. Z. Luo and G. J.Tang, "Spacecraft Optimal Rendezvous Controller Design using Simulated Annealing," *Aerospace Science and Technology,* vol. 9, pp. 732-737, 2005.

[86] S. Gao and Y. Han, "Relative Position Control Based on H-inf Robust Control for Spacecraft Rendezvous Final Approach," in *3rd International Conference on Measuring Technology and Mechatronics Automation*, Shanghai, China, 2011, pp. 984-988.

[87] A. Miele, M. W. Weeks, and M. Ciarcia, "Optimal Trajectories for Spacecraft Rendezvous," *Journal of Optimal Theory Application,* vol. 132, pp. 353-376, 2007.

[88] H. Li, Y. Luo, J. Zhang, and G. Tang, "Optimal Multi-Objective Linearized Impulsive Rendezvous under Uncertainty," *Acta Astronautica,* vol. 66, pp. 439-445, 2011.

[89] Y. Z. Luo, G. J.Tang, and Y. Lei, "Optimal Multi-objective Linearized Impulsive Rendezvous," *Journal of Guidance, Control and Dynamics,* vol. 30, no. 2, pp. 383-389, 2007.

[90] P. C. Hughes, *Spacecraft Attitude Dynamics*: Dover Publications, Inc, 2004.

[91] M. R. Akella, "Rigid Body Attitude Tracking without Angular Velocity Feedback," *System and Control Letters,* vol. 42, pp. 321-326, 2001.

[92] H. Miwa and M. R. Akella, "Global Adaptive Stabilization using Output Feedback for Spacecraft Attitude Tracking," *Advances in the Astronautics and Sciences,* pp. 345-357, 2002.

[93] W. Cai, X. H. Liao, and Y. D. Song, "Indirect Robust Adaptive Fault-Tolerant Control for Attitude Tracking of Spacecraft," *Journal of Guidance, Control and Dynamics,* vol. 31, no. 5, pp. 1456-1463, 2008.

[94] M. R. Long, "Spacecraft Attitude Tracking Control," Master of Science in Aerospace Engineering Thesis, Virginia Polytechnic Institute and State University, 1999.

[95] A. Sanyal, A. Fosbury, N. Chaturvedi, and D. S. Bernstein, "Inertia Free Spacecraft Attitude Tracking with Disturbance Rejection and Almost Global Stabilization," *Journal of Guidance, Control and Dynamics,* vol. 32, no. 4, pp. 1167-1178, 2009.

[96] Z. Chen and J. Huang, "Attitude Tracking and Disturbance Rejection of Rigid Spacecraft by Adaptive Control," *IEEE Transactions on Automatic Control,* vol. 54, no. 3, pp. 600-605, 2009.

[97] A. A. Gami, M.Shafiq, A.Kassem, and R.Ahmed, "Feedforward Adaptive Learning based Tracking of Spacecraft Attitude," in *Mediterranean Conference on Control and Automation*, Athens, 2007, pp. 1-8.

[98] M. Krstic, I. Kanellakopoulos, and P. V. Kokotovic, "Adaptive Nonlinear Control without Overparameterization," *System and Control Letters,* vol. 19, pp. 177-185, 1992.

[99] C. Li and G. Ma, "Adaptive Backstepping Control for Attitude Tracking of a Spacecraft," in *IEEE International Symposium on Industrial Electronics*, Vigo, Spain, 2007, pp. 83-88.

[100] D. T. Stansbery and J. R. Cloutier, "Position and Attitude Control of a Spacecraft using the State-Dependent Riccati Equation Technique," in *American Control Conference*, Chicago, IL, 2000, pp. 1867-1871.

[101] T. Nagashio, T. Kida, T. Ohtani, and Y. Hamada, "Design and Implementation of Robust Symmetric Attitude Controller for ETS-VIII Spacecraft," *Control Engineering Practice,* vol. 18, pp. 1440-1451, 2010.

[102] M. Krstic and P. Tsiotras, "Inverse Optimality Results for the Attitude Motion of a Rigid Spacecraft," in *American Control Conference*, Albuquerque, NM, 1997, pp. 1884-188.

[103] C. Pukdeboon and A. S. I. Zinober, "Optimal Sliding Mode Controllers for Attitude Tracking of Spacecraft," in *IEEE International Conference on Control Applications*, Saint Petersburg, Russia, 2009, pp. 1708-1713.

[104] Y. Xia, Z. Zhu, M. Fu, and S. Wang, "Attitude Tracking of Rigid Spacecraft with Bounded Disturbance," *IEEE Transactions on Industrial Electronics,* vol. 58, no. 2, pp. 664-659, 2011.

[105] A. Chakrabortty, M. Arcak, and P. Tsiotras, "Robust Design of a Spacecraft Attitude Tracking Control System with Actuator Uncertainties," in *47th IEEE Conference on Decision and Control*, Cancun, Mexico, 2008, pp. 1587-1592.

[106] A. Mohammad and S. S. Ehsan, "Fuzzy Sliding Mode Controller Design for Spacecraft Attitude Tracking in terms of Quaternion," in *27th Chinese Control Conference*, Kunming, China, 2008, pp. 753-757.

[107] P. Singla, K. Subbarao, and J. L. Junkins, "Adaptive Output Feedback Control for Spacecraft Rendezvous and Docking Under Measurement Uncertainty," *Journal of Guidance, Control and Dynamics,* vol. 29, no. 4, pp. 892-902, 2006.

[108] K. Subbarao and S. Welsh, "Nonlinear Control of Motion Synchronization for Satellite Proximity Operations," *Journal of Guidance, Control and Dynamics,* vol. 31, no. 5, pp. 1284-1294, 2008.

[109] H. Liaw and B. Shirinzadeh, "Robust Adaptive Constrained Motion Tracking Control of Piezo-actuated Flexure-based Mechanisms for Micro/Nano Manipulation," *IEEE Transactions on Industrial Electronics,* vol. 58, no. 4, pp. 1406-1415, 2011.

[110] F. Karray, A. Grewal, M. Glaum, and V. Modi, "Stiffening Control of a class of Nonlinear Affine Systems," *IEEE Transactions on Aerospace and Electronic Systems,* vol. 33, no. 2, pp. 473-484, 1997.

[111] S. N. Singh and R. Zhang, "Adaptive Output Feedback Control of Spacecraft with Flexible Appendages by Modeling Error Compensation," *Acta Astronautica,* vol. 54, pp. 229-243, 2004.

[112] T. Nagashio and T. Kida, "Robust Control of Flexible Mechanical Systems by Utilizing Symmetry and Its Application to Large Space Structures," *IEEE Transactions on Control System Technology,* vol. 17, no. 3, pp. 671-680, 2009.

[113] G. Zhang, Y. Wang, W. Li, and Y. Zhang, "Nonlinear Control of Flexible Spacecraft Based on LMI Constrained Convex Optimization," in *2nd International Symposium on Systems and Control in Aerospace and Astronautics*, Shenzhen, China, 2008, pp. 10-12.

[114] S. D. Gennaro, "Output Attitude Tracking for Flexible Spacecraft," *Automatica,* vol. 38, no. 1719, p. 1726, 2002.

[115] S. D. Gennaro, "Output Feedback Stabilization of Flexible Spacecraft," in *35th IEEE Conference on Decision and Control*, Kobe, Japan, 1996, pp. 497-502.

[116] S. D. Gennaro, "Adaptive Robust Tracking for Flexible Spacecraft in presence of Disturbances," *Journal of Optimization Theory and Application,* vol. 98, no. 3, pp. 545-568, 1998.

[117] M. Shaharavi and M. Kabganian, "Attitude Tracking and Vibration Suppression of Flexible Spacecraft using Implicit Adaptive Control Law," in *American Control Conference*, Portland, OR, 2005, pp. 913-918.

[118] S. D. Gennaro, "Attitude Tracking for Flexible Spacecraft from Quaternion Measurements," in *41st IEEE Conference on Decision and Control*, 2002, pp. 4090-4091.

[119] S. D. Gennaro, "Passive Attitude Control of Flexible Spacecraft from Quaternion Measurements," *Journal of Optimization Theory and Application,* vol. 116, no. 1, pp. 41-60, 2003.

[120] E. Jin and Z. Sun, "Passivity-based Control for a Flexible Spacecraft in the presence of Disturbances," *International Journal of Nonlinear Mechanics,* vol. 45, pp. 348-356, 2010.

[121] Q. Hu, M. I. Friswell, W. David J, and S. Neild, "Nonlinear Proportional-Derivative-Type Controller for Flexible Spacecraft Attitude Stabilization under Bounded Disturbances," in *21th Annual International Conference on Chinese Control and Decision Conference*, Guilin, China, 2009, pp. 17-19.

[122] Q. Hu, "Semi-globally Input-to-State Stable Controller Design for Flexible Spacecraft Attitude Stabilization under Bounded Disturbances," *Acta Astronautica,* vol. 66, pp. 567-576, 2010.

[123] E. Jin and Z. Sun, "Robust Attitude Tracking Control of Flexible Spacecraft for Achieving Globally Asymptotic Stability," *International Journal of Robust and Nonlinear Control,* vol. 19, pp. 1201-1223, 2009.

[124] M. C. Pai and A. Sinha, "Sliding Mode Control of Vibration in a Flexible Structure via Estimated States and H-inf/u techniques," in *American Control Conference*, Chicago, IL, 2000, pp. 1118-1123.

[125] M. C. Pai and A. Sinha, "Increasing Robustness of Input Shaping Method to Parametric Uncertainties and Time-Delays," *Journal of Dynamic Systems, Measurement, and Control,* vol. 133, pp. 1-8, 2011.

[126] Q. Hu, "Input Shaping and Variable Structure Control for Simultaneous Precision Positioning and Vibration Reduction of Flexible Spacecraft with Saturation Compensation," *Journal of Sound and Vibration (Chinese),* vol. 318, pp. 18-35, 2008.

[127] Q. Hu, X. Gao, and G. Ma, "Reference Model Variable Structure Output Feedback for Attitude Maneuvers Control of Flexible Spacecrafts," *Intelligent Automation and Soft Computing,* vol. 15, no. 1, pp. 53-62, 2009.

[128] S. D. Gennaro, "Active Vibration Suppression in Flexible Spacecraft Attitude Tracking," *Journal of Guidance, Control and Dynamics,* vol. 21, no. 3, pp. 400-408, 1998.

[129] S. N. Singh and A. D. De'Araujo, "Adaptive Control and Stabilization of Elastic Spacecraft," *IEEE Transactions on Aerospace and Electronic Systems,* vol. 35, no. 1, pp. 115-121, 1999.

[130] S. D. Gennaro, "Output Stabilization of Flexible Spacecraft with Active Vibration Suppression," *IEEE Transactions on Aerospace and Electronic Systems,* vol. 39, no. 3, pp. 747-759, 2003.

[131] A. Grewel and V. J. Modi, "Multibody Dynamics and Robust Control of Flexible Spacecraft," *IEEE Transactions on Aerospace and Electronic Systems,* vol. 36, no. 2, pp. 491-500, 2000.

[132] Q. Hu and B. Xiao, "Robust Adaptive Backstepping Attitude Stabilization and Vibration Reduction of Flexible Spacecraft Subject to Actuator Saturation," *Journal of Vibration and Control,* vol. 0, no. 0, pp. 1-15, 2010.

[133] A. Iyer and S. N. Singh, "Sliding Mode Control of Flexible Spacecraft under Disturbance Torque," in *27th Conference on Decision and Control*, Austin, TX, 1988, pp. 718-722.

[134] Q. Hu, "Robust Adaptive Attitude Tracking Control with L 2 Gain Performance and Vibration Reduction of an Orbiting Flexible Spacecraft," *Journal of Dynamic Systems, Measurement, and Control,* vol. 133, pp. 1-11, 2011.

[135] Q. Hu, "Variable Structure Maneuvering Control with Time-varying Sliding Surface and Active Vibration Damping of Flexible Spacecraft with Input Saturation," *Acta Astronautica,* vol. 64, pp. 1085-1108, 2009.

[136] Q. Hu, "Adaptive Output Feedback Sliding-mode Maneuvering and Vibration Control of Flexible Spacecraft with Input Saturation," *IET-Control Theory and Applications,* vol. 2, no. 6, pp. 467-478, 2008.

[137] Q. Hu, L. Xie, and H. Gao, "A Combined Positive Position Feedback and Variable Structure Approach for Flexible Spacecraft under Input Nonlinearity," in *9th International Conference on Control, Automation, Robotics and Vision*, Singapore, 2006, pp. 1-6.

[138] L. Zhu, W. Song, and Q. Hu, "Active Vibration Suppression and Attitude Maneuvers of Flexible Spacecraft via Fuzzy Sliding Control," in *Chinese Control and Decision Conference*, Yantai, China, 2008, pp. 3665-3669.

[139] L. Zhu, Y. Liu, D. Wang, and Q. Hu, "Backstepping-based Attitude Maneuver Control and Active Vibration Reduction of Flexible Spacecraft," in *Chinese Control and Decision Conference*, Yantai, China, 2008, pp. 887-891.

[140] Q. Hu, J. Cao, and Y. Zhang, "Robust Backstepping Sliding Mode Attitude Tracking and Vibration Damping of Flexible Spacecraft with Actuator Dynamics," *Journal of Aerospace Engineering,* vol. 22, no. 2, p. 14, 2007.

[141] M. Lither and S. Dubowsky, "State, Shape and Parameter Estimation of Space Objects from Range Images," in *IEEE International Conference on Robotics and Automation*, New Orleans, LA, 2004, pp. 2974-2979.

[142] H. Schaub and J. L. Junkins, *Analytical Mechanics of Space Systems* vol. 2nd. Reston, VA: AIAA, 2009.

[143] L. Meirovitch, "A Stationary Principle for the Eigenvalue Problem for Rotating Structures," *AIAA Journal,* vol. 14, pp. 1387-1394, 1976.

[144] J. D. Turner and H. M. Chun, "Optimal Distributed Control of a Flexible Spacecraft during a Large-Angle Maneuver," *Journal of Guidance, Control and Dynamics,* vol. 7, no. 3, pp. 257-264, 1984.

[145] M. Xin and H. Pan, "Nonlinear Optimal Control of Spacecraft Approaching a Tumbling Target," in *American Control Conference*, St. Louis, 2009.

[146] M. Xin and H. Pan, "Integrated Nonlienar Control of Spacecraft Position, Attitude, and Flexible Motion for Satellite Proximity Operations," in *AIAA Guidance, Navigation, and Control Conference*, Chicago, IL, 2009.

[147] M. Xin and H. Pan, "Robust Control of PVTOL Aircraft with a Nonlienar Optimal Control Solution," *Journal of Aerospace Engineering,* vol. 23, no. 4, p. 10, 2010.

[148] M. Xin and H. Pan, "Integrated Nonlinear Optimal Control of Spacecraft in Proximity Operations," *International Journal of Control,* vol. 83, no. 2, p. 16, 2010.

[149] M. Xin and H. Pan, "Indirect Robust Control of Spacecraft via Theta-D Optimal Control Solution," in *AIAA Infotech@Aerospace Conference*, Atlanta, GA, 2010.

[150] M. Xin and H. Pan, "Indirect Robust Control of Spacecraft via Optimal Control Solution," *IEEE Transactions on Aerospace and Electronic Systems,* in press, 2011.

[151] A. E. Bryson and Y. C. Ho, *Applied Optimal Control: Optimization, Estimation and Control* vol. 2nd. New York, NY: Taylor & Francis, 1975.

[152] M. Xin, S. N. Balakrishnan, D. T. Stansbery, and E. J. Ohlmever, "Nonlinear Missile Autopilot Design with θ-D Technique," *Journal of Guidance, Control and Dynamics,* vol. 27, pp. 406-417, 2004.

[153] M. Xin, S. N. Balakrishnan, and E. J. Ohlmever, "Integrated Guidance and Control of Missile with θ-D Method," *IEEE Transactions on Control Systems Technology,* vol. 14, pp. 981-992, 2006.

[154] D. A. Vallado, *Fundamentals of Astrodynamics and Applications* vol. 3rd. El Segundo, CA: Microcosm and Springer, 2007.

[155] H. K. Khalil, "Fundamental Properties: Comparison Principle," in *Nonlinear Systems*, 3rd ed: Prentice Hall, 2001, pp. 102-104.

[156] H. K. Khalil, "Nonlinear Systems," 3rd ed Upper Saddle River, NJ: Prentice Hall, 2001, p. 192.